fMRI investigations of visual cortex dynamics: Impact of peripheral visual field restrictions

Thesis
for the degree of

doctor rerum naturalium (Dr. rer. nat.)

approved by the Faculty of Natural Sciences of
Otto von Guericke University Magdeburg

by **M.Sc. Gokulraj Prabhakaran**
born on 17. March 1988 in Chennai, India

Reviewer: apl. Prof. Dr. rer. nat. Michael Hoffmann
Prof. Dr. Serge Dumoulin

submitted on: 14. February 2022
defended on: 01. December 2022

Abstract

One of the key challenges of modern visual neuroscience is to learn how neuroplasticity shapes visual cortex in the face of deprived input. Those insights are also fundamental for therapeutic and diagnostic initiatives aimed at restoring vision where the plasticity and remapping of visual cortex is a critical factor. Currently, the neuroplasticity of visual cortex is best studied with the combination of functional MRI (fMRI) and computational neuroimaging models. It is however, imperative that those methods are also transferable to and interpretable in the clinical context, so they can complement standard ophthalmological tests in order to improve diagnostics and therapy. In this thesis, I have investigated the scope and limits of large-scale cortical reorganization in relation to peripheral visual field (VF) restrictions, as well as addressed on approaches to translate fMRI-based findings into clinical workflow. Specifically, I have investigated the following topics:

i) Patients with peripheral VF-defects, as in glaucoma or retinitis pigmentosa (RP) show changes in the receptive field (pRFs) characteristics of the intact central representation. Using fMRI-based mapping of the central VF at 3 T we tested the dynamics of cortical pRF properties in a comparative approach, where the VF restrictions (scotomas) that are characteristic for retinal pathologies were simulated in healthy individuals (n=8). For a simulated scotoma condition, we observed a significant displacement in the pRF positions of the neuronal population of the foveal representation (≤3°) towards the periphery ($p<0.05$, corrected) and an overall increase in their pRF size. The shifts were observed across the early visual areas (V1-V3), though without any hierarchical trend, and the magnitude of shifts were associated with the extent of the VF-restriction. In a context of reduced peripheral stimulation, our findings in controls with simulated scotomas suggest that previous similar findings in patients are explainable by the normal cortical organization principles, and originate from plausible methodological biases and/or physiological mechanisms. The findings emphasize the use of appropriate and comparable controls in studies addressing plasticity and exert caution in interpreting changes in pRF properties in vision disorders as straightforward evidence of large-scale reorganization of the visual cortex.

ii) Brain activity in the cortical projection zones of retinal lesion (LPZ) following visual input deprivation can erroneously be mistaken for cortical remapping. In central vision disorders, such as macular degeneration (MD) and congenital RP, these LPZ responses were shown to be side-effects of task-elicited

demands. Here, we extended these studies to acquired vision disorders by investigating the fMRI response signatures in patients with advanced glaucoma (n=4), in comparison to two reference groups, RP (n=3) and healthy controls with simulated peripheral VF-defects (n=7). The glaucomatous LPZ showed the presence of aberrant LPZ responses in the early visual cortex only with the performance of stimulus-related task [p(corrected) for V1: 0.024, V2: 0.069, V3: 0.006], which was not observed in the controls with simulated VF deficits. No significant modulation of responses was observed in the LPZ when the participant passively viewed the stimulus or performed a stimulus-independent task. The response behavior of RP patients was similar to glaucoma and in line with existing reports, indicating the robustness of these findings. In summary, we provided further evidence that aberrant LPZ responses are shaped by top-down mechanism elicited by task-demands rather than the remapping of visual cortex, and are also a general feature of human visual system across the spectrum of visual dysfunctions.

iii) Inclusion of measurements of visual cortex activity is critical in determining the success of upcoming and promising initiatives to restore vision. Those methods are however strongly required to be clearly and effectively transferable into clinical routine. To study the relationship between fMRI and standard ophthalmological assessments, we reconstructed the VFs of patients with advance glaucoma (n=4), RP (n=2) and controls with artificial defects (n=6) from cortical responses in the early visual cortex and compared them to the gold standard subjective standard automated perimetry (SAP) based VFs. pRF-mapping-predicted VFs were found to show a strong matching accuracy with SAP-based VFs [accuracy: 74%], providing evidence of the feasibility and reliability of fMRI-based approaches to provide an objective assessment of VFs. A second less-demanding approach using a simple and robust visual stimulation (on-off block design) and individualized anatomy-driven retinotopic-atlas information (atlas-based approach) to reconstruct VFs was also shown to have equivalently good congruence with SAP [accuracy: 65%]. This indicates that the atlas-based approach may be used as a surrogate for VF-predictions where mapping-based methods are not possible, for e.g. in patients with fixation instabilities, very advanced VF-defects or encountering other difficulties when performing task. Importantly, the findings are likely to help mitigate some limitations in translating fMRI-based methods to clinical work-up.

In conclusion, the findings presented in this thesis provide no evidence for bottom-up large-scale reorganization of the visual cortex in peripheral vision disorders, such as glaucoma and RP. This was ascertained by addressing known major indications mimicking neuroplasticity in the context of normal cortical organization and functional behavior. Finally, by showcasing the translatability of fMRI as a clinical tool, the thesis is expected not only to provide significant insights into the development and reorganization of the visual system, but also pave way for better disease management and therapeutic decisions.

Zusammenfassung

Eine der wichtigsten Herausforderungen der modernen visuellen Neurowissenschaften besteht darin, herauszufinden, wie die neuroplastischen Vorgänge den visuellen Kortex angesichts fehlender Informationen formt. Diese Erkenntnisse sind auch von grundlegender Bedeutung für therapeutische und diagnostische Initiativen zur Wiederherstellung des Sehvermögens, bei denen Plastizität und Reorganisation des visuellen Kortex ein kritischer Faktor sind. Dazu lässt sich die Neuroplastizität des visuellen Kortex sehr gut mit der Kombination von funktionellem MRT (fMRI) und computergestützter Neuroimaging-Modellierung untersuchen. Es ist jedoch zwingend erforderlich, dass diese Methoden auch auf den klinischen Kontext übertragbar und interpretierbar sind, damit sie ophthalmologische Standardtests zur Verbesserung von Diagnostik und Therapie ergänzen können. In dieser Dissertation wurden der Umfang und die Grenzen einer großflächigen kortikalen Reorganisation in Bezug auf Einschränkungen des peripheren Gesichtsfelds (VF) untersucht und Ansätze zur Umsetzung fMRI-basierter Erkenntnisse im klinischen Arbeitsablauf getestet. Konkret wurden folgende Themen untersucht:

i) Patienten mit peripheren VF-Defekten, wie bei Glaukom oder Retinitis pigmentosa (RP), zeigen Veränderungen im rezeptiven Feld (pRFs) der intakten zentralen Repräsentation. Mittels fMRT-basierter Kartierung des zentralen VF bei 3 T wurde die Dynamik kortikaler pRF-Eigenschaften in einem vergleichenden Ansatz getestet, wobei die für Netzhautpathologien charakteristischen VF-Einschränkungen (Skotome) bei gesunden Personen (n=8) simuliert wurden. Für die Bedingung mit einem simulierten Skotom konnte eine signifikante Verschiebung der pRF-Positionen der neuronalen Population der fovealen Repräsentation (≤3°) in Richtung der Peripherie ($p<0,05$, korrigiert) beobachtet werden sowie eine allgemeine Zunahme ihrer pRF-Größe. Die Verschiebungen wurden in den frühen visuellen Bereichen (V1-V3) beobachtet, jedoch ohne einen hierarchischen Trend, ferner hing das Ausmaß der Verschiebungen mit dem Ausmaß der VF-Einschränkung zusammen. In Hinblick auf reduzierte periphere visuelle Reizung legen unsere Ergebnisse bei Kontrollen mit simulierten Skotomen nahe, dass frühere ähnliche Befunde bei Patienten durch die normalen kortikalen Organisationsprinzipien erklärbar sind, und auf plausible methodologische Verzerrungen und/oder physiologische Mechanismen zurückzuführen sind. Die Ergebnisse unterstreichen die Notwendigkeit geeigneter und vergleichbarer Kontrollen in Studien, die sich mit Plastizität befassen, und mahnen zur Vorsicht bei der Interpretation von

Veränderungen der pRF-Eigenschaften bei Sehstörungen als direktem Beweis für eine umfangreiche Reorganisation des visuellen Kortex.

ii) Die Gehirnaktivität in den kortikalen Projektionszonen der Netzhautläsion (LPZ) nach dem Entzug von visueller Informationen kann mit kortikaler Reorganisation verwechselt werden. Bei zentralen Sehstörungen, wie Makuladegeneration (MD) und angeborener RP, wurden diese LPZ-Reaktionen als Nebenwirkungen von aufgabenbezogenen Anforderungen gezeigt. Hier haben wir diese Studien auf erworbene Sehstörungen bei Glaukom ausgeweitet, indem wir die fMRT-Antwortsignaturen bei Patienten mit fortgeschrittenem Glaukom (n=4) im Vergleich zu zwei Referenzgruppen, (I) RP (n=3) und (II) gesunden Kontrollpersonen mit simulierten peripheren VF-Defekten, untersucht haben (n=7). Die glaukom-bedingte LPZ zeigte das Vorhandensein von abweichenden LPZ-Reaktionen im frühen visuellen Kortex nur bei Ausführung von reizabhängigen Aufgaben [p(korrigiert) für V1: 0,024, V2: 0,069, V3: 0,006], was bei den Kontrollen mit simulierten VF-Defiziten nicht beobachtet wurde. Im LPZ wurde keine signifikante Modulation der Antworten beobachtet, wenn der Teilnehmer den Sehreiz passiv betrachtete oder eine reizunabhängige Aufgabe ausführte. Das Antwortverhalten von RP-Patienten ähnelt dem von Glaukompatienten und entsprach vorherigen Berichten, was die Robustheit dieser Ergebnisse untermauert. Zusammenfassend lässt sich sagen, dass wir weitere Beweise dafür geliefert haben, dass abweichende LPZ-Antworten durch „Top-down“-Mechanismen beeinflusst werden, die durch aufgabenbezogene Anforderungen ausgelöst werden, und nicht durch Neuzuordnungen im visuellen Kortex. Dies scheint ein allgemeines Merkmal des menschlichen visuellen Systems im Spektrum visueller Störungen zu sein.

iii) Die Einbeziehung von Messungen der Aktivität des visuellen Kortex ist entscheidend für den Erfolg der bevorstehenden und vielversprechenden Initiativen zur Wiederherstellung des Sehvermögens. Diese Methoden müssen jedoch eindeutig und effektiv in die klinische Routine übertragbar sein. Um die Beziehung zwischen fMRT und ophthalmologischen Standarduntersuchungen zu betrachten, rekonstruierten wir die VFs von Patienten mit fortgeschrittenem Glaukom (n=4), RP (n=2) und Kontrollen mit simulierten Defekten (n=6) aus kortikalen Reaktionen im frühen visuellen Kortex und verglichen sie mit dem subjektiven Goldstandard der automatisierten Perimetrie (SAP). Es zeigte sich, dass die mit pRF-Mapping vorhergesagten VFs eine hohe Übereinstimmung mit den SAP-basierten VFs aufwiesen [Genauigkeit: 74 %], was die Durchführbarkeit und Zuverlässigkeit fMRT-basierter Ansätze zur objektiven Bewertung von VFs belegt. Ein zweiter weniger anspruchsvoller Ansatz, der eine einfache und robuste visuelle Stimulation (On-Off-Blockdesign) und individualisierte anatomie-bezogene retinotope Atlasinformationen zur Rekonstruktion von VFs verwendet (atlasbasierter Ansatz), zeigte ebenfalls eine ähnlich gute Kongruenz mit SAP [Genauigkeit: 65 %]. Dies deutet darauf hin, dass der atlasbasierte Ansatz als Surrogat für VF-Vorhersagen verwendet werden kann, wenn kartierungsbasierte Methoden nicht möglich sind, z.B.

bei Patienten mit Fixationsinstabilitäten, sehr fortgeschrittenen VF-Defekten oder anderen Schwierigkeiten bei der Durchführung von Aufgaben. Wichtig ist dabei auch, dass die Ergebnisse dazu beitragen können, Einschränkungen bei der Übertragung von fMRT-basierten Methoden auf die klinische Untersuchung zu verringern.

Zusammenfassend lässt sich sagen, dass die in dieser Dissertation präsentierten Ergebnisse keine Evidenz für eine umfangreiche „bottom-up“ Reorganisation des visuellen Kortex bei peripheren Sehstörungen wie Glaukom und RP liefern. Dazu wurden Indikatoren, die die Neuroplastizität im Kontext normaler kortikaler Organisation und Funktion nachahmen, untersucht und identifiziert. Diese Dissertation soll nicht nur wichtige Erkenntnisse über die Entwicklung und Reorganisation des visuellen Systems liefern, indem sie die Übertragbarkeit der fMRT als klinisches Instrument aufzeigt, sondern auch den Weg für ein besseres Krankheitsmanagement und für therapeutische Entscheidungen ebnen.

Contents

List of figures

Chapter 1

Introduction

"We see the world with our eyes, but we perceive the information with our brain" making it critical to investigate ophthalmic disorders not only from the perspective of the eye, but also the cortex, in particular the visual cortex. In patients with retinal lesions, there is a concomitant deprivation of visual input from the damaged retina to its corresponding locations in the visual cortex. An important question here is how the visual cortex responds to the visual field (VF) loss. Specifically, does the visual cortex adapt from its normal functional organization to accommodate for the lack of visual input or is it rather too inert to change? A fundamental characteristic of the visual cortex that allows for the investigation of cortical reorganization is its topographic organization i.e. correspondence of neighboring cortical neurons to neighboring locations stimulated in the visual field that preserves the spatial integrity of the retinal image (Engel et al., 1997). Taking advantage of this property, functional magnetic resonance imaging (fMRI) is currently the state-of-the art tool for non-invasive mapping of visual field in the visual cortex, commonly referred to as retinotopic mapping (Sereno et al., 1995). There are multiple maps of the visual field delineating the visual cortex into spatially and hierarchically organized visual areas, with some areas devoted for generic processing of the visual information and some for specialized functions (Wandell et al., 2007).

In addition to VF mapping, a quantitative evaluation of the visual field is also possible via the estimation of receptive field (RF) properties of neurons in the visual cortex (Dumoulin and Wandell, 2008). A neuron's RF is the portion of visual field (position and size) which when presented with a stimulus changes the neuron's responses. In contrast to single neuron animal models, fMRI estimates are derived from a population of neurons. Importantly, alterations in the characteristics of these population RFs (pRF) are observed in patients with restricted visual input. Consideration of these changes at a neuronal population level as explicit evidence of reorganization is however still under debate (Ferreira et al., 2017; Zhou et al., 2017), given that similar changes in the pRF dynamics are also reported in visually healthy individuals when patient-like VF deficits are simulated (Baseler et al., 2011; Haak et al., 2012). Such findings have indicated that altered pRF properties as reported with VF loss can be explained by the principles of normal cortical organization. These investigations however have been predominantly focused on central vision disorders as in macular degeneration (MD) (Morland, 2015), but not on peripheral vision

disorders for e.g. glaucoma and retinitis pigmentosa (RP). It is critical to bridge this gap in consideration to distinct processing of central and peripheral vision. In chapter 5, we used fMRI and computational neuroimaging methods to investigate the dynamics of pRF characteristics in healthy individuals for various sizes of simulated peripheral VF defects and to explore its relevance for existing reports of altered pRF properties in glaucoma and RP.

With the already well established knowledge of the visual cortex organization and its topographical representation (Engel et al., 1997; Sereno et al., 1995; Wandell et al., 2007), it is possible to predict the cortical representation of retinal lesions, i.e. the lesion projection zone (LPZ) of the visual cortex. A second common way of reporting evidence for large scale reorganization post VF loss is reporting the presence of aberrant cortical responses in the LPZ of patients with retinal lesions (Baker et al., 2008, 2005; Dilks et al., 2009). These responses however are shown to be elicited only in the presence of a visual task and suggested to be an effect of task-related feedback, an anomaly that is explainable by the normal cortical response behavior (Masuda et al., 2010, 2008). Such findings question the interpretation of abnormal cortical responses to be a straightforward indication of neuroplasticity and warrants further evidence. Insights into the responsiveness of LPZs are nevertheless critical in the context of vision restoration and rehabilitation strategies yet they are currently unavailable for a highly prevalent eye disease such as glaucoma. In this thesis (chapter 6), employing fMRI, we assessed the scope of the afore-mentioned LPZ response in peripheral vision disorders (glaucoma and RP) and its task-dependence to improve understanding of the visual cortex plasticity in adults.

Deciphering the limits of cortical plasticity is a vital factor in the selection of the optimal treatment strategies for the given eye disease. For instance, upcoming therapeutic advances to restore lost vision as in gene therapy are explored on the assumptions of no large scale cortical reorganization in the adult visual cortex (Ashtari et al., 2017). On the other hand, rehabilitation strategies are based on the contrasting view that the visual system is able to alter its organization (Authié et al., 2017; Cattaneo and Vecchi, 2011). It is thus important to establish the balance between the stability and plasticity of the adult visual cortex to understand which approaches will be most beneficial for the patients. This is however only possible when findings from fMRI are appropriately translated into clinical context and its feasibility is established. For this purpose, we investigated the correspondence of objective VF-assessments based on cortical response patterns in the visual cortex in comparison to VF-assessments from standard automated perimetry (SAP), the gold standard technique used in clinical routine and explored the complementary nature of the two approaches (chapter 7).

In summary, in this thesis I aimed to determine the scope and limits of large-scale cortical reorganization with peripheral visual field restrictions in the context of altered pRF characteristics (chapter 5) and abnormal LPZ responses (chapter 6). I

addressed the afore-mentioned indications of plasticity from the perspective of normal visual cortex organization and questioned the validity of this evidence. Finally, I explored the feasibility of and need for translating findings from fMRI investigations into the clinical work-up, in the interest of imminent advanced approaches to restore vision (Chapter 7).

Chapter 2

Background

2.1 Human visual system

Vision, as we see, results from a system of complex and sophisticated transformations and computations of the visual input at different levels, between the eye and the brain. The human visual pathway is broadly divided into anterior pathway comprising the retina, optic nerve, optic chiasm, lateral geniculate nucleus (LGN), and the posterior pathway comprising optic radiations and visual cortex (Figure 1).

2.2 From the retina to the visual cortex

Upon entering an eye, the light is focused by the cornea and lens and is projected on the retina in the back of the eye, thus forming an image. The retina is a multilayered network, where the initial transformation of the visual signal occurs at its first layer where light sensitive photoreceptors (rods and cones) convert the light stimulus into electrical activity (Dowling and Joseph L. Dowling, 2016). The cones are oriented predominantly towards high resolution (acuity) visual function at high light levels, i.e. photopic conditions, whereas the rods are tuned for very low light levels or scotopic conditions. This difference in functionality is also reflected by the difference in the density and non-uniform distribution of the photoreceptors in the retina (Provis et al., 1998). Specifically, (1) the fovea, a region of very high spatial acuity subtending the central 2 degrees of visual angle in the retina resulting in a high resolution central vision, contains only cones, while (2) periphery contains both rods and cones (20:1) which translates into lower visual acuity (Curcio et al., 1990). The generated electrical potential is further shaped and networked through the subsequent layers comprising the different types of neuronal cells [amacrine, bipolar, horizontal and retinal ganglion cells (RGCs)]. The axonal projections from the RGCs form a bundle of nerve fibers i.e. the optic nerve and exit the eye through the optic disc commonly referred to as the blind spot. A partial decussation of the optic fibers, particularly the nasal retinal fibers from each retina occurs at the optic chiasm (Kupfer et al., 1967). This results in both of the brain hemispheres receiving information from both of the eyes, but in a specific pattern, i.e. visual hemifields are represented on the contralateral hemispheres i.e. the right hemisphere receives

information only from the left visual field and the left hemisphere from the right visual field respectively. The fibers exiting the optic chiasm form the right and left optic tracts which primarily project to the corresponding six layered LGN which projects via the optic radiation to the visual cortical areas in the occipital lobe (the area of research in this thesis) leading to the perception of visual information.

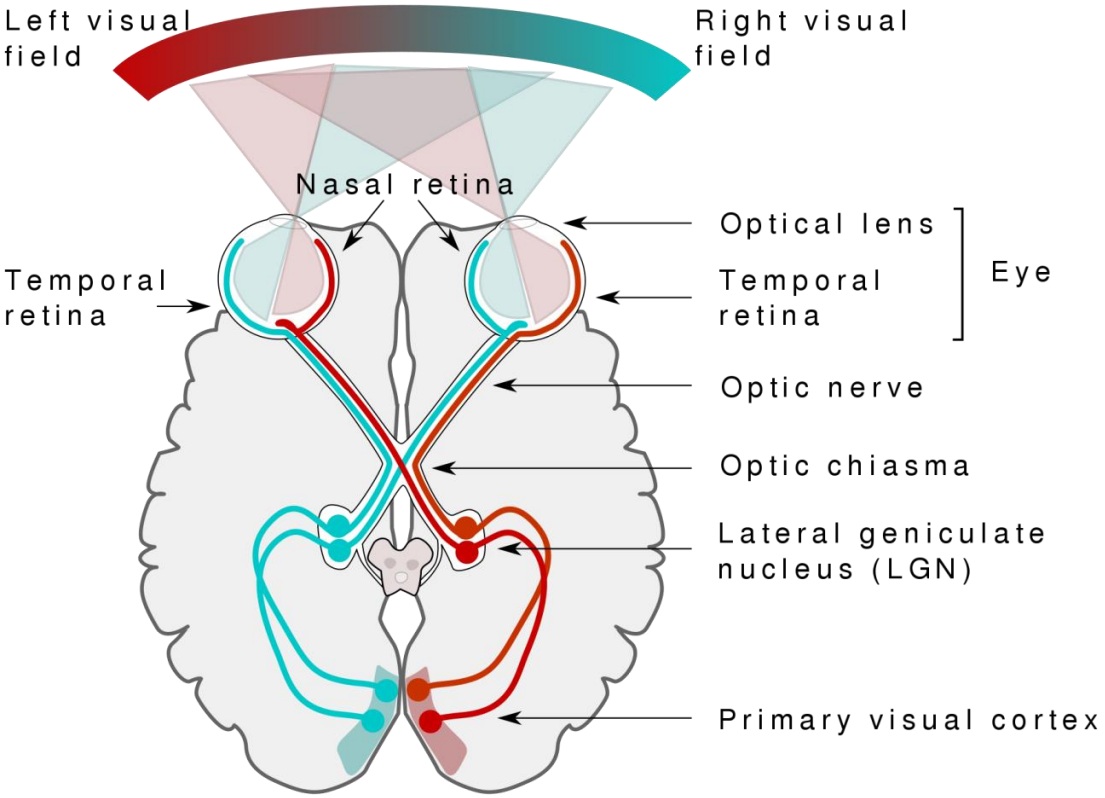

Figure 1. The human visual pathway. Information flow from the retina to the primary visual cortex is represented in the figure. Image from the outer world, in the form of light reaches the retina and gets translated in the electrical signal. The signal further propagates through the optic fibers along the optic nerve and partially decussates at the optic chiasm depending on the fibers origin (i.e. nasal or temporal) and terminates in the LGN. The optic radiation traverse from the LGN and the retinal representation reaches the visual cortex. The architecture of the visual system is developed in such a way that each hemisphere of the visual cortex receives information from both the eye but only from its contralateral visual field. Source: Miquel Perello Nieto, licensed under CC BYSA 4.0, via Wikimedia Commons (https://commons.wikimedia.org/wiki/File:Human_visual_pathway.svg

2.3 Visual cortex organization and cortical representation of the visual field

The majority of output from the LGN terminates in the primary visual cortex (also known as a V1) located alongside the calcarine sulcus extending to the occipital pole. The primary visual cortex plays a vital role in distributing visual information for further levels/stages of visual processing. In addition to the representation of contralateral hemifield in the visual cortex, the topographic information from the retinal image is also preserved in V1 input. This property is known as retinotopic organization i.e. neighboring locations in the visual field are represented in the neighboring locations in the visual cortex (Engel et al., 1997). Because of this arrangement, the neurons with receptive fields in the central and peripheral visual fields are located in the posterior and anterior portions of the calcarine, respectively. The representation is however non-linear with a large area of V1 devoted for foveal input processing and central vision, a phenomenon, termed as cortical magnification (Duncan and Boynton, 2003; Rovamo and Virsu, 1979). Further, the lower quadrant of a hemifield is represented in the dorsal bank of the calcarine and the upper quadrant in the ventral bank (Dougherty et al., 2003) (Figure 2A).

Following the initial processing of visual information in V1, the processed signal is transmitted to the extrastriate visual area V2 and subsequently from V2 to V3. Anatomically, V2 appears to encapsulate over V1 and V3 over V2. The representations of these areas also follow retinotopic organization, however there is a discontinuity in the dorsal and lower visual field along the horizontal meridian resulting in two quarter hemifield representation in the dorsal and ventral regions for both V2 and V3 (Wandell et al., 2007). Although the primary and extrastriate visual areas are the regions of interest in this thesis, several other higher-order visual areas (more than 20) respecting the topographic organization principle have been identified via fMRI investigations (Wandell et al., 2007) (Figure 2B). In general, the transformation from a visual abstract to perceivable information begins with processing of low level stimulus features by the early visual areas followed by processing of complex and specialized features by higher level visual areas (Grill-Spector et al., 2001; Malach et al., 1995). The presence of multiple retinotopically organized visual areas, each with neuronal population processing different aspects of an image determines the functional specialization of an area, for e.g. area MT with motion-selective neurons (Kourtzi and Kanwisher, 2000).

Alongside the feed-forward bottom-up hierarchical transfer of information, the areas of the visual cortex also receives reciprocal top-down information via feed-back projections (Lamme et al., 1998). Similar to the other cortical areas, the visual cortex is also layered and consists of six layers across which the information on the directionality of visual information is segregated (Callaway, 2004). For instance, a feed-forward input usually arrives in layer 4 whereas a feed-back input terminates in the superficial layers (1 & 2). The interplay of the feed-forward and feed-back

interactions between the visual areas mediate processes like perceptual organization and attention by modulating the dynamics of cortical responses to sensory input and is critical in shaping the normal organization of the visual cortex (Muckli et al., 2015).

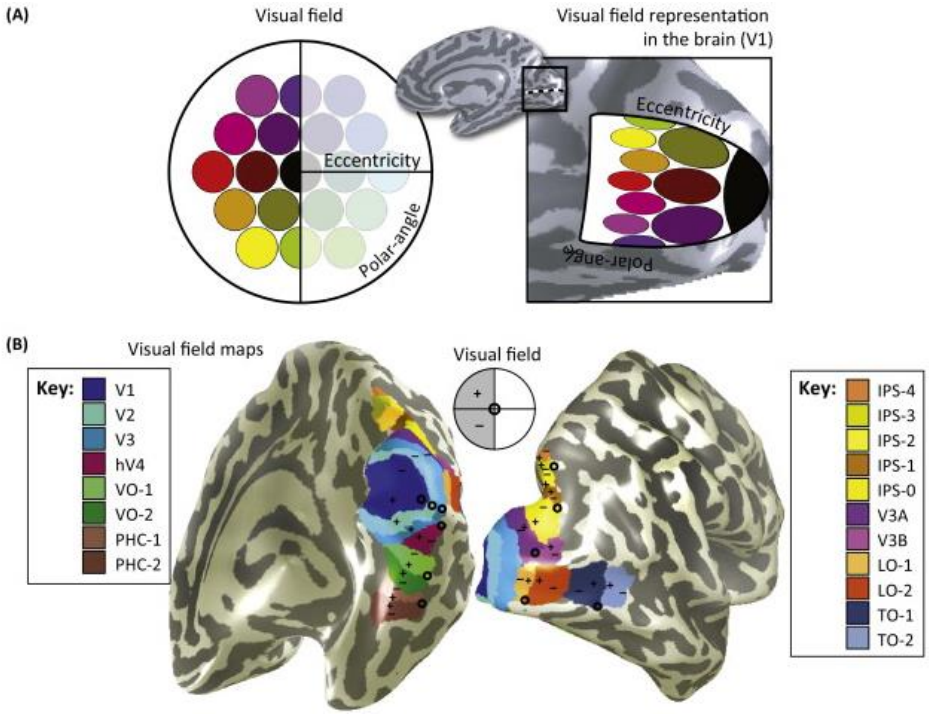

Figure 2. Mapping of visual field in the visual cortex and its organization. (A) Illustration of the retinotopic organization, cortical magnification and inversion of the retinal image in the primary visual cortex V1; (B) schematic of the different retinotopically organized visual areas in the medial (left) and lateral (right) view. "+", "-" and "o" indicates upper, lower and foveal VF locations respectively. Reprinted with permission from (Hoffmann and Dumoulin, 2015); Congenital visual pathway abnormalities: a window onto cortical stability and plasticity; Elsevier copyright: 2015.

2.4 Cortical reorganization following visual field loss

In the context of advancing therapeutic approaches and rehabilitation strategies for vision disorders (Beauchamp et al., 2020; Jutley et al., 2017; Roska and Sahel, 2018), it is critical to understand the interplay of cortical stability and plasticity following deprivation of visual input. Although some degree of developmental plasticity exists in congenital eye diseases with early life onsets (Baseler et al., 2002), in acquired or inherited vision disorders with late onset, there exists contradictory evidences in

ascertaining plasticity. This is attributed to the use of differential definitions of cortical reorganization by different research groups in the interpretation of their findings (Baker et al., 2005; Dilks et al., 2009; Masuda et al., 2010, 2008; Morland, 2015). Specifically, a stricter definition of reorganization is based on the existing knowledge about normal cortical organization, and considering if the results observed in patients with visual field defects are explainable by the principles of normal organization. In contrast, a liberal definition takes differences between healthy individuals and patients as the sole criterion for reorganization. fMRI has not only opened up the possibility to map the cortical representation of visual field, but also to assess the visual cortex organization in patients with vision loss. Two approaches are predominantly used in the existing literature for investigations on the scope of reorganization and their findings are taken as evidence for plasticity: (1) changes in the receptive field properties of neuronal population (pRF), for instance, change in the pRF position and size (Ferreira et al., 2017; Zhou et al., 2017), and (2) presence of unexpected aberrant cortical responses in the regions of visual cortex deprived of visual input, commonly referred as the lesion projection zones (LPZ) (Baker et al., 2008, 2005; Dilks et al., 2009). Studies following the stricter definition of reorganization have explained these above-mentioned evidences by the normal cortical response behavior and more importantly even in healthy individuals, questioning the nature and limits of bottom-up cortical reorganization in adulthood following vision loss (Haak et al., 2012; Masuda et al., 2010, 2008). These contrarian interpretations of human visual cortex plasticity were investigated in central vision disorders e.g. macular degeneration (Morland, 2015). However, there is very limited discussion in terms of peripheral vision disorders as in glaucoma and retinitis pigmentosa (Ferreira et al., 2017; Masuda et al., 2010; Zhou et al., 2017). As such, bridging this gap is the core theme of this thesis work.

2.5 Peripheral vision disorders – retina and beyond

2.5.1 Glaucoma

Progressive degeneration of retinal ganglion cells (RGCs) causes irreversible loss of vision in glaucoma (Jonas et al., 2017) and is a leading cause of blindness worldwide (Quigley and Broman, 2006). The progression of the vision loss advances from the peripheral to the central visual field, but can be also monocular or even affect only individual quadrants or hemifields. The routine diagnostic workup for glaucoma detection involves assessment of (1) structural changes in optic disc/cup and thinning of retinal nerve fiber layer (RNFL), (2) visual field loss, and (3) intraocular pressure. Elevated IOP is the major and the only modifiable risk factor, towards which most of the conventional therapeutic approaches for the management of glaucoma are directed (Jonas et al., 2017). There are however several cases of glaucoma patients with normal IOP or continuing progression even after IOP control indicating involvement of other factors along the visual pathway, such as the visual cortex.

Importantly, deprivation of visual input to the visual cortex induced by retinal damage results in both: (1) structural changes, for e.g. decreased gray matter volume (Boucard et al., 2009; Wang et al., 2016) (2) functional changes, for e.g. reduced fMRI BOLD responses consistent with the loss of vision and damage of optic disk (Duncan et al., 2007a, 2007b) of the visual cortex. Retinotopic fMRI also provided evidence for cortical reorganization in the context of altered topographic representation, for e.g. enlarged para-foveal representations of the visual cortex (Zhou et al., 2017). It is however to be noted that these reports are based on the liberal definition of reorganization and need further validation with the stricter criterion for plasticity, which has been addressed in this thesis. Figure 3 shows for a representative glaucoma participant visual field loss from perimetry and the corresponding restricted representation in the visual cortex.

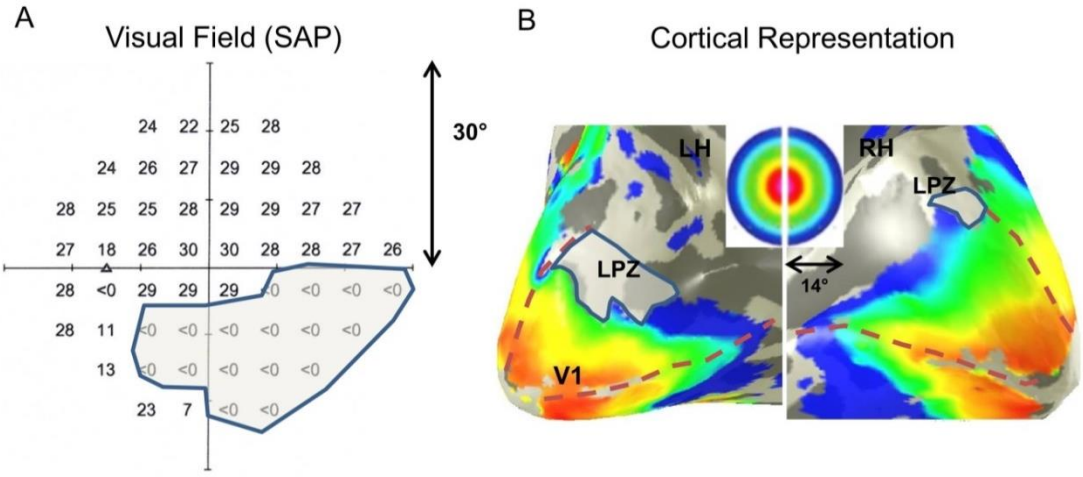

Figure 3. Cortical representation of LPZ. (A) Humphrey standard automated perimetry (SAP) predicted visual field of a glaucoma participant with retinal lesions in the lower VF-defects (marked by a transparent patch with a blue border and denoted by sensitivity < 0 dB). (B) Population receptive field (pRF) mapping derived visual field eccentricities of the same participant projected on their subjective inflated right and left visual cortex. Dashed red line indicates the primary visual cortex (V1). The pseudo-color progression from orange to blue represents the eccentricities from 0° to 14°. Corresponding lesion projection zones (LPZ) of the retinal lesion are marked by the blue boundaries.

2.5.2 Retinitis Pigmentosa (RP)

RP is an inherited eye disorder with progressive degeneration of photoreceptors, progressing from rod to cone damage(Hamel, 2006). Loss of visual field begins with

patchy losses in the periphery progressing to ring shaped scotomas and tunnel vision in advanced stages, eventually leading to blindness. The clinical diagnostic signs for the detection of RP involve the presence of night blindness, peripheral visual defects, pigment deposits in fundus images and electroretinogram (ERG) investigations (Hamel, 2006). The age of onset ranges from infancy to adulthood making the disease a prime candidate model for research addressing cortical reorganization. Structural integrity of visual pathways and the visual cortex appears to be intact, indicating a preserved thalamo-cortical and cortico-cortical connections (Cunningham et al., 2015; Ferreira et al., 2017; Schoth et al., 2006). However, remapping of V1 (based on the liberal definition) has been reported with altered retinotopic representation in the form of shifting of central retinal inputs to peripheral locations (Ferreira et al., 2017) with stronger remapping for advanced visual field loss.

2.6 Translation of cortex-driven information into clinical evaluation

In the context of age-associated eye diseases such as glaucoma, by the time there is noticeable VF defects as measured with SAP, there might be a loss of several optic nerve axons (Jonas et al., 2017). Interestingly, it has also been suggested that, in addition to RNFL thinning and optic nerve cupping, changes in the visual cortex activity might precede signs of visual field impairment (Murphy et al., 2016). Given the plausibility of visual cortices' relation with the disease and its progression, incorporating fMRI findings into the clinical workup might play a vital role in identifying early glaucoma mechanisms and subsequently in the early detection of the disease. Furthermore, this is also a critical need with an increase in average life expectancy and consequently more patients reaching the stage of advanced VF-defects in their life-time with glaucoma being an age-progressive disorder.

The advent of advanced therapeutic approaches e.g. retinal gene therapy (Aguirre, 2017; Ashtari et al., 2015) requires information not only at the level of the retina but also at the level of the visual cortex. From the perspective of therapy planning, insights into the scope of neuroplasticity in the visual cortex are critical as some of these approaches are developed on the premises of a limited plasticity of the adult visual cortex. Insights into the modulations in the functional activity of the brain once these approaches are performed are also fundamental in the evaluation of the therapy success. In consideration of all these needs, fMRI becomes an indispensable tool which needs to be appropriately translated to clinical routine for these promising advancements to be of utmost benefit in disease management and treatment.

Chapter 3

Methods

Over the past 20 years, advancements in the field of non-invasive measurements of cortical responses and computational neuroimaging approaches have provided the vision science community with tools to study visual dysfunction not only at the level of eye and retina, but also the visual cortex (Smirnakis, 2016; Wandell and Winawer, 2015). Those advancements, together with standard ophthalmological tests, enabled complementary investigations of development and progression of diseases affecting vision. In this thesis, I have addressed the limits of neuroplasticity in the adult visual cortex with help of state-of-the-art non-invasive modalities and analytical techniques. In particular, I predominantly used (1) functional MRI (fMRI) to measure functional responses in the visual cortex, (2) population receptive field (pRF) mapping-based modeling approaches to map the cortical representation of VFs and quantify RF of visual cortex neurons, and (3) standard automated perimetry (SAP) for clinical evaluation of VF-defects. In this chapter, I briefly discuss the theoretical and methodological background of these approaches.

3.1 Visual field testing

Assessment of visual field is one of the initial ophthalmological tests performed in the clinical routine for diagnosis and follow-up of eye diseases. Standard automated perimetry (SAP) is primarily used for this purpose and regarded as the gold standard. The most commonly used automated perimeters, which were also employed in studies described in this thesis, are the Humphrey Field Analyzer (HFA) and the Octopus. Different extents of the VF can be probed, for e.g. the central 30° or 24° or 10°. For our purpose, we measured the visual sensitivity of the central 30 degrees of the VF which was divided into grids of size 6x6 degrees. During SAP measurement, a light stimulus appears at each grid location in a systematic manner to estimate the retinal contrast sensitivity at each location (test points) in comparison to normative data, and measured in decibels (dB). These threshold dB values indicate the lowest possible luminance of the stimulus at which it still can be seen. The higher the value the higher the sensitivity. Consequently, a value of 0 dB represents a test location where the stimulus cannot be seen even for the brightest stimulus conditions and hence is likely to reflect a scotoma. Figure 3A shows the SAP predicted VF-defects (threshold plot) of a representative glaucoma patient. In the studies presented in this

thesis, SAP was predominantly used for two purposes, for (1) characterization of the VF-defect in the study patients and (2) quantitative comparisons with the fMRI-based VFs (chapter 7).

3.2 Functional magnetic resonance imaging (fMRI)

Functional MRI provides an indirect measure of neuronal activity in the brain non-invasively based on the property of neurovascular coupling, i.e. relationship of neuronal activity and local cerebral blood flow (Logothetis and Wandell, 2004). Briefly, in order to function the neurons require oxygen that is bound to the hemoglobin (oxyhemoglobin) in the blood. In the event of an increased neuronal activity, the need for oxygen raises which is answered by a surge in local blood supply. This results in a change in the blood oxygen concentration i.e. increase in oxy-hemoglobin and decrease in deoxy-hemoglobin (hemoglobin without bound oxygen). The core idea of fMRI measurements is to use this difference in oxygen concentration as an endogenous contrast, and an indirect indicator of neuronal activity. The theoretical basis for generating MRI signal from this mechanism is due to the difference in susceptibility to magnetic distortions of the oxy-hemoglobin (diamagnetic) and deoxy-hemoglobin (paramagnetic and high susceptibility). Consequently, the decreased concentration of deoxy-hemoglobin in the regions of high neuronal activity results in increased MRI signal intensity. Because of the dependence on blood oxygen level, cortical imaging with fMRI is commonly referred to as the BOLD (Blood Oxygen Level Dependent) imaging (Ogawa et al., 1990b, 1990a).

Gradient Echo Planar Imaging (EPI) sequence is predominantly used for acquiring fMRI images (Glover, 2011; Mansfield, 1977). During fMRI, the MRI signal intensity is measured for each voxel at different time points, as defined by the repetition time (TR). This results in voxel-wise time course of BOLD images which are subjected to further analysis as required. Notably, BOLD images have good spatial resolution, typically in the order of $2\text{-}3^3$ mm^3 voxels (3 T MRI scanners), which is sufficient for many neuroscientific studies, however, at the same time suffer from limited temporal resolution. Furtherly, quality of fMRI images is negatively affected by their susceptibility to artifacts caused by for e.g. head motion and physiological responses. Advanced developments in preprocessing and analysis methods have counteracted the limitations of fMRI and established it to be an indispensable tool for non-invasive neuroimaging.

3.3 Population receptive field (pRF) Mapping

In vision science, application of computational neural models has pushed the limits of fMRI from being a tool for localization of regions responding to a stimulus to characterization of RF properties of neurons (Wandell and Winawer, 2015). Specifically, each neuron has its own RF which is the location in the VF that

stimulates the neuron. In contrast to single cell animal studies, fMRI based neural models measure the pooled characteristics of a neuronal population within a voxel, and hence appropriately termed as population receptive field (pRF) models (Dumoulin and Wandell, 2008). Given the topographical organization of the visual cortex, pRF models revolve around the premises of building quantitative models to estimate voxel-wise RF estimates. Figure 4 shows the schematic of a conventional pRF model comprising of three broad components, (1) stimulus representation, (2) RF representation and (3) fMRI response prediction. The representation of the stimulus entails the properties of the visual stimulus that was used in the fMRI to elicit cortical responses. Theoretically, any stimulus with a well-defined spatial and temporal characteristic can be used for this purpose. In our studies, we used the conventional drifting checkerboard bar stimulus (Dumoulin and Wandell, 2008) which sampled across the entire VF systematically. The stimulus information at each time point is provided to the model as a binary mask representing the stimulus location. The shape of the pRF is modeled as 2D isotropic circular Gaussian with three stimulus-referred parameters (positon in the VF (x, y) and the spatial spread (σ), in visual degrees). The predicted fMRI time series is computed by a point-wise multiplication of the stimulus mask with the pRF model and convolved with the hemodynamic response function (HRF) to account for the hemodynamic response delay. For each cortical voxel, the pRF model parameters are adjusted to reduce the difference between the predicted and the measured fMRI time series and the best fitting combination of parameters (x, y and σ) is estimated. The optimal model parameters are used to derive eccentricity ($\sqrt{x^2 + y^2}$), polar angle ($\text{atan}(\frac{y}{x})$) and pRF size (σ) for each voxel, which are subsequently used in the generation of visual field maps.

Importantly, fMRI in combination with neuronal models provides a quantitative framework capable of investigation of the dynamics of the structure and function of visual cortex in a comparative approach (for e.g. between participant cohorts or across conditions) with interpretable units of measurements. The ability of this fundamental requisite to unravel the reality of neuroplasticity in the adult visual cortex explains the wide-spread adoption of pRF modeling approach across the spectrum of vision disorders (Wandell and Winawer, 2015).

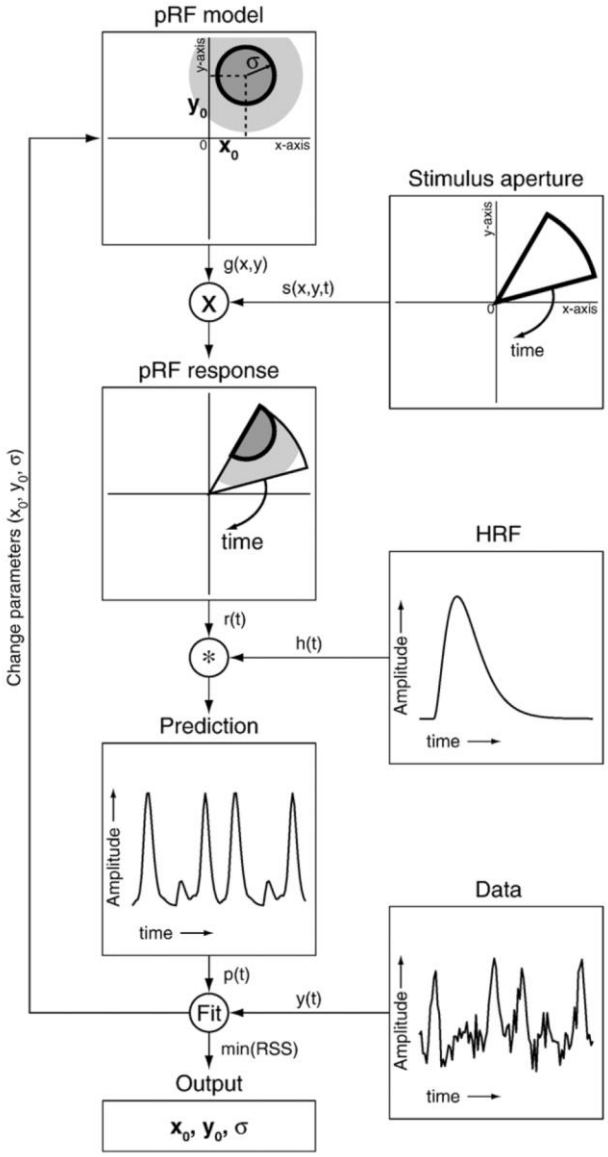

Figure 4. Schematic of a population receptive field (pRF) model illustrating the pipeline of the pRF model; Briefly, for each VF location, the pRF model takes in to account the spatial and temporal information of a stimulus [s(x,y,t)] and shape of the model receptive field [g(x,y)] defined by three stimulus-referred parameters [position: x_0 and y_0; spatial spread (σ)] to predict a pRF response [r(t)]. This is convolved with a canonical hemodynamic response (HRF) function [h(t)] to compute the predicted fMRI time series [p(t)]. The model parameters (x_0, y_0 and σ) are adjusted to minimize the sum of squared residuals (RSS) between the predicted and the observed time series [y(t)] for each and the best fitting parameters are chosen as the optimal pRF-estimates for each voxel. Reprinted with permission from (Dumoulin and Wandell, 2008); Population receptive field estimates in human visual cortex; Elsevier copyright: 2008.

Chapter 4

Research questions and steps taken to address them

The primary aim of the thesis was to establish the scope and degree of plasticity available to the adult human visual cortex in the event of peripheral visual field (VF) restrictions. For this purpose, we studied, using fMRI, two peripheral ophthalmic disorders, glaucoma and retinitis pigmentosa (RP) as well as visually healthy individuals with simulated patient-like visual field restrictions. Given the therapeutic relevance of the findings from the above studies, we further investigated the utility and translation of fMRI into the clinical routine. Specifically, the following questions as outlined below were addressed in the subsequent chapters.

4.1 Do pRF properties associated with VF restrictions indicate plasticity?

In chapter 5, we investigated the plausibility of observing altered pRF properties as reported previously in patients with peripheral VF defects (Ferreira et al., 2017; Zhou et al., 2017), in healthy individuals with simulated peripheral scotoma. The artificial VF loss was introduced indirectly by reducing the extent of the stimulated visual field with a peripheral gray mask. fMRI-based pRF mapping was performed on eight young controls (age: 21-28) for three different stimulus size conditions (stimulus radius: 14° (reference), 7° and 4° (scotoma conditions)). Through answers to the following sub-questions, I assessed the gravity of evidence asserted by the changes in pRF estimates for long term reorganization and its limits,

- Are there changes in the pRF properties of the stimulated visual cortex when an artificial scotoma is imposed?
- In the presence of potential changes:
  - Does the size of VF restriction impact the degree and extent of the observed variations?
  - What are the plausible underlying methodological/ modeling or physiological mechanisms?

  - How do these changes propagate across the visual hierarchy (V1, V2 and V3)?

4.2 Do aberrant LPZ responses in peripheral vision disorders indicate plasticity?

In substantiation to existing reports of aberrant LPZ responses in macular degeneration (MD) and retinitis pigmentosa (RP) (Baker et al., 2005; Masuda et al., 2010, 2008), in chapter 6, we investigated the dynamics of functional activity in glaucomatous LPZs and its interpretation as indication for plasticity. fMRI responses were acquired in four glaucoma patients with very advanced VF deficits with a robust ON-OFF visual stimulation (drifting contrast pattern in different directions). Three different conditions were tested: (1) no explicit task, (2) task related to the stimulus, and (3) non-stimulus dependent task. In addition to glaucoma, data from patients with RP (n=3) and age-matched healthy individuals (n=7) with simulated peripheral VF defects were included as reference cohorts. We investigated the afore-said phenomenon in the context of normal cortical response behavior with the following questions.

- Do our findings in the reference RP group corroborate with earlier reports?
- Is the LPZ in glaucoma patients responsive to visual stimulation? If yes:
  - Are these responses exclusively task and task-type dependent?
  - Is the dynamics similar across the visual hierarchy?
  - Can the response patterns be explained as a function of VF loss and structural integrity of the visual cortex?
- What happens in the simulated LPZs of the controls? If differential response patterns exist to those of the patients, what are the plausible mechanisms behind this?

4.3 Are fMRI-based VF assessments fMRI comparable to conventional methods?

Standard automated perimetry (SAP) is the conventional gold standard clinical tool used for diagnosing VF defects in ocular diseases. In chapter 7, we explored the utility of fMRI as a method for objective assessment of VF in patients with glaucoma (n=4), RP (n=2) and healthy controls (n=6) with simulated scotomas. fMRI based VFs were reconstructed employing two approaches based on (1) the pRF estimates of position and size (mapping-based) from fMRI-based pRF mapping, and (2) the cortical responses to a block design simple full field visual stimulation and existing retinotopic atlases (atlas-based). In a quantitative approach, the reconstructed VFs

were compared with subjective SAP-derived VFs. The feasibility of the approach was established through the following questions.

- Are mapping based VFs congruent to SAP-derived VFs?
- Is there a differential performance of the mapping-based and atlas-based approaches?
- Does the presence of a stimulus-related task influence the accuracy of the reconstructed VFs (atlas-based approach)?
- Does the ability of fMRI to reconstruct VFs depend on the extent of VF defects?

4.4 Steps undertaken to achieve research goals

To address the afore-mentioned research questions and achieve the goals of the thesis, I did the following steps:

- Recruitment of participants (patients/controls) and integration of ophthalmological data.
- Acquisition and analysis of fMRI and anatomical MRI data.
- Design and modification of visual stimuli for fMRI-paradigms.
- Adaptation of analysis toolboxes and validation of advanced modeling approaches.
- Establishment of algorithms and scripts to,
    - run computationally demanding models and analysis pipelines over high performance computing cluster,
    - automatize data processing and analysis workflow,
    - translate and transform results from one software convention to another, and from one modality to another.
- Quantitative and statistical data analysis and interpretation of findings and manuscript-writings.

Chapter 5

VF restrictions and dynamics of pRF properties

This chapter contains the permitted reprint of the study **"Foveal pRF properties in the visual cortex depend on the extent of stimulated visual field"** published in NeuroImage:

Prabhakaran, G.T., Carvalho, J., Invernizzi, A., Kanowski, M., Renken, R.J., Cornelissen, F.W., Hoffmann, M.B., 2020. Foveal pRF properties in the visual cortex depend on the extent of stimulated visual field. NeuroImage 222, 117250.

https://doi.org/10.1016/j.neuroimage.2020.117250

NeuroImage 222 (2020) 117250

Contents lists available at ScienceDirect

NeuroImage

journal homepage: www.elsevier.com/locate/neuroimage

Foveal pRF properties in the visual cortex depend on the extent of stimulated visual field

Gokulraj T. Prabhakaran [a], Joana Carvalho [b], Azzurra Invernizzi [b], Martin Kanowski [c], Remco J. Renken [b,d], Frans W. Cornelissen [b], Michael B. Hoffmann [a,e,*]

[a] Department of Ophthalmology, Otto-von-Guericke University, Magdeburg, Germany
[b] Laboratory of Experimental Ophthalmology, University Medical Center Groningen, University of Groningen, Groningen, the Netherlands
[c] Department of Neurology, Otto-von-Guericke University, Magdeburg, Germany
[d] Cognitive Neuroscience Center, University Medical Center Groningen, University of Groningen, the Netherlands
[e] Center for Behavioural Brain Sciences, Magdeburg, Germany

ARTICLE INFO

Keywords:
Visual cortex
Human
fMRI
Visual field defect
Fovea
Retinotopy

ABSTRACT

Previous studies demonstrated that alterations in functional MRI derived receptive field (pRF) properties in cortical projection zones of retinal lesions can erroneously be mistaken for cortical large-scale reorganization in response to visual system pathologies. We tested, whether such confounds are also evident in the normal cortical projection zone of the fovea for simulated peripheral visual field defects. We applied fMRI-based visual field mapping of the central visual field at 3 T in eight controls to compare the pRF properties of the central visual field of a reference condition (stimulus radius: 14°) and two conditions with simulated peripheral visual field defect, i.e., with a peripheral gray mask, stimulating only the central 7° or 4° radius. We quantified, for the cortical representation of the actually stimulated visual field, the changes in the position and size of the pRFs associated with reduced peripheral stimulation using conventional and advanced pRF modeling. We found foveal pRF-positions (≤3°) to be significantly shifted towards the periphery ($p<0.05$, corrected). These pRF-shifts were largest for the 4° condition [visual area (mean eccentricity shift): V1 (0.9°), V2 (0.9°), V3 (1.0°)], but also evident for the 7° condition [V1 (0.5°), V2 (0.5°), V3 (0.9°)]. Further, an overall enlargement of pRF-sizes was observed. These findings indicate the dependence of foveal pRF parameters on the spatial extent of the stimulated visual field and are likely associated with methodological biases and/or physiological mechanisms. Consequently, our results imply that, previously reported similar findings in patients with actual peripheral scotomas need to be interpreted with caution and indicate the need for adequate control conditions in investigations of visual cortex reorganization.

1. Introduction

Receptive field (RF) characteristics of neurons driven by visual input and their dynamics have for long been of fundamental interest in order to understand the mechanisms underlying visual processing. In contrast to invasive single-neuron electrophysiological recordings, functional MRI (fMRI) based RF measures reflect the aggregate characteristics of a population of neurons in a single voxel, termed population receptive field (pRF), where a pRF refers to the region in the visual field (VF) that elicits a response in the voxel. Over the last decade, a model based fMRI approach termed population receptive field mapping (Dumoulin and Wandell, 2008), has been widely used in investigating visual cortex functioning and contributed to our understanding of pRF characteristics of the visual cortex in healthy vision (Harvey and Dumoulin, 2011; Lee et al., 2013; Wandell and Winawer, 2015; Zeidman et al., 2018; Zuiderbaan et al., 2012). Furthermore, pRF modeling allowed us to quantitatively assess potential alterations of pRF characteristics in the visual cortex in the face of retinal lesions (Barton and Brewer, 2015; Baseler et al., 2011), developmental disorders (Ahmadi et al., 2019; Carvalho et al., 2019; Hoffmann et al., 2012; Hoffmann and Dumoulin, 2015) and trauma (Haak et al., 2014; Halbertsma et al., 2019; Papanikolaou et al., 2014). While alterations could be interpreted as evidence for potential cortical remapping and as an explanation for changes in fMRI responses following visual field defects (Baker et al., 2008; Dilks et al., 2009; Ferreira et al., 2017; Zhou et al., 2017), there is growing evidence for more conservative views on the nature and extent of adult visual cortex plasticity (Masuda et al., 2010, 2008; Wandell and Smirnakis, 2009).

* Correspondence to: Universitäts-Augenklinik, Otto-von-Guericke Universität, Leipziger Str. 44, 39120 Magdeburg, Germany.
E-mail address: michael.hoffmann@med.ovgu.de (M.B. Hoffmann).

https://doi.org/10.1016/j.neuroimage.2020.117250
Received 28 January 2020; Received in revised form 29 July 2020; Accepted 3 August 2020
Available online 14 August 2020

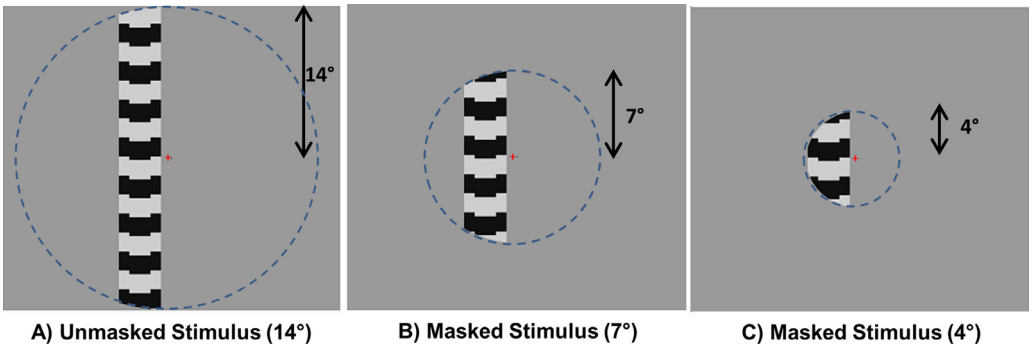

Fig. 1. Illustration of the three stimulus size configurations; unmasked (**A**) and the masked stimulus (**B** and **C**) configurations. The size of the unmasked stimuli was 14° (radius) and was restricted for the masked stimuli by simulating mean luminance masks in the peripheral VF (> 7° and > 4°) of the 14° stimulus space, stimulating only the central 7° and 4° respectively. Blue dashed boundaries indicate the spatial extent of the stimulated visual field (depicted here only for illustration purpose and were not visible during stimulus presentation) during the different conditions, whereas the spatial and temporal properties of the stimuli did not change. Participants fixated a small cross placed at the center of the stimuli and reported a change in the fixation color using a button press.

E.g., larger pRFs in the lesion projection zones (LPZ) in the primary visual cortex in patients with macular degeneration were also evident in controls with simulated lesions (Barton and Brewer, 2015; Baseler et al., 2011; Haak et al., 2012), thus questioning the concept of large-scale long-term reorganization in the visual cortex. While this bias has been well investigated in the lesion projection zone for deprived foveal stimulation (Haak et al., 2012; Morland, 2015), studies on the pRF dynamics in the normal projection zone associated of the fovea during deprived peripheral stimulation are currently emerging. In fact, recent investigations of patients with peripheral visual field defects, due to retinitis pigmentosa (RP) (Ferreira et al., 2017) or glaucoma (Zhou et al., 2017), report a displacement of pRFs in the normal projection zone, i.e., foveal pRFs to parafoveal or eccentric position. These shifts were taken as evidence for cortical remapping, in comparison to healthy controls with intact VF representations. While the authors of these studies acknowledge the limitations of a lack of appropriate control comparisons, it is unresolved whether the observed effects also occur for simulated peripheral visual field defects. This differentiation, however, is instrumental to dissociate long-term pathology-induced plasticity from short-term adaptation effects associated with the extent of visual stimulation.

In the present study, we intended to bridge this gap by reporting pRF measurements in healthy participants for three different stimulus sizes; a normal retinal representation of the visual space (14°) and two restricted representations comprising only the central 7° and 4°, respectively. The size of the stimulus was reduced by applying two differently sized mean luminance masks in the peripheral visual field (> 7° and > 4°) of the 14° stimulus space. We investigated the effect of reduced peripheral stimulation on the pRF estimates of the central visual field representation in primary (V1) and extra-striate (V2 and V3) visual cortex. Our study revealed a pRF displacement towards the stimulus border and an enlargement of foveal pRFs (< 3°) for the restricted stimulus condition (7° and 4°), in comparison to the 14° pRF estimates. As possible explanations of these effects, we discuss the contribution of both physiological mechanisms and potential methodological and modeling causes.

2. Methods

2.1. Participants

Eight individuals (age: 21–28; 4 males and 4 females) with normal vision (best-corrected decimal visual acuity ≥ 1.0 (Bach, 1996)) took part in the study. All participants gave their informed written consent. The study was approved by the ethics committee of the University of Magdeburg and the procedure adhered to the tenets of the Declaration of Helsinki.

2.2. MR stimulus

The visual stimulus, programmed in MATLAB (Mathworks, Natick, Massachusetts, USA) using Psychtoolbox-3 (Brainard, 1997; Pelli, 1997), was projected (resolution: 1920 × 1080 pixels) to a screen at the rear end of the magnet bore. Participants viewed the stimulus monocular with their dominant eye at a distance of 35 cm through an angled mirror. The stimulus was a moving checkerboard pattern (mean luminance: 109 cd/m^2; contrast: 99%; check size: 1.57°) exposed through a bar aperture (3.45°) moving in eight different directions (2 horizontal, 2 vertical and 4 diagonal; Dumoulin and Wandell, 2008). The bar moved across a circular aperture subtending 14° radius in 16 steps with each step lasting 1 TR (step rate = 1.75°/TR; TR = 1.5 s), resulting in a total time of 24 s per bar direction. The temporal sequence of the stimulus presentation comprised a sweep in one of the horizontal or vertical direction (24 s) followed by a sweep in a diagonal direction (see Supplementary Fig. S1A bottom, for stimulus schematics). Only the first 12 s of the diagonal sweeps were presented and the later 12 s were replaced by a mean luminance gray. In addition to the 14° condition, we estimated in separate scans during the same session the pRFs for two other stimulus size conditions, i.e., 7° and 4° radius, by masking the peripheral section of the 14° stimulus (Fig. 1). Hence we refer to the 7° and 4° stimulus conditions as masked conditions and the 14° stimulus as the unmasked condition. The spatial and temporal properties of the stimulus remained same for all the three conditions but only the extent of stimulation varied. The duration of each of these conditions was 192 s. Each condition was repeated four times in an interleaved design. The participants were instructed to focus their attention on a small fixation cross placed at the center of the stimuli and report a change in the fixation color via button press.

2.3. MRI acquisition

All MRI measurements were obtained with a 3 Tesla Siemens Prisma scanner using only the lower part of a 64-channel head coil. This results in a 34-channel coil covering most of the brain while allowing an unrestricted view to the projection screen. fMRI scans were acquired using a T2*-weighted BOLD gradient-EPI sequence (TR | TE = 1500 | 30 ms & voxel size = 2.5^3 mm^3). The first 8 volumes from each scan were removed automatically by the scanner to allow for steady magnetization. Each scan comprised a total of 136 volumes. One anatomical T1-weighted scan (MPRAGE, 1 mm isotropic voxels, TR | TI | TE = 2500 | 1100 | 2.82 ms) was collected for each participant to allow for gray-white matter segmentation and surface based analyses.

2.4. Data preprocessing and analysis

T1-weighted anatomical scans were segmented for gray-white matter boundaries using Freesurfer (https://surfer.nmr.mgh.harvard.edu/) and manually corrected for possible segmentation errors using ITK gray software (https://github.com/vistalab/itkgray). The gray-white boundaries were reconstructed to generate a 3-dimensional rendering of the cortical surface (Wandell et al 2000). fMRI scans of each individual participant were corrected for within and between scan head motion artefacts using AFNI (https://afni.nimh.nih.gov/). For each participant, motion-corrected fMRI time series of the different stimulus size conditions (14°, 7°, and 4°) were averaged together into separate groups with MATLAB based Vistasoft tools (https://github.com/vistalab/vistasoft) and were aligned spatially to the anatomical scan using Kendrick Kay's alignment toolbox (https://github.com/kendrickkay/alignvolumedata).

2.5. pRF modeling

We estimated the pRF parameters independently for our three stimulus conditions using a custom implemented advanced pRF modeling method based on Bayesian inference and Markov Chain Monte Carlo (MCMC) sampling (Adaszewski et al., 2018; Carvalho et al., 2019; Zeidman et al., 2018). In a comparative approach, we also looked at the conventional pRF estimates (Dumoulin and Wandell, 2008) to inspect for any model specific variations in the estimates. Since the Bayesian pRF modeling builds on the conventional method, we start with the description of the latter's procedure.

2.5.1. Conventional pRF

For each voxel, the voxel's fMRI time-series was used to estimate the aggregate receptive field properties of the underlying neuronal population using a 2D-Gaussian pRF model (described by three stimulus-referred parameters; position preferred in the visual field (x and y in Cartesian coordinates) and the spatial spread (σ)). The model predicts fMRI response of a voxel from the time course of the stimulus convolved with a canonical hemodynamic response function (HRF; Friston et al., 1998). Approximately 100,000 plausible combinations of pRF parameters (x, y,σ) were generated to compute predictions of the observed BOLD time-series of each voxel. The optimal pRF parameters, best fitting the predicted and actual voxel time-series were estimated by minimizing the sum of squared errors (RSS) between the two. Position parameters were used to derive pRF eccentricity $\sqrt{(x^2 + y^2)}$ and polar angle $\tan^{-1}(\frac{y}{x})$ and pRF size was derived from the spatial spread of the fitted 2D Gaussian model.

2.5.2. Bayesian MCMC

As we followed the nomenclature and mathematical notations for the Bayesian modeling (Zeidman et al., 2018) and MCMC sampling (Adaszewski et al., 2018; Carvalho et al., 2019) used elsewhere, we present here a more generic description of the method. With the conventional pRF method, we have fixed model parameters and use the variation between the predicted and the observed data to infer the most probable estimates of a voxel without any information on the probability of the estimates. In contrast to this, the Bayesian approach computes the posterior probability (*posterior*) of the predicted pRF parameter combination. The posterior follows the Bayes' rule (Eq. (1)) translating as the probability of a pRF parameter combination (location: x, y and spread σ) given the observed BOLD time series ($BOLD_{TS}$), hemodynamic response function (HRF) and the stimulus representation ($\prod$).

$$P(x, y, \sigma | BOLD_{TS}, HRF, \Pi) = P(x, y, \sigma).P(BOLD_{TS}, HRF, \Pi | x, y, \sigma) \quad (1)$$

We computed the posterior as the product of probability of a parameter combination (prior) and the probability of the observed voxel response given a parameter combination (likelihood). The likelihood of a parameter combination was computed as the probability density function of the error between the predicted and the observed voxel time-series given a set of pRF parameters (as in conventional pRF). We restricted the plausible pRF position (x, y) parameter to the area of our unmasked stimulus (14° radius), whereas for the conventional pRF the field of view ranged between [−2*radius, 2*radius], i.e. [−28° to 28°], resulting in the pRFs to be placed beyond the stimulated visual field. To start with, we initialized the pRF position parameters with a non-flat prior which accounts for the cortical magnification factor, i.e. we assume a higher probability for the pRFs to be centered foveally than in a peripheral position. However, for the pRF size (σ) parameter, a flat prior with equal probability for all possible widths within the permissible range [0.5° to 14°] was assigned.

We used the Markov Chain Monte Carlo (MCMC) approximation to efficiently sample the visual field, i.e. areas of the visual field with higher variance explained were more densely sampled. Per voxel 17,500 samples were computed, which form the posterior distribution. We start with a set of initial pRF parameters (x, y, σ) and propose a new set of parameters based on the initial ones. The MCMC algorithm followed a coarse to fine approach for choosing the proposed parameters i.e. the step size was larger for the initial samples whereas it reduced with the iterations. We compute and compare the posteriors for the initial and the proposed parameters. If the proposed parameters adhere to the observed data better than the initial parameters, we accept the proposed parameters and assign the combination as the new initial parameters; else there is still a chance to accept the proposed parameters. For this a probability of random acceptance was defined, if the difference in likelihood between the proposed and initial parameters is bigger than the $N(0,1)$, the parameters are updated. As we repeated this procedure for 17500 iterations, the parameters start to converge around the true measures underlying the neuronal population of a voxel. Our priors for the parameter combinations were not based on empirical data, which might result in the initial posterior samples to deviate from the true measure and skew the posterior distribution. To mitigate this possible bias, we discarded the posteriors of the initial 10% (1750) samples for further analysis. The Bayesian approach, for each voxel provides us a quantitative inference of the underlying distribution of the pRF model parameters (uncertainty). We used the full width at half maximum (FWHM) of the posterior distribution of the parameters as our measure of uncertainty, thereby investigating any changes in the behavior of the posterior distribution of each voxel for the different stimulus size conditions.

2.6. ROI definition and statistical analysis

Polar angle maps from the unmasked 14° condition for each participant were projected onto their inflated cortical surface. We delineated the borders of the primary (V1) and extra-striate (V2 and V3) visual cortex by following the phase reversals in the polar angle data (Sereno et al., 1995). All the further region of interest (ROI) analyses and statistics were performed with custom written scripts and statistical toolbox functions in MATLAB. Only voxels with an explained variance above 15% for the unmasked stimulus condition (14°) were included for all the subsequent analysis presented here (applying no threshold did not influence the findings we report here).

3. Results

3.1. Cortical representation of the stimulus

Firstly, we examined the representation of the Bayesian derived pRF eccentricities (preferred position in the visual field VF) in the cortex for the different stimulus conditions. For the unmasked 14° stimulus, the maps from all the participants followed a retinotopic organization in the primary (V1) and extra striate visual cortex (V2 and V3) spanning the entire stimulus radius of 14°. Whereas with the masked 4° and 7° conditions, as expected, we observed a restricted representation in the

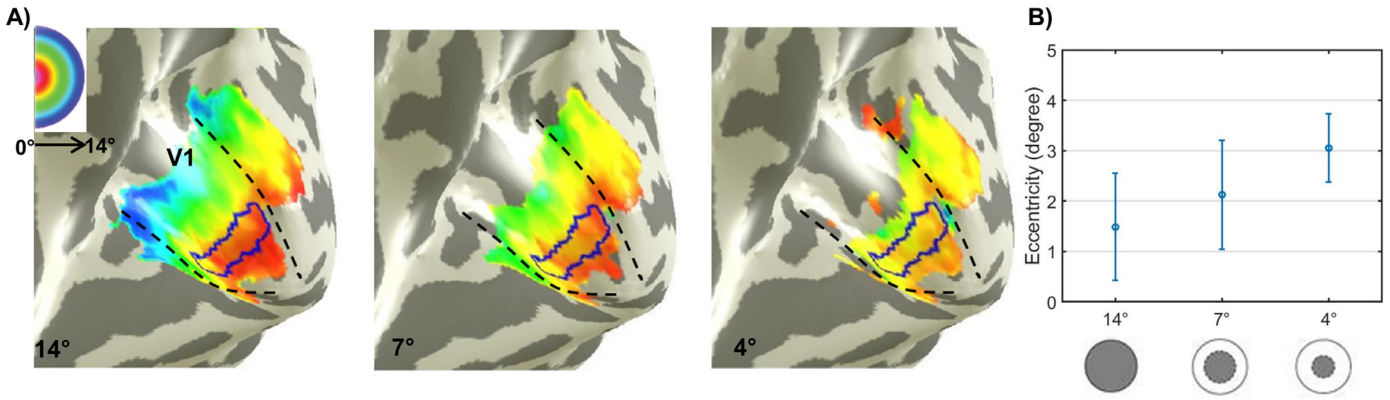

Fig. 2. Bayesian MCMC derived pRF eccentricities **(A)** of a representative participant mapped on inflated right visual cortex for the different stimulus sizes – 14° (unmasked), 7° and 4° (masked). Dashed black lines delineate the primary visual cortex V1. False-color representation from dark orange to dark blue in the unmasked stimulus illustrates the retinotopically organized eccentricities from 0° to 14°. Restricted cortical representation and changes in the pseudo-color progression are visualized in the masked condition maps, respective to their stimulus size. Panel **B** plots the mean and standard deviation of eccentricities within a small randomly defined paracentral ROI in V1 (indicated by the blue boundaries in the map) for the three stimulus sizes. Insets at the bottom of panel B shows a sample depiction of the stimulus configurations (grayed section represents the stimulated visual field). The plots clearly demonstrate the increase in eccentricity upon the restriction of the stimulus size.

cortex, in congruence with the stimulated VF, i.e. spanning a reduced eccentricity range. This is depicted for a representative participant in Fig. 2A. In addition to the restriction of the representation, we also observed a trend in the voxels' pRF centers to be more eccentric for the 4° and 7° conditions than for the 14° stimulus. This indicates an attraction of these pRFs towards the stimulus border. We illustrate this change in a sample participant by defining a small random paracentral ROI in V1 depicted by the blue borders in Fig. 2A. The ROI included only those voxels which were stimulated for all three stimulus conditions. Fig. 2B shows the plot of the mean preferred eccentricity of the voxels in the ROI for the three stimulus sizes. For the 14° stimulus condition, the mean preferred eccentricity in the VF was 1.5°, whereas for the 7° and 4° conditions, it increased to 2.1° and 3.1°, respectively. The plots clearly show that for the masked conditions pRF positions were more eccentric than for the 14° condition. This effect was larger for the smallest stimulus size, i.e. for the 4° condition. In conjunction to these reported changes in modeled estimates, we also found systematic changes in the voxel-wise time-series (early or delayed peaks in relation to the temporal and directional sequence of the bar) of the smaller stimulus conditions in comparison to the 14° time-series (see Supplementary Fig. S1 for the time-series plots of the same representative individual as in Fig. 2A).

3.2. Stimulus size dependent changes in pRF properties

3.2.1. Displacement of pRF preferred position

Next we assessed the spatial extent of these observed shifts in the pRF position with reduced stimulus size at the group level. For this purpose, we grouped the voxels into bins of 1° based on the 14° Bayesian derived pRF eccentricities, and determined for each visual area (V1, V2, and V3) and bin, the mean shift in eccentricity for the 4° or 7° conditions in comparison to the unmasked condition ($\text{Eccentricity}_{14^\circ} - \text{Eccentricity}_{4^\circ \text{ or } 7^\circ}$) (Fig. 3; mean eccentricity shift (n=8) plotted with standard error of the mean (SEM)). Due to our interest in understanding the pRF dynamics in the stimulated VF, we restricted our further analysis to the stimulated eccentricities of the restricted stimulus conditions (i.e. 4 bins for the 4° and 7 bins for the 7° conditions). For the 4° condition, we observed the mean eccentricity of the bins to be more eccentric than for the 14° condition and the difference was, as expected, negative for the stimulated eccentricities (Fig. 3A). This increase was particularly pronounced for the central eccentricities (< 3°) in contrast to those adjacent to the border of the stimulus, i.e. 3°–4°. The trend progresses similarly across V1, V2 and V3. Although we report a similar position displacement for the 7° condition (Fig. 3B) for the 1° and 2° bins, the shifts were smaller than for the 4° condition and did not propagate across the further eccentricities. A similar pattern of eccentricity shifts was also observed for the estimates from the conventional pRF approach (see Supplementary Fig. S2 A and B) and for a Bayesian model incorporating surround suppression (Difference of Gaussian, DoG; Zuiderbaan et al., 2012). Subsequently, we performed independent 2-way ANOVAs [Factor 1 *eccentricity* (bins), Factor 2 *model* (Bayesian pRF and conventional pRF)] on these reported shifts for each visual area (V1, V2 and V3) and stimulus combinations (14°–4° and 14°–7°; Table 1). The ANOVAs revealed a main effect of *eccentricity* in the reported shifts (Table 1A). Although, the shifts observed for the 7° stimulus condition were larger for the Bayesian approach than for conventional pRF-mapping, the ANOVAs did neither show a significant effect of *model* to the displacements ($p > 0.093$ (with an exception of marginal significance for 1/6 ANOVAs; p>0.04)) nor an interaction of *eccentricity* and *model* ($p > 0.75$) in any of the visual areas (see Table 1A for region and stimulus condition specific statistics). Post-hoc 2-sample t-tests with Holm–Bonferroni correction (Holm, 1979) showed the observed shifts with 4° stimulus size to be significant ($p < 0.05$) for the eccentricities < 3° for all visual areas, except for V3 with significant shifts only for eccentricities < 2°. For the 7° stimulus condition, pRFs were significantly displaced only for the central 2 degrees.

In addition to the eccentricity measures, we compared the distribution of Bayesian derived eccentricities for each bin for the 14° condition with either the 4° or 7° condition (Fig. 3C (14°–4°) and D (14°–7°)). As detailed in Methods, we used the FWHM of the distribution as our measure of uncertainty, as this reflects the range of RF positions represented by the neuronal population within each bin. As expected, the FWHM increased for the masked conditions over the unmasked condition especially in the central eccentricities. The wider distribution in the center with reduced stimulus size indicates that the neuronal populations in these voxels now represent a larger range of VF positions and the estimates obtained for these conditions are most likely to be biased. There is a high correspondence of larger uncertainty for the eccentricity bins with the biggest displacement.

As our measures show the aggregate estimates of all the voxels in a bin, the shifts observed could be the result of either (1) few voxels having very large displacements or (2) a substantial number of voxels with moderate displacements. To deduce the proportion of voxels contributing to the reported shifts, we defined an ROI with voxels representing the central eccentricities (<3°) in the 14° stimulus size condition and measured voxel-wise shifts in eccentricity for the 7° and 4° stimulus conditions. Fig. 4 shows the distribution of these shifts (14°–7° and 14°–4°) across all participants (n=8) for visual areas V1, V2 and V3. For the central

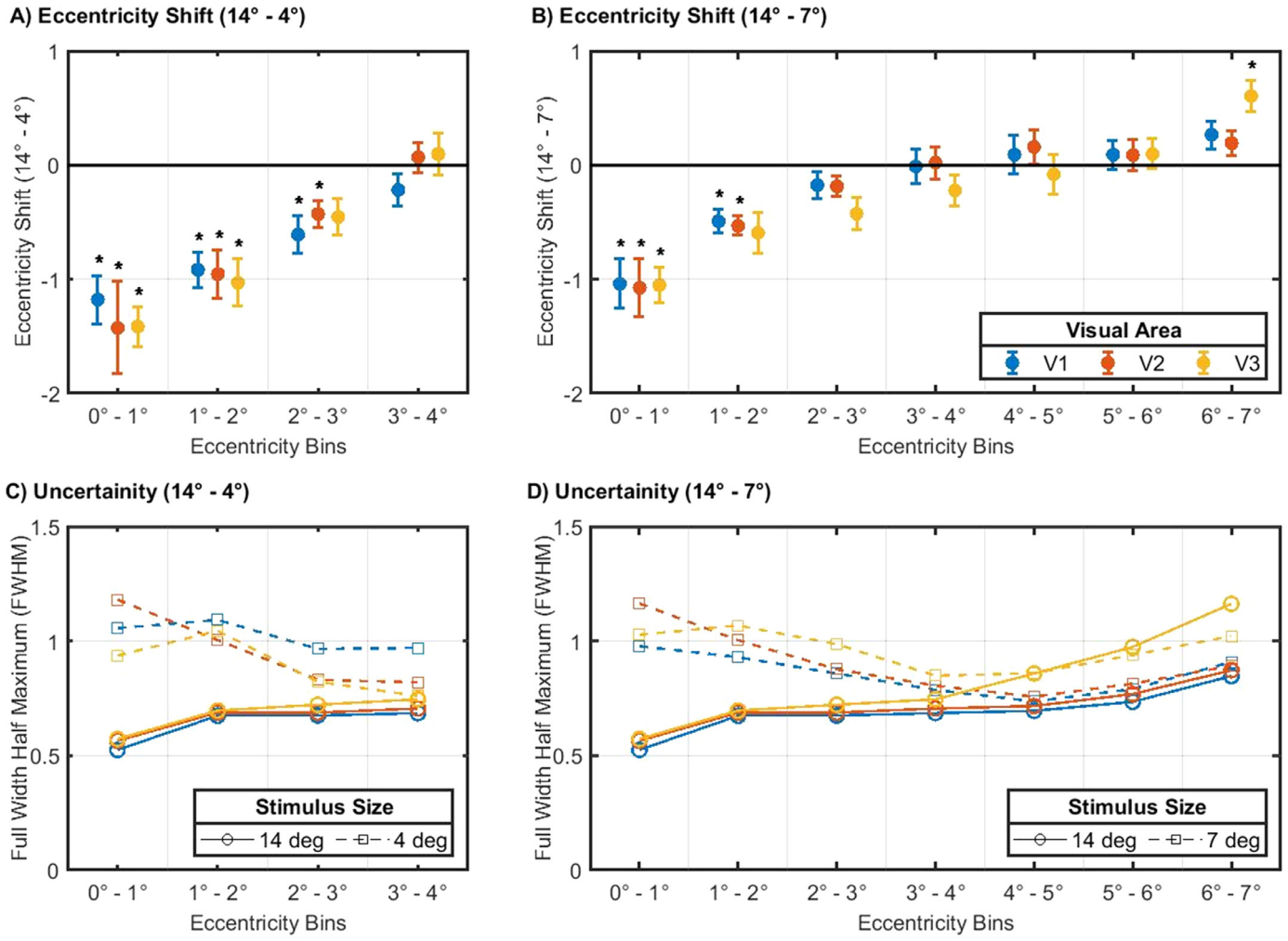

Fig. 3. Differences in Bayesian-MCMC-derived pRF-eccentricity measures, i.e. unmasked 14° condition minus the masked smaller stimulus conditions, i.e. **(A)** $\text{Eccentricity}_{(14^\circ - 4^\circ)}$ **(B)** $\text{Eccentricity}_{(14^\circ - 7^\circ)}$. For each participant, voxels were grouped into bins of 1° based on their 14° condition eccentricities (x-axis). All the analysis was restricted only to the stimulated eccentricities of the restricted stimulus conditions (i.e. 4 bins for the 4° and 7 bins for the 7° conditions) and included only those voxels which explained at least 15% of the time-series variance for the unmasked configuration. In the y-axis, for each eccentricity bin, the group level (n=8) mean shift in eccentricity and standard error are plotted for visual areas, V1 (blue), V2 (Red) and V3 (orange). Shift of the foveal eccentricities (<3°) in the negative direction implies a more eccentric preferred pRF position for the 4° or 7° stimulus compared to the 14° condition. The shifts were larger for the 4° stimulus than the 7° stimulus and similar across V1, V2 and V3. Visual areas, eccentricity bins and stimulus conditions with significant effects (p<0.05) after Holm–Bonferroni correction are indicated by "*". Bottom panels (**C and D**) shows the bin-wise comparison of FWHM of the eccentricity distribution (Bayesian measure of uncertainty) for the 14° (circle) vs. 4° or 7° (square) conditions. Note the increased uncertainty for the masked conditions, in particular for the bins with larger shifts.

representation, we observed a substantial proportion of voxels to shift peripherally for the masked conditions across the visual hierarchy (see indications of median shifts in Fig. 4) as well as an absence of secondary peaks. This indicates that the observed shifts are not driven by very few voxels with ectopic RFs.

3.2.2. *Enlargement of pRF-size*

After the analysis of the pRF position, we analyzed whether Bayesian derived pRF sizes are also affected by stimulus size. Fig 5A and B shows the bin-wise mean pRF-size shifts between the 14° and the 4° or 7° conditions. Similar to the preferred pRF position, we observed increased pRF-size estimates in the stimulated eccentricities for smallest stimulus size (4°), whereas it was negligible for the 7° condition. The shifts decreased as a function of eccentricity and we did not observe any systematic pattern across the visual areas. Conventional pRF-size estimates also exhibited comparable shifts with reduced stimulus size (supplementary Fig. S2 C and D). We performed a 2-way ANOVA [Factor 1 *eccentricity* (bins), Factor 2 *model* (Bayesian pRF and conventional pRF))] (Table 1B). The effect of *model* did not reach significance. A main effect of *eccentricity* was evident for the observed size-shifts for V2 and V3, but not for V1 (for both 14°–4° and 14°–7°). For the 4° condition, post-hoc t-tests corrected for multiple comparison showed significant shifts in V2 (eccentricity bins 1–3) and V3 (bin 1), and for the 7° condition, the shifts in V2 (bins 1–5) and V3 (bins 1–3) were significant with the Bayesian pRF approach. Similar to pRF eccentricity, the uncertainty i.e. FWHM of pRF-size distribution was larger for the masked condition (Fig. 5C and D).

3.3. *Modeling restricted stimulus representation*

All the above reported analysis for all the three different stimulus sizes was modeled assuming an unmasked (14°) stimulus condition. As a sanity check, we assessed the presence of the observed effects while explicitly incorporating the actual stimulus representation in the models for the smaller stimulus size conditions. We did not observe any reduction of the stimulus size effects for this approach. Actually, we report shifts that were not restricted to the central eccentricities and that exceeded those found for our original approach, i.e. no modeling the reduced stimulus representation (see Supplementary Fig. S3). Taken

Table 1
Two-way ANOVA of the reported eccentricity (A) and pRF size (B) shifts for each visual area (V1, V2 and V3) and stimulus combinations (14°–4° and 14°–7°). Factor 1: eccentricity (bins); Factor 2: model (Bayesian pRF or conventional pRF). Only the bins within stimulated eccentricities were used in the analysis.

Table 1 A: Eccentricity shift

Visual area	Stimulus combination	Eccentricity		Model		Interaction	
		F-Stat	p-Value	F-Stat	p-Value	F-Stat	p-Value
V1	14°–4°	11.5	<0.001	0.3	0.588	0.07	0.971
	14°–7°	15.9	<0.001	2.8	0.153	0.06	0.997
V2	14°–4°	13.9	<0.001	0.68	0.416	0.08	0.969
	14°–7°	15.9	<0.001	2.88	0.093	0.61	0.719
V3	14°–4°	18.8	<0.001	0.17	0.678	0.29	0.829
	14°–7°	16.6	<0.001	4.3	0.041	0.57	0.754

Table 1 B: pRF-size shift

Visual Area	Stimulus Condition	Eccentricity		Model		Interaction	
		F-Stat	*p*-Value	*F*-Stat	*p*-Value	*F*-Stat	*p*-Value
V1	14°–4°	1.02	0.387	1.3	0.257	0.02	0.994
	14°–7°	0.78	0.590	1.40	0.239	0.16	0.987
V2	14°–4°	9.41	<0.001	0.52	0.474	0.12	0.950
	14°–7°	9.9	<0.001	3.1	0.081	0.35	0.911
V3	14°–4°	5.77	0.0017	0.0007	0.979	0.12	0.946
	14°–7°	4.94	<0.001	0.55	0.460	0.11	0.995

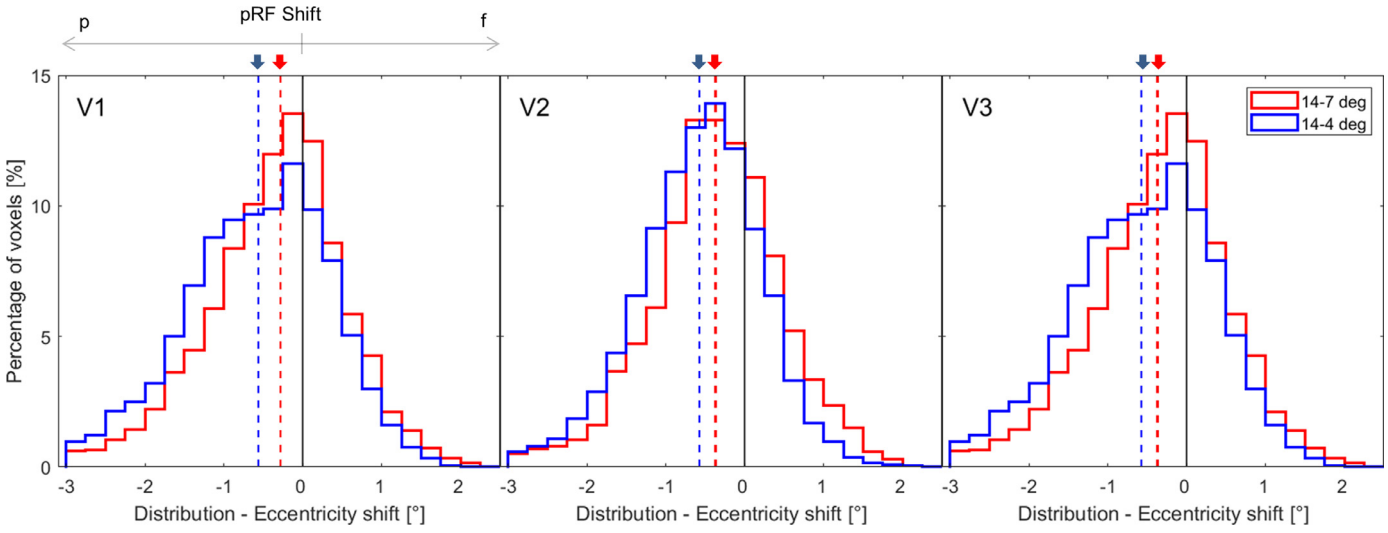

Fig. 4. Distribution of shifts (n=8) in Bayesian-MCMC-derived pRF-eccentricity of voxels representing the foveal eccentricities (< 3°) for V1 (left), V2 (middle) and V3 (right); 14°-7° (red) and 14°-4° (blue). Black solid line at 0° represents no shift in eccentricity between the unmasked and masked condition. Red and blue arrow-heads indicate the centrifugal median shifts (dashed lines) in eccentricity for the 7° and 4° stimulus condition, respectively. 'p' and 'f' above the gray arrow indicates shifts towards peripheral and foveal directions, respectively.

together, the observed effects were not reduced, when knowledge about the simulated visual field defects entered the model.

4. Discussion

The findings from our study revealed, 1) shifts (displacement and enlargement) of the foveal pRFs (< 3°) from their preferred positions and size as estimated with 14° stimulus, when reducing the stimulus size, 2) shifts for the 4° exceeding than those for the 7° stimulus condition, 3) a propagation of the shifts across V1, V2 and V3, but without any hierarchical trend, 4) no significant differences between the modeling approaches (Bayesian pRF or conventional pRF). The novelty of our findings is that they were observed in the normal projection zone of the fovea, as opposed to reports on changes of the pRF-properties in the lesion projection zone of the damaged fovea (Dumoulin and Knapen, 2018; Morland, 2015; Wandell and Smirnakis, 2009).

Similar changes in the receptive field estimates of the representation of the fovea in the early visual areas were reported by some studies on patients with peripheral visual field deficits, including RP (Ferreira et al., 2017) and glaucoma (Zhou et al., 2017). The authors proposed that the observed shifts are evidence of cortical reorganization in these patients, but at the same time in their interpretation acknowledged the possibility of control biases. Our results demonstrate that such alterations in the pRF estimates can also be observed in healthy individuals via mimicking scotomas of patients with peripheral retinal pathologies. This suggests that the previous findings in patients reflect normal cortical response behavior in a context of reduced peripheral stimulation. Consequently, our findings emphasize that care needs to be exerted before interpreting alterations in receptive field properties in patients with VF restrictions as definitive evidence for cortical reorganization. In particular, appropriate controls, e.g. with simulated visual field defects, are of great value investigating the scope of cortical plasticity.

A critical question prompted by the above findings concerns the nature and origin of the observed pRF estimate dependence on stimulus size. The aim of our study was to check the existence of such stimulus

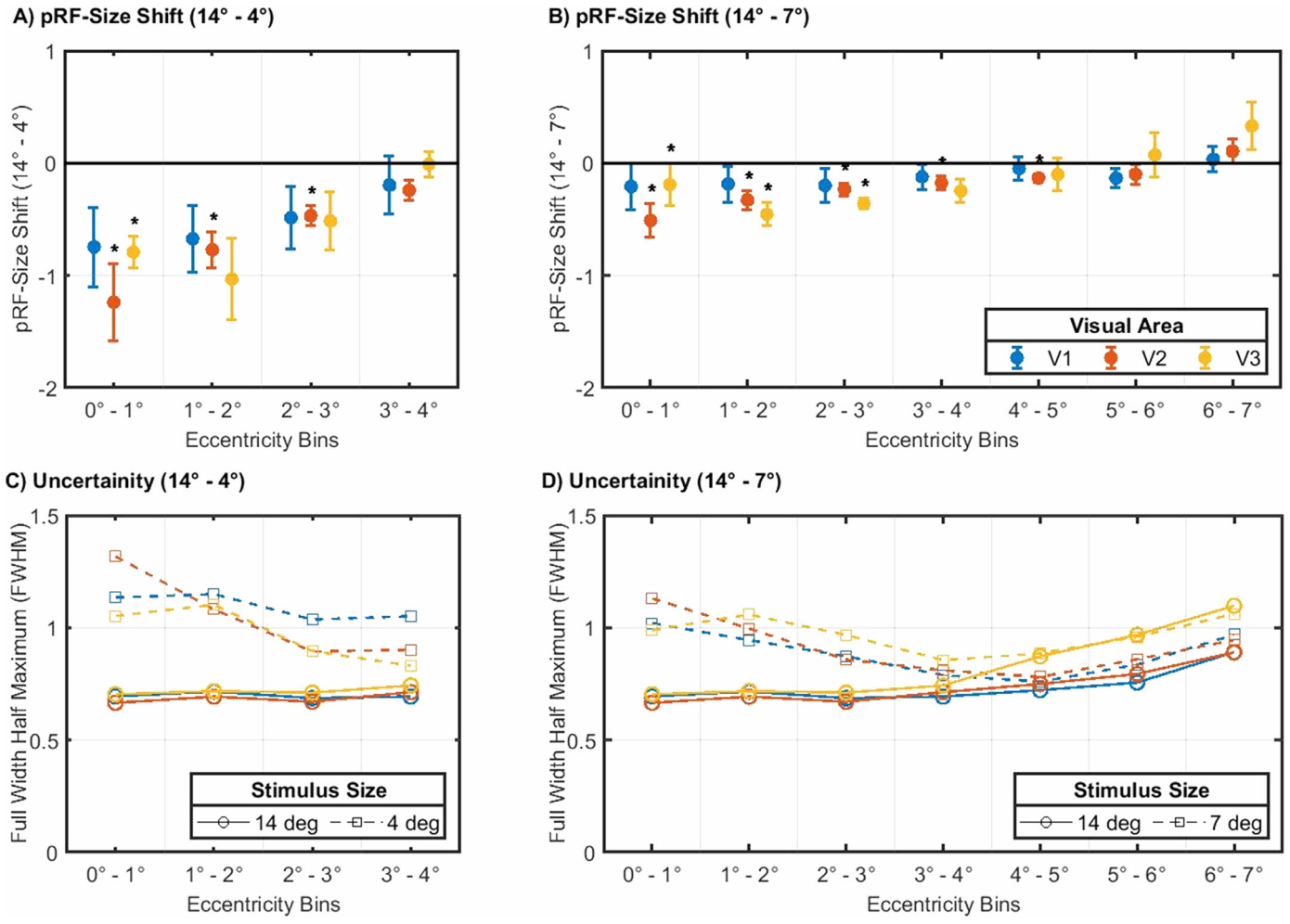

Fig. 5. Differences in Bayesian-MCMC-derived pRF-size upon reduced stimulation extent. Differences calculated as (A) pRF-size(14°–4°) (B) pRF-size(14°–7°) for V1 (blue), V2 (Red) and V3 (orange). Grouping of voxels into eccentricity bins was performed as for Fig 3. For the *y*-axis the group level (n=8) mean shifts in pRF-size and standard error of the mean (SEM) are plotted. A change in the negative direction implies larger pRF sizes for the 4° or 7° stimulus compared to the 14° stimulus. We report larger absolute shifts for the 4° stimulus, whereas the 7° shifts were very small. Visual areas, eccentricity bins and stimulus conditions with significant effects (p<0.05) after Holm–Bonferroni correction are indicated by "*". Bottom panels (C and D) show the bin-wise comparison of FWHM of the pRF-size distribution (Bayesian measure of uncertainty) for the 14° (circle) and 4° or 7° (square) conditions. Increased FWHM measures can be seen for the bins with larger pRF-size shifts, in particular for the 4° estimates.

size dependent biases in pRF mapping. The next step is to identify the underlying causes and mechanism in future studies. Below, we suggest and discuss plausible explanations of the observed effects, i.e., (1) potential methodological or modeling biases associated with pRF mapping and (2) physiological mechanisms, i.e. changes in neuronal receptive field properties.

4.1. Modeling and stimulus configuration

Previous studies have reported biased pRF estimates in the neighborhood of the boundaries of simulated foveal (Baseler et al., 2011; Binda et al., 2013; Haak et al., 2012) and quadrantopic scotomas (Papanikolaou et al., 2015) in healthy individuals. Binda et al. (2013) proposed that such biases could be mitigated by taking into account the scotoma in the pRF model and using a randomized multifocal stimulus. Importantly, for the predominantly used non-randomized size-invariant bar stimulus, modeling the scotoma did not have a substantial effect on the biased estimates. This is consistent with our findings for the explicit inclusion of the reduced stimulus representation in the estimation models. We report stimulus size dependent pRF shifts that are not restricted to foveal eccentricities and larger than those observed when assuming an unmasked stimulus condition for modeling (Supplementary Fig. S3). Another study comparing different stimulus configurations for pRF mapping (Alvarez et al., 2015) illustrated eccentricity scaling and use of polar rather than Cartesian stimuli, to have a significant effect on the goodness of fits and pRF size estimates. Similar to our study, they also reported a display size bias in the pRF size by changing the viewing distance (but not by masking the stimulus periphery). Larger pRFs were observed in participants who experienced a 16° display (n=2) compared to those who experienced a 9° display (n=6). Although these results were in contrast to our finding of a mean expansion of the pRFs (at the group level) for the smaller stimulus size, we noticed heterogeneous single subject results (especially in V1) for the conventional pRF approach. Three out of our eight participants had smaller pRFs for the masked vs. unmasked stimulus condition (see SEM in Supplementary Fig. S2 (C and D), in particular in V1). However, this heterogeneity was not observed for the Bayesian model (see SEM in Fig. 5 (A and B)), where all the participants showed pRF-size increase with reduced stimulus size, indicating the utility of the Bayesian approach in mitigating some methodological biases of conventional pRF modeling. Despite the possibility that biases associated with modeling and stimulus configurations could result in the shifts we report here, there are always tradeoffs in choosing the optimal stimulus design or modeling approach, e.g., the low power of multifocal stimulus (Binda et al., 2013; Ma et al., 2013), high predictive power but reduced accuracy of polar-

coordinate based wedge and ring stimuli (Alvarez et al., 2015) or limitations of ascertaining absolute scotomas in patients to be included in the model. As over-manipulation of the stimulus and modeling characteristics can also limit the replicability and reproducibility of studies, the effective approach to circumvent potential methodological biases would be to match the experimental conditions between the controls and patients as closely as possible.

4.2. Ectopic receptive fields

As fMRI based pRF estimates reflect only the aggregate RF properties of all the neurons in the voxel, the observed shifts are possible even if the response characteristics of only a subset of the neuronal population changes. Haak et al. (2012) observed an activation of very few foveal voxels in healthy individuals even when only the peripheral VF was stimulated and highlighted the existence of neurons with ectopic receptive fields (RF) in the regions of cortex representing the central VF. Even though our masked stimulus might silence this ectopic neuronal subpopulation, it is highly unlikely that this mechanism could drive the shifts we observe. First, only a minority of voxels is expected to have ectopic receptive fields in the central representation; however our results show that at least 50% of voxels contribute to the displacements in the foveal representation. Secondly, silencing of ectopic neurons would ideally shrink the distribution of the neuronal population within a voxel, consequently, the position scatter should be away from the stimulus border i.e. parafoveal to foveal. Therefore, a more global neuronal mechanism might be inducing the observed changes in the pRF characteristics. Below, we outline how these variations might originate from extra-classical RF modulations and from attentional modulation.

4.3. Surround Suppression and Attention modulation

Surround suppression. fMRI-BOLD response amplitudes have been demonstrated to decrease with the introduction of a iso-oriented stimulus in the surround (Kastner et al., 2001; Nurminen et al., 2009; Williams et al., 2003; Zenger-Landolt and Heeger, 2003). In our case, the presence or absence of peripheral stimulation might in a way behave as the surround modulating the collective neural responses and shift the balance between excitatory (facilitation) and inhibitory (suppression) neuronal responses induced by the center-surround RF configurations (extra classical). Our results suggest that, for the masked conditions, the absence of a high-contrast iso-oriented surround mitigates the effects of surround suppression, resulting in the pRFs to be driven by much more excitatory neuronal activity.

Attention modulation. Previous studies reported response modulations in the visual cortex with voluntary attention and its influence in receptive field estimates (Desimone and Duncan, 1995; Kastner and Ungerleider, 2000; Kay et al., 2015; Klein et al., 2014; Puckett and DeYoe, 2015). In our study, the participants fixated on a cross in the center of the stimulus and performed an attention demanding task by reporting color changes of the fixation dot during all the conditions. In addition to this voluntary attention, masking the stimulus might induce an involuntary shift of attention towards the border of the stimulus (exogenous) and a shift in the balance between these two attentional modes might result in the pRF variations, we report here. Single cell studies in Macaque (Womelsdorf et al., 2008, 2006) showed that when attention is shifted from one location to another within the receptive field of the respective neuron, the RF centers of these neurons shift to the attended location.

While these mechanisms, surround suppression and attentional field influence, are equally able to explain our data, the reported pRF variations might arise from an interaction of both mechanisms (Reynolds and Heeger, 2009) and other factors.

4.4. Limitations and future directions

At present we do not know which of the aforementioned mechanisms might be the most relevant to cause the observed variations in pRF measures, as our study was designed to identify the experimental effect, but not to pinpoint their exact origin. Consequently, further studies with different models, for e.g. incorporating surround suppression (Zuiderbaan et al., 2012), spatial nonlinearities (Kay et al., 2013), and no pre-defined pRF shape (Carvalho et al., 2019), are needed to deduce the nature of these shifts, which might provide hints on the robustness of retinotopic maps.

Our results raise the question, which of the results for the different stimulation conditions reflects the veridical cortical visual field mapping. In the context of our study, it is not possible to resolve this issue. For instance, even though we have the unmasked condition as the reference, it still has a mask outside 14° and might have differential estimates if compared to e.g. a 24° stimulus. If our reported effects were driven by methodological biases, the underlying mapping for the different conditions might be more stable and robust than observed. However, a physiological basis behind the effects would add evidence to a more flexible view of the retinotopic representation. It should also be considered that we were evaluating population responses: i.e. the specific contribution of different subpopulations to the pRF measures might depend on the stimulation conditions we applied. As a consequence, differences in these subpopulations' RF measures might lead to an apparent flexibility of the retinotopic representation. Such questions might be answered by comparative studies with other pRF modeling approaches and more importantly cross-modal, e.g. fMRI- and electrophysiology based, RF estimates. Forthcoming research should also investigate pRF data from patients and healthy controls with and without comparable experimental conditions (for e.g. artificial scotomas, visual acuity) to help us better understand and demonstrate the existence and impact of control biases in studies looking for potential cortical reorganization.

5. Conclusion

In summary, we demonstrated in healthy controls, the dependence of foveal pRF estimates on the spatial extent of the stimulation. We report enlargement and displacement of foveal pRFs towards the stimulus border when we reduced the size of the stimulus by masking and thereby restricting the peripheral stimulation. The shifts were more pronounced for the 4° than the 7° stimulus size and propagated across the primary (V1) and the extra striate (V2 and V3) visual cortex. Our results imply that, similar findings in patients with actual VF restrictions might also reflect normal cortical response behavior in a context of reduced peripheral stimulation. They therefore underscore that care must be taken to separate effects of stimulus properties, such as size, and of cortical reorganization in visual system pathologies. This emphasizes the importance of careful control measures in studies addressing neuronal plasticity.

Declaration of competing interest

None

CRediT authorship contribution statement

Gokulraj T. Prabhakaran: Conceptualization, Methodology, Formal analysis, Investigation, Data curation, Writing - review & editing. **Joana Carvalho:** Software, Writing - review & editing. **Azzurra Invernizzi:** Software, Writing - review & editing. **Martin Kanowski:** Methodology, Writing - review & editing. **Remco J. Renken:** Software, Writing - review & editing. **Frans W. Cornelissen:** Software, Writing - review & editing, Funding acquisition. **Michael B. Hoffmann:** Conceptualization, Methodology, Supervision, Writing - review & editing, Funding acquisition.

Data and code availability

The data and the code will be made available via a repository.

Acknowledgments

This project was supported by European Union's Horizon 2020 research and innovation programme under the Marie Sklodowska-Curie grant agreements No. 675033 (EGRET plus), No. 641805 (NextGenVis) and No. 661883 (EGRET cofund) to MBH & FWC. JC and AI were additionally supported by a grant from the Graduate School of Medical Sciences (GSMS) of the University Medical Center Groningen (UMCG). The funding organization did not have any role in the study design, collection, analysis and interpretation of the data, or publication of this research. We also thank the two anonymous reviewers for their valuable comments and suggestions which have greatly helped us improve the manuscript.

Supplementary materials

Supplementary material associated with this article can be found, in the online version, at doi:10.1016/j.neuroimage.2020.117250.

References

Adaszewski, S., Slater, D., Melie-Garcia, L., Draganski, B., Bogorodzki, P., 2018. Simultaneous estimation of population receptive field and hemodynamic parameters from single point BOLD responses using Metropolis-Hastings sampling. Neuroimage 172, 175–193. doi:10.1016/j.neuroimage.2018.01.047.

Ahmadi, K., Fracasso, A., van Dijk, J.A., Kruijt, C., van Genderen, M., Dumoulin, S.O., Hoffmann, M.B., 2019. Altered organization of the visual cortex in FHONDA syndrome. Neuroimage 190, 224–231. doi:10.1016/j.neuroimage.2018.02.053.

Alvarez, I., de Haas, B., Clark, C.A., Rees, G., Schwarzkopf, D.S., 2015. Comparing different stimulus configurations for population receptive field mapping in human fMRI. Front. Hum. Neurosci. 9, 96. doi:10.3389/fnhum.2015.00096.

Bach, M., 1996. The Freiburg Visual Acuity test–automatic measurement of visual acuity. Optom. Vis. Sci. 73, 49–53.

Baker, C.I., Dilks, D.D., Peli, E., Kanwisher, N., 2008. Reorganization of visual processing in macular degeneration: replication and clues about the role of foveal loss. Vis. Res. 48, 1910–1919. doi:10.1016/j.visres.2008.05.020.

Barton, B., Brewer, A.A., 2015. fMRI of the rod scotoma elucidates cortical rod pathways and implications for lesion measurements. PNAS 112, 5201–5206. doi:10.1073/pnas.1423673112.

Baseler, H.A., Gouws, A., Haak, K.V., Racey, C., Crossland, M.D., Tufail, A., Rubin, G.S., Cornelissen, F.W., Morland, A.B., 2011. Large-scale remapping of visual cortex is absent in adult humans with macular degeneration. Nat. Neurosci. 14, 649–655. doi:10.1038/nn.2793.

Binda, P., Thomas, J.M., Boynton, G.M., Fine, I., 2013. Minimizing biases in estimating the reorganization of human visual areas with BOLD retinotopic mapping. J. Vis. 13, 13. doi:10.1167/13.7.13.

Brainard, D.H., 1997. The psychophysics toolbox. Spat. Vis. 10, 433–436.

Carvalho, J., Invernizzi, A., Ahmadi, K., Hoffmann, M.B., Renken, R.J., Cornelissen, F.W., 2019. Micro-probing enables fine-grained mapping of neuronal populations using fMRI. Neuroimage, 116423 doi:10.1016/j.neuroimage.2019.116423.

Desimone, R., Duncan, J., 1995. Neural mechanisms of selective visual attention. Annu. Rev. Neurosci. 18, 193–222. doi:10.1146/annurev.ne.18.030195.001205.

Dilks, D.D., Baker, C.I., Peli, E., Kanwisher, N., 2009. Reorganization of visual processing in macular degeneration is not specific to the "preferred retinal locus.". J. Neurosci. 29, 2768–2773. doi:10.1523/JNEUROSCI.5258-08.2009.

Dumoulin, S.O., Knapen, T., 2018. How visual cortical organization is altered by ophthalmologic and neurologic disorders. Annu. Rev. Vis. Sci. 4, 357–379. doi:10.1146/annurev-vision-091517-033948.

Dumoulin, S.O., Wandell, B.A., 2008. Population receptive field estimates in human visual cortex. Neuroimage 39, 647–660. doi:10.1016/j.neuroimage.2007.09.034.

Ferreira, S., Pereira, A.C., Quendera, B., Reis, A., Silva, E.D., Castelo-Branco, M., 2017. Primary visual cortical remapping in patients with inherited peripheral retinal degeneration. Neuroimage Clin. 13, 428–438. doi:10.1016/j.nicl.2016.12.013.

Friston, K.J., Fletcher, P., Josephs, O., Holmes, A., Rugg, M.D., Turner, R., 1998. Event-related fMRI: characterizing differential responses. Neuroimage 7, 30–40. doi:10.1006/nimg.1997.0306.

Haak, K.V., Cornelissen, F.W., Morland, A.B., 2012. Population receptive field dynamics in human visual cortex. PLoS One 7, e37686. doi:10.1371/journal.pone.0037686.

Haak, K.V., Langers, D.R.M., Renken, R., van Dijk, P., Borgstein, J., Cornelissen, F.W., 2014. Abnormal visual field maps in human cortex: a mini-review and a case report. Cortex 56, 14–25. doi:10.1016/j.cortex.2012.12.005.

Halbertsma, H.N., Haak, K.V., Cornelissen, F.W., 2019. Stimulus- and neural-referred visual receptive field properties following hemispherectomy: a case study revisited. Neural Plast. 2019. doi:10.1155/2019/6067871.

Harvey, B.M., Dumoulin, S.O., 2011. The relationship between cortical magnification factor and population receptive field size in human visual cortex: constancies in cortical architecture. J. Neurosci. 31, 13604–13612. doi:10.1523/JNEUROSCI.2572-11.2011.

Hoffmann, M.B., Dumoulin, S.O., 2015. Congenital visual pathway abnormalities: a window onto cortical stability and plasticity. Trends Neurosci. 38, 55–65. doi:10.1016/j.tins.2014.09.005.

Hoffmann, M.B., Kaule, F.R., Levin, N., Masuda, Y., Kumar, A., Gottlob, I., Horiguchi, H., Dougherty, R.F., Stadler, J., Wolynski, B., Speck, O., Kanowski, M., Liao, Y.J., Wandell, B.A., Dumoulin, S.O., 2012. Plasticity and stability of the visual system in human achiasma. Neuron 75, 393–401. doi:10.1016/j.neuron.2012.05.026.

Holm, 1979. A simple sequentially rejective multiple test procedure. Scand J Stat 6 (2) 65–70. doi:10.2307/4615733.

Kastner, S., De Weerd, P., Pinsk, M.A., Elizondo, M.I., Desimone, R., Ungerleider, L.G., 2001. Modulation of sensory suppression: implications for receptive field sizes in the human visual cortex. J. Neurophysiol. 86, 1398–1411. doi:10.1152/jn.2001.86.3.1398.

Kastner, S., Ungerleider, L.G., 2000. Mechanisms of visual attention in the human cortex. Annu. Rev. Neurosci. 23, 315–341. doi:10.1146/annurev.neuro.23.1.315.

Kay, K.N., Weiner, K.S., Grill-Spector, K., 2015. Attention reduces spatial uncertainty in human ventral temporal cortex. Curr. Biol. 25, 595–600. doi:10.1016/j.cub.2014.12.050.

Kay, K.N., Winawer, J., Mezer, A., Wandell, B.A., 2013. Compressive spatial summation in human visual cortex. J. Neurophysiol. 110, 481–494. doi:10.1152/jn.00105.2013.

Klein, B.P., Harvey, B.M., Dumoulin, S.O., 2014. Attraction of position preference by spatial attention throughout human visual cortex. Neuron 84, 227–237. doi:10.1016/j.neuron.2014.08.047.

Lee, S., Papanikolaou, A., Logothetis, N.K., Smirnakis, S.M., Keliris, G.A., 2013. A new method for estimating population receptive field topography in visual cortex. Neuroimage 81, 144–157. doi:10.1016/j.neuroimage.2013.05.026.

Ma, Y., Ward, B.D., Ropella, K.M., Deyoe, E.A., 2013. Comparison of randomized multifocal mapping and temporal phase mapping of visual cortex for clinical use. Neuroimage Clin. 3, 143–154. doi:10.1016/j.nicl.2013.08.004.

Masuda, Y., Dumoulin, S.O., Nakadomari, S., Wandell, B.A., 2008. V1 projection zone signals in human macular degeneration depend on task, not stimulus. Cereb. Cortex 18, 2483–2493. doi:10.1093/cercor/bhm256.

Masuda, Y., Horiguchi, H., Dumoulin, S.O., Furuta, A., Miyauchi, S., Nakadomari, S., Wandell, B.A., 2010. Task-dependent V1 responses in human retinitis pigmentosa. Investig. Ophthalmol. Vis. Sci. 51, 5356–5364. doi:10.1167/iovs.09-4775.

Morland, A.B., 2015. Organization of the central visual pathways following field defects arising from congenital, inherited, and acquired eye disease. Annu. Rev. Vis. Sci. 1, 329–350. doi:10.1146/annurev-vision-082114-035600.

Nurminen, L., Kilpeläinen, M., Laurinen, P., Vanni, S., 2009. Area summation in human visual system: psychophysics, fMRI, and modeling. J. Neurophysiol. 102, 2900–2909. doi:10.1152/jn.00201.2009.

Papanikolaou, A., Keliris, G.A., Lee, S., Logothetis, N.K., Smirnakis, S.M., 2015. Nonlinear population receptive field changes in human area V5/MT+ of healthy subjects with simulated visual field scotomas. Neuroimage 120, 176–190. doi:10.1016/j.neuroimage.2015.06.085.

Papanikolaou, A., Keliris, G.A., Papageorgiou, T.D., Shao, Y., Krapp, E., Papageorgiou, E., Stingl, K., Bruckmann, A., Schiefer, U., Logothetis, N.K., Smirnakis, S.M., 2014. Population receptive field analysis of the primary visual cortex complements perimetry in patients with homonymous visual field defects. Proc. Natl. Acad. Sci. USA 111, E1656–E1665. doi:10.1073/pnas.1317074111.

Pelli, D.G., 1997. The VideoToolbox software for visual psychophysics: transforming numbers into movies. Spat. Vis. 10, 437–442.

Puckett, A.M., DeYoe, E.A., 2015. The attentional field revealed by single-voxel modeling of fMRI time courses. J. Neurosci. 35, 5030–5042. doi:10.1523/JNEUROSCI.3754-14.2015.

Reynolds, J.H., Heeger, D.J., 2009. The normalization model of attention. Neuron 61, 168–185. doi:10.1016/j.neuron.2009.01.002.

Sereno, M.I., Dale, A.M., Reppas, J.B., Kwong, K.K., Belliveau, J.W., Brady, T.J., Rosen, B.R., Tootell, R.B., 1995. Borders of multiple visual areas in humans revealed by functional magnetic resonance imaging. Science 268, 889–893.

Wandell, B.A., Chial, S., Backus, B.T., 2000. Visualization and measurement of the cortical surface. J. Cogn. Neurosci. 12, 739–752. doi:10.1162/089892900562561.

Wandell, B.A., Smirnakis, S.M., 2009. Plasticity and stability of visual field maps in adult primary visual cortex. Nat. Rev. Neurosci. 10, 873–884. doi:10.1038/nrn2741.

Wandell, B.A., Winawer, J., 2015. Computational neuroimaging and population receptive fields. Trends Cogn. Sci. 19, 349–357. doi:10.1016/j.tics.2015.03.009.

Williams, A.L., Singh, K.D., Smith, A.T., 2003. Surround modulation measured with functional MRI in the human visual cortex. J. Neurophysiol. 89, 525–533. doi:10.1152/jn.00048.2002.

Womelsdorf, T., Anton-Erxleben, K., Pieper, F., Treue, S., 2006. Dynamic shifts of visual receptive fields in cortical area MT by spatial attention. Nat. Neurosci. 9, 1156–1160. doi:10.1038/nn1748.

Womelsdorf, T., Anton-Erxleben, K., Treue, S., 2008. Receptive field shift and shrinkage in macaque middle temporal area through attentional gain modulation. J. Neurosci. 28, 8934–8944. doi:10.1523/JNEUROSCI.4030-07.2008.

Zeidman, P., Silson, E.H., Schwarzkopf, D.S., Baker, C.I., Penny, W., 2018. Bayesian population receptive field modelling. Neuroimage 180, 173–187. doi:10.1016/j.neuroimage.2017.09.008.

Zenger-Landolt, B., Heeger, D.J., 2003. Response suppression in v1 agrees with psychophysics of surround masking. J. Neurosci. 23, 6884–6893.

Zhou, W., Muir, E.R., Nagi, K.S., Chalfin, S., Rodriguez, P., Duong, T.Q., 2017. Retinotopic fMRI reveals visual dysfunction and functional reorganization in the visual cortex of mild to moderate glaucoma patients. J. Glaucoma 26, 430–437. doi:10.1097/IJG.0000000000000641.

Zuiderbaan, W., Harvey, B.M., Dumoulin, S.O., 2012. Modeling center-surround configurations in population receptive fields using fMRI. J. Vis. 12, 10. doi:10.1167/12.3.10.

Chapter 6

Task-dependent LPZ activity in glaucoma

This chapter contains the permitted reprint of the study "**Functional dynamics of deafferented early visual cortex in glaucoma"** published in Frontiers in Neuroscience:

Prabhakaran, G.T., Al-Nosairy, K.O., Tempelmann, C., Wagner, M., Thieme, H., Hoffmann, M.B., 2021. Functional dynamics of de-afferented early visual cortex in glaucoma. Front. Neurosci. 15.

https://doi.org/10.3389/fnins.2021.653632

frontiers in Neuroscience

ORIGINAL RESEARCH
published: 26 July 2021
doi: 10.3389/fnins.2021.653632

Functional Dynamics of Deafferented Early Visual Cortex in Glaucoma

*Gokulraj T. Prabhakaran[1], Khaldoon O. Al-Nosairy[1], Claus Tempelmann[2], Markus Wagner[1], Hagen Thieme[1] and Michael B. Hoffmann[1,3]**

[1] Department of Ophthalmology, Otto-von-Guericke University, Magdeburg, Germany, [2] Department of Neurology, Otto-von-Guericke University, Magdeburg, Germany, [3] Center for Behavioral Brain Sciences, Otto-von-Guericke University, Magdeburg, Germany

In advanced retinitis pigmentosa with retinal lesions, the lesion projection zone (LPZ) in the early visual cortex can be driven during visual tasks, while it remains unresponsive during passive viewing. We tested whether this finding translates to advanced glaucoma, a major cause of acquired blindness. During visual stimulation, 3T fMRI scans were acquired for participants with advanced glaucoma (n = 4; age range: 51–72) and compared to two reference groups, i.e., advanced retinitis pigmentosa (n = 3; age range: 46–78) and age-matched healthy controls with simulated defects (n = 7). The participants viewed grating patterns drifting in 8 directions (12 s) alternating with uniform gray (12 s), either during passive viewing (PV), i.e., central fixation, or during a one-back task (OBT), i.e., reports of succeeding identical motion directions. As another reference, a fixation-dot task condition was included. Only in glaucoma and retinitis pigmentosa but not in controls, fMRI-responses in the lesion projection zone (LPZ) of V1 shifted from negative for PV to positive for OBT (p = 0.024 and p = 0.012, respectively). In glaucoma, these effects also reached significance in V3 (p = 0.006), while in V2 there was a non-significant trend (p = 0.069). The general absence of positive responses in the LPZ during PV underscores the lack of early visual cortex bottom-up plasticity for acquired visual field defects in humans. Trends in our exploratory analysis suggesting the task-dependent LPZ responses to be inversely related to visual field loss, indicate the benefit of patient stratification strategies in future studies with greater sample sizes. We conclude that top-down mechanisms associated with task-elicited demands rather than visual cortex remapping appear to shape LPZ responses not only in retinitis pigmentosa, but also in glaucoma. These insights are of critical importance for the development of schemes for treatment and rehabilitation in glaucoma and beyond.

Keywords: fMRI, glaucoma, lesion projection zone, plasticity, visual cortex, feedback

OPEN ACCESS

Edited by:
Jan Kremers, University Hospital Erlangen, Germany

Reviewed by:
Miguel Castelo-Branco, Coimbra Institute for Biomedical Imaging and Translational Research (CIBIT), Portugal
Elisa Castaldi, University of Florence, Italy

****Correspondence:***
Michael B. Hoffmann
michael.hoffmann@med.ovgu.de

Specialty section:
This article was submitted to Perception Science, a section of the journal Frontiers in Neuroscience

Received: *14 January 2021*
Accepted: *23 June 2021*
Published: *26 July 2021*

Citation:
Prabhakaran GT, Al-Nosairy KO, Tempelmann C, Wagner M, Thieme H and Hoffmann MB (2021) Functional Dynamics of Deafferented Early Visual Cortex in Glaucoma. Front. Neurosci. 15:653632. doi: 10.3389/fnins.2021.653632

INTRODUCTION

Glaucoma, a progressive degeneration of retinal ganglion cells (RGCs), results in an irreversible loss of vision, eventually leading to blindness (Jonas et al., 2017). Worldwide it is the second most prevalent cause of acquired blindness, next to cataract (Quigley and Broman, 2006). Most of the conventional therapeutic strategies, by medication or surgery, are directed toward the management

or control of the major risk factor in glaucoma, increased intraocular pressure (IOP). In fact, these interventions are known to reduce the progression rate of the disease (Jonas et al., 2017). However, the beneficial effects of recent advances in early detection and progression-delaying treatment of glaucoma are counteracted by increased life expectancy. As a consequence, a substantial proportion of glaucoma patients will become severely visually impaired and eventually bilaterally blind during their lifetime (Quigley and Broman, 2006; Kapetanakis et al., 2016). This motivates current research initiatives, not only to focus on better disease treatment tools, but also to further our understanding of the management of visual impairment in advanced glaucoma. In fact, the ultimate goal is to explore effective avenues for the restoration of visual input, which is motivated by ongoing research progress, ranging from cell-based therapies at the retinal level to interventions at the cortical level (reviewed in Jutley et al., 2017; Roska and Sahel, 2018). For this purpose, knowledge about the state and functionality of the deafferented visual cortex in glaucoma is instrumental. In fact, in addition to the retinal damage caused by glaucoma, the concomitant deprivation of visual input from the retina to the cortex has been shown to result in structural and functional changes at the cortical level, in particular in the primary (V1) and extra-striate (V2 and V3) visual cortex (Duncan et al., 2007; Dai et al., 2013; Frezzotti et al., 2014; Boucard et al., 2016; Wang et al., 2016; Zhou et al., 2017).

fMRI-based retinotopic mapping demonstrated the interplay of plasticity and stability in congenital visual pathway abnormalities and inherited retinal diseases (Hoffmann et al., 2012; Hoffmann and Dumoulin, 2015; Ferreira et al., 2017; Ahmadi et al., 2019, 2020). In contrast, reorganization of the primary visual cortex is much more limited in patients with acquired visual field defects as studied in detail for macular degeneration (Baker et al., 2008; Masuda et al., 2008; Dilks et al., 2009; Liu et al., 2010; Baseler et al., 2011; Plank et al., 2013). Although glaucoma is a prevalent disease, the scope of cortical plasticity in the deafferented portions of the early visual cortex in advanced glaucoma has only received little attention. Zhou et al. (2017) reported an enlarged para-foveal representation in the visual cortex of glaucoma patients, but recent investigations of simulated peripheral response dropouts in controls (Prabhakaran et al., 2020) suggest that such effects do not necessarily reflect veridical long-term cortical reorganization. This mirrors the views of previous reports analyzing the limited nature of visual cortex plasticity for foveal de-afferentation (Baseler et al., 2011; Haak et al., 2012; Barton and Brewer, 2015). Accordingly, reductions of amplitude and extent of fMRI BOLD responses in the visual cortex of glaucoma patients (Duncan et al., 2007; Song et al., 2012; Borges et al., 2015; Murphy et al., 2016) and thinning of gray matter in the de-afferented visual cortex (Yu et al., 2014, 2015; Boucard et al., 2016) suggest the absence of large-scale reorganization post visual field loss.

Importantly, in the context of vision restoration and rehabilitation strategies, investigations of the responsivity of lesion projection zones (LPZ) in the visual cortex, i.e., cortical representations of the retinal lesions, are key to understanding the reality of adult visual cortex reorganization capabilities. Consequently, investigations are needed to assess cortical responses in the LPZ and their relation to visual stimulation and visual tasks. In fact, for patients with non-glaucomatous retinal disorders, cortical activations in the LPZ were reported. Remarkably they appear to depend on the presence of a visual task to be performed on the presented stimuli. In a series of case observations Masuda et al., demonstrated these task-dependent V1-responses in patients with macular degeneration (MD) and retinitis pigmentosa (RP), i.e., for central (Masuda et al., 2008, 2020) and peripheral visual field defects (Masuda et al., 2010), respectively. These task-dependent effects have now been confirmed in a larger cohort of RP patients (n = 13) using spatially specific stimulation (Ferreira et al., 2019). These signals are taken as evidence for an absence of bottom-up plasticity and are discussed as side effects of task-related feed-back and attentional demands from higher visual areas. Although highly relevant for the management of advanced glaucoma, such insights into the responsiveness of the LPZ in the early visual cortex are currently completely missing for the entity of glaucoma patients.

In the present study, we assessed the task-dependence of cortical responses in the LPZ in a set of glaucoma patients (GL), carefully selected to have extensive glaucoma-related peripheral visual field defects, and compared the findings to those in two reference groups, i.e., advanced RP and controls with simulated peripheral visual field defects. In fact, LPZ response signatures and task-dependencies in RP and glaucoma matched and were analogous to those reported previously in MD, but absent in controls. Consequently, the lack of relevant bottom-up plasticity appears to be a general feature of the human visual system.

MATERIALS AND METHODS

Participants

Demographics of the participants is given in **Table 1**. Participants with extensive visual field (VF) defects due to advanced open-angle glaucoma (GL; n = 4) or to retinitis pigmentosa (RP; n = 3; RP2 also had secondary glaucoma, see **Table 1**) and age-matched visually healthy controls (HC) with normal vision [best-corrected decimal visual acuity $\geq$ 1.0 (Bach, 1996); n = 7] took part in the study. Written informed consents and data usage agreements were signed by all participants. The study was conducted in adherence to the tenets of the Declaration of Helsinki and was approved by the ethics committee of the University of Magdeburg.

Visual Field Testing and Fixation Stability

Standard automated perimetry (SAP) was performed using 24–2 Swedish Interactive Threshold Algorithm protocol (SITA-Fast; Goldmann size III white-on-white stimuli; Humphrey Field Analyzer 3; Carl Zeiss Meditec AG; Jena, Germany). For three participants, VF to the central 30° was tested using another perimeter (OCTOPUS® Perimeter 101, Haag-Streit International, Switzerland; dG2; dynamic strategy; Goldmann size III). For the patient cohort (except 1; GL3), fixation stability was determined with a fundus-controlled microperimeter (MP-1 microperimeter, Nidek, Padua, Italy) during fixation of a central fixation target.

TABLE 1 | Participant demographics and clinical characteristics.

Participants	Age	Sex	Stimulated eye (fMRI)	Visual acuity	Visual field (MD—dB)	Fixation stability[1] (2°)	Onset age (yrs)	Duration (yrs)
GL1	68	Female	Left	1.0	−13.9	100%	59	9
GL2	70	Male	Left	0.4	−25.8	100%	65	5
GL3	51	Female	Right	0.8	−32.5	na	48	3
GL4	72	Male	Left	0.8	−30.7	100%	47	25
RP1	56	Female	Left	0.6	−23.5	97%	26	30
RP2[2]	78	Male	Left	0.05	−30.7	99%	59	19
RP3	46	Female	Right	0.05	−27.3	31%	11	34
HC1	64	Male	Left	1.6	1.0	na	na	na
HC2	79	Female	Left	1.3	0.0	na	na	na
HC3	56	Male	Left	1.3	0.0	na	na	na
HC4	73	Male	Left	1.0	−0.9	na	na	na
HC5	75	Male	Left	1.3	0.0	na	na	na
HC6	71	Female	Right	1.0	−1.4	na	na	na
HC7	63	Female	Left	1.0	na	na	na	na

GL, glaucoma; RP, retinitis pigmentosa; HC, control participants; MD, Visual field mean deviation as measured with standard automated perimetry (SAP); na, not available.
[1]Proportion of central fixations within a fixation window of 2° radius as determined with a fundus-controlled perimeter (see section "Materials and Methods.").
[2]RP participant with secondary glaucoma; visual field defects are predominantly driven by the primary disease, i.e., RP, consequently, RP2 is classified as RP.

Fixations were tracked with 25 Hz and the proportion of fixations falling within the central 2° radius was determined using built-in MP1 analysis (**Table 1**).

Visual Stimulation for fMRI

Stimulus Conditions and Rationale

Three different tasks were performed independently in separate runs within the same session: (1) one-back task (OBT), (2) passive viewing (PV), and (3) fixation-dot task (FDT). The underlying rationale was to dissociate top-down modulations and bottom-up input to the visual cortex by applying visual stimulation with a moving pattern with (OBT) and without a stimulus related task (PV). Specifically, during (1) OBT, the participants were instructed to report a repetition of same drifting directions of the pattern in two consecutive trials using a button press. They were required to fixate on the central dot while performing the task. One-back repetition trials were ensured to be at least 15% of the total number of trials and were randomized. All the participants were able to perform the stimulus-locked task without much difficulty. (2) During PV, the participants passively viewed the stimulus while fixating the central dot, i.e., they were explicitly instructed not to do the OBT during the PV. (3) The FDT task was introduced as a reference condition to test whether the effects of PV could be enhanced by fixing the participants' attention at the center to make it more difficult to perform a self-paced stimulus related task, e.g., the OBT. For FDT (not locked to the stimulus, i.e., running during both on- and off-blocks) the participants responded via button press when the color of the fixation dot changed. In all controls and most of the patients, the switch-colors used were black and white; however, in some patients different colors were used depending on the ability of participants to notice the change. The color change occurred throughout the cycle i.e., during both the stimulus presentation and the mean luminance gray. The spatial and temporal properties of the stimuli were kept consistent for all the three conditions. Each of the different task-condition was repeated for three times in an interleaved order (ABCCBAABC; A-PV, B-OBT, C-FDT) and the sequence was kept the same for all participants. Before each run, the participants were informed of the current task by the MRI technician through an audio setup in the scanner.

Visual Stimulation

Psychtoolbox-3 (Brainard, 1997; Pelli, 1997) was used to program the visual stimuli in MATLAB (Mathworks, Natick, Massachusetts, United States). The stimulus employed comprised high-contrast patterns drifting in eight different directions that were projected to a screen at the rear end of the magnet bore, with a resolution of 1,920 × 1,080 pixels. Participants viewed the stimulus monocularly via the better eye [patients: based on SAP (MD and extent of VF-loss); controls: dominant eye] at a distance of 35 cm via an angled mirror. This resulted in an effective stimulus size subtending approximately 24 and 14° radius in the horizontal and the vertical directions, respectively. All the patients viewed the stimulus projected on the entire screen, whereas, in the controls, we simulated an artificial peripheral scotoma by exposing only the central 7° of the stimulus through a circular aperture. The temporal sequence of each run followed a block design with 10 cycles of 12 s motion block (stimulus presentation) alternating with 12 s of mean luminance gray (24 s per cycle). Within each motion block, the direction of the contrast pattern was randomly changed every second (i.e., 12 trials per block; **Figure 1**). In each 1 s trial, the stimulus was presented for 750 ms followed by a 250 ms mean luminance gray. Participants were instructed to maintain fixation on a centrally located fixation dot. The stimulated eye of the participants were monitored and evaluated via an eye tracker qualitatively during fMRI measurements. The spatial properties of the stimulus are quite robust to account for any possible eye-movement related

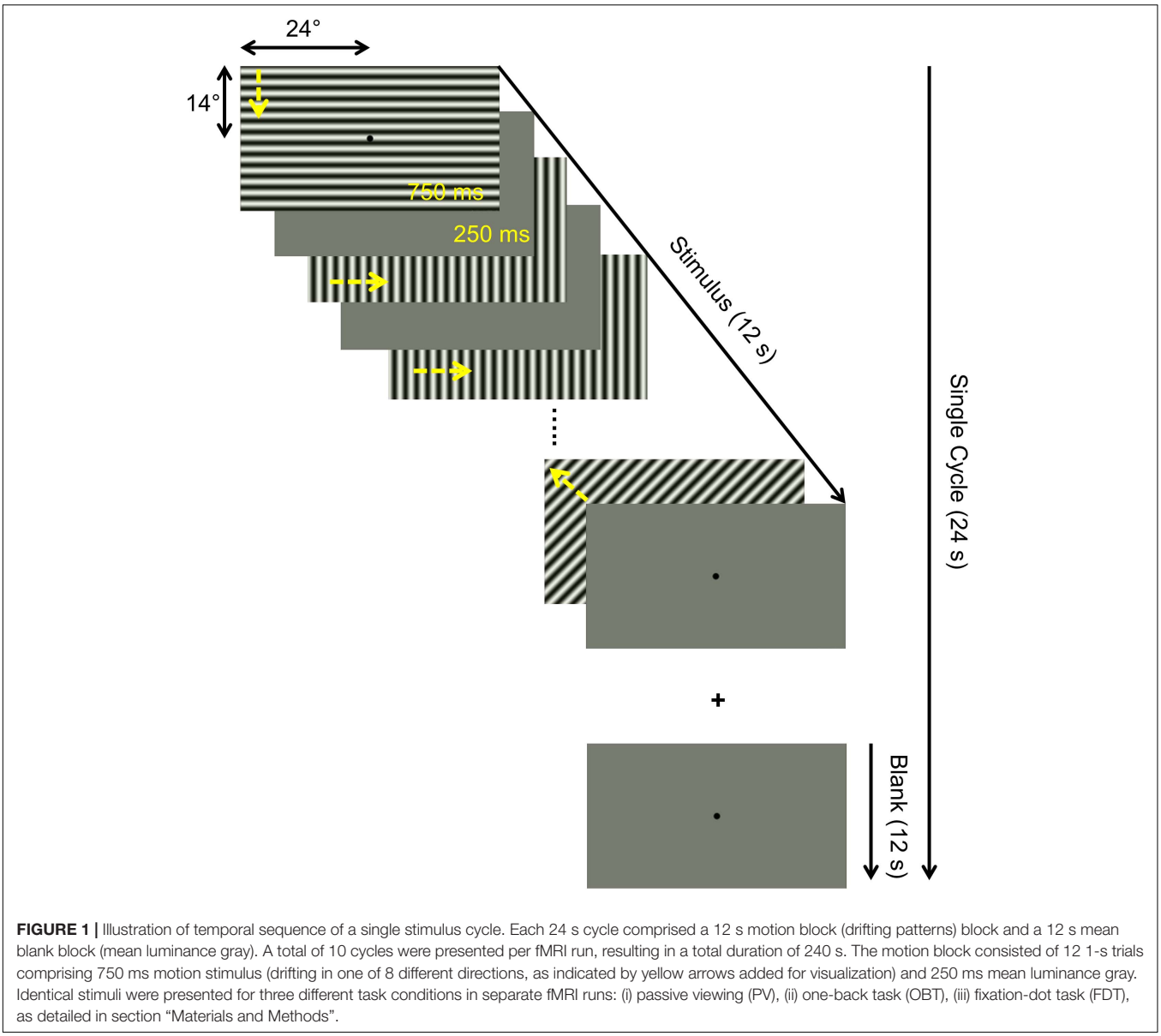

FIGURE 1 | Illustration of temporal sequence of a single stimulus cycle. Each 24 s cycle comprised a 12 s motion block (drifting patterns) block and a 12 s mean blank block (mean luminance gray). A total of 10 cycles were presented per fMRI run, resulting in a total duration of 240 s. The motion block consisted of 12 1-s trials comprising 750 ms motion stimulus (drifting in one of 8 different directions, as indicated by yellow arrows added for visualization) and 250 ms mean luminance gray. Identical stimuli were presented for three different task conditions in separate fMRI runs: (i) passive viewing (PV), (ii) one-back task (OBT), (iii) fixation-dot task (FDT), as detailed in section "Materials and Methods".

influence in the fMRI response. In particular, even in patients with little eye-movements, the representation of the scotoma and intact VF remains the same because of the presence of the stimulus on the entire screen.

In addition, to delineate the visual areas, fMRI-based population receptive field (pRF) mapping scans were obtained from each participant in a second session on a separate day. A checkerboard stimulus pattern (mean luminance: 109 cd/m^2; contrast: 99%; check size: 1.57°) moving in eight different directions (2 horizontal, 2 vertical and 4 diagonal; Dumoulin and Wandell, 2008) was exposed through a bar aperture. The width of the bar subtended 1/4th (3.45°) of the stimulus radius (13.8°). The spatial and temporal properties of the stimulus have been described in Prabhakaran et al. (Prabhakaran et al., 2020). The duration of each pRF mapping scan was 192 s and the scan was repeated 6 times for the patient cohort and 4 times for the controls. The participants responded to a fixation-dot color change via button press.

MRI Acquisition

All MRI and fMRI data were collected on a 3 Tesla Siemens Prisma scanner (Erlangen, Germany). In order to allow for an unrestricted view of the entire projection screen, we used only the lower section of a 64-channel head coil, resulting in a 34-channel coil covering most of the brain. fMRI scans parallel to the AC-PC line were acquired using a T2*-weighted BOLD gradient-EPI sequence (TR | TE = 1,500 | 30 ms and voxel size = 2.5^3 mm^3). A total of 160 fMRI time series images (volumes) were obtained for each run after the removal of the first 8 volumes by the scanner itself to allow for steady magnetization. The fMRI parameters were the same for the pRF mapping data, except for the number of volumes (136). One high-resolution whole brain

anatomical T1-weighted scan (MPRAGE, 1 mm isotropic voxels, TR | TI | TE = 2,500 | 1,100 | 2.82 ms) was collected for each participant to allow for cortical visualization of fMRI responses. An inversion recovery EPI sequence (TR | TI | TE = 4,000 | 1,100 | 23 ms) with spatial coverage (FOV) and resolution identical to the T2* EPI was obtained to aid in the alignment of structural and functional data.

Data Preprocessing

Gray-white matter boundaries in the T1-weighted anatomical images were segmented using Freesurfer[1]. ITK-gray was used to manually inspect the Freesurfer segmentation and correct for possible segmentation errors[2]. A 3-D rendering of the cortical surface was generated by reconstruction of the segmented boundaries (Wandell et al., 2000). Within and between fMRI scans, head motion artifacts were corrected using AFNI[3]. For each participant, motion-corrected fMRI time series of the repetitions of each stimulation condition (i.e., PV, OBT, FDT, and pRF mapping data) were averaged into separate groups with MATLAB-based Vistasoft tools (mrVista[4]). The inversion recovery EPI was aligned spatially with the anatomical scan in two steps; first manually with rxAlign function in mrVista and then automatically using Kendrick Kay's alignment toolbox[5]. The obtained alignment matrix was used to align the fMRI images with the anatomy.

Data Analysis

Phase-Specified Coherence (Coherence$_{ps}$)

We computed voxel-wise coherence at the fundamental stimulus frequency and phase corrected for hemodynamic delay (phase-specified coherence) to quantitatively investigate changes in the strength of the BOLD response for the different task conditions. We used the definition and formula to calculate the phase-specified coherence (coherence$_{ps}$) that has been previously used (Masuda et al., 2008) and is also available as a function in the mrVista toolbox.

$$\text{Coherence}_{ps} = \frac{A_0}{\sqrt{\Sigma A_f^2}} \cos(\phi_0 - \varphi)$$

where A_0 and ϕ_0 are the signals amplitude and phase at the stimulation frequency, respectively, A_f are the amplitudes of each Fourier component, and φ is the delay in the hemodynamic response (estimated for each participant from the positive fMRI responses). The phase at the stimulus frequency was estimated from the averaged fMRI time-series of all the task conditions in a small 5 mm ROI drawn in the region of the cortex that had reliable positive BOLD response across all the conditions. Coherence$_{ps}$ can take values between −1 and +1; voxels with positive measure reflect stimulus synchronized fMRI response modulation and negative measures reflect modulation to the mean luminance gray (no or negative stimulus related BOLD response).

Visual Area Delineation

We defined the borders of primary (V1) and extra-striate visual cortex (V2 and V3) for each participant using fMRI-based pRF-mapping data. Employing a 2D-Gaussian pRF model approach described previously (Dumoulin and Wandell, 2008; Prabhakaran et al., 2020), we estimated for each voxel their preferred position in the visual field (x and y in Cartesian coordinates). Eccentricity $\sqrt{(x^2+y^2)}$ and polar angle $\tan^{-1}(\frac{y}{x})$ measures were derived from these position parameters. Polar angle estimates were projected onto an inflated cortical surface and the visual areas were delineated by following the phase reversals in the polar angle data (Sereno et al., 1995). As in advanced glaucoma and RP, retinal and subsequent cortical lesions render this delineation process difficult, due to deafferentation and hence disrupted maps, it was complemented by visual area definitions based on the Benson atlas (Benson et al., 2014). The Bensons atlas applies for each individual an anatomically defined template of retinotopy and thus informs pRF-mapping based visual area definitions. The anterior extent of the visual areas was manually drawn based on the participants pRF mapping data and Benson atlas extracted eccentricity predictions (14° in the vertical meridian representation and 24° in the horizontal meridian representation) in correspondence to our stimulus size. Based on the coherence$_{ps}$ measures from passive viewing (PV), we divided each visual area into two ROIs; voxels with positive responses were classified as the normal projection zone (NPZ) and those with negative responses as the lesion projection zone (LPZ).

All further region of interest (ROI) analyses were performed with custom written scripts in MATLAB and statistics in SPSS 26 (Statistical Package for the Social Sciences, IBM). For each visual area (V1, V2, and V3) and ROIs (LPZ and NPZ), separate two-way repeated measures ANOVAs were performed to test for the effects of *task* (PV, OBT, and FDT) and *group* (glaucoma, RP, control) on coherence$_{ps}$ and their significance, if any. Paired *t*-tests were used for *post hoc* comparisons and corrected for multiple comparison with the Holm-Bonferroni correction (Holm, 1979).

RESULTS

Task-Dependent Responses in Lesion Projection Zone (LPZ)

Firstly, as a validation and replication of the existing literature, we examined the scope of aberrant cortical responses in the deafferented visual cortex of a reference group of three participants with RP. Consistent with the results from Masuda and colleagues (Masuda et al., 2010) in their cohort of three RP participants primary visual cortex (V1), we found task-dependent activity in the peripheral LPZ in V1 (OBT-PV: $t = 16.8$; $p = 0.012$), and non-significant trends in V2 (OBT-PV: $t = 6.2$; $p = 0.075$) and V3 (OBT-PV: $t = 3.7$; $p = 0.198$) (see **Figure 2**, **Supplementary Figure 1**, and **Supplementary Table 1**).

[1]https://surfer.nmr.mgh.harvard.edu/

[2]https://github.com/vistalab/itkgray

[3]https://afni.nimh.nih.gov/

[4]https://github.com/vistalab/vistasoft

[5]https://github.com/kendrickkay/alignvolumedata

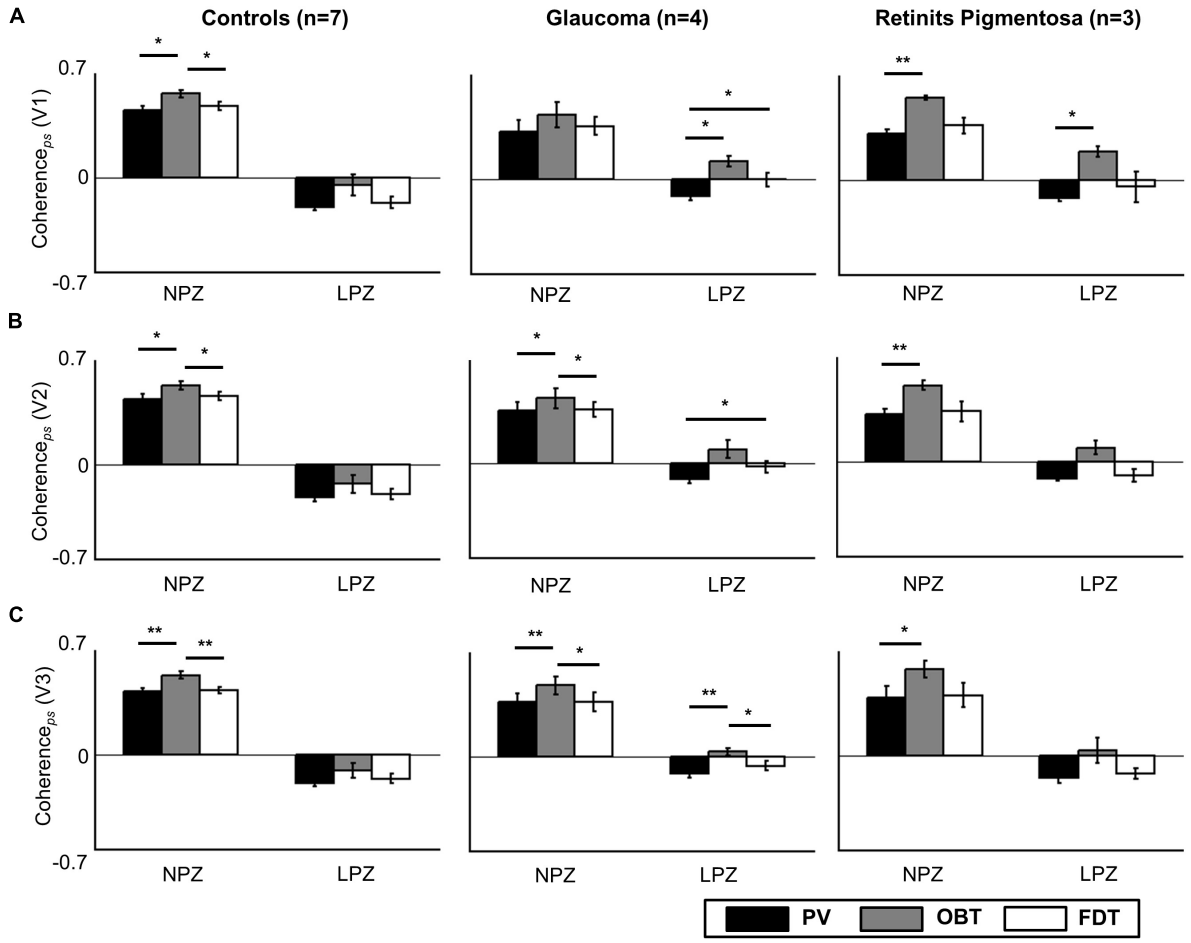

FIGURE 2 | Task dependence of coherence$_{ps}$ in V1 **(A)**, V2 **(B)**, and V3 **(C)** for the control (n = 7), glaucoma (n = 4), and retinitis pigmentosa groups (n = 3; mean ± SEM). Controls and patients differ specifically for LPZ. Only in the patient groups' LPZ, negative coherence$_{ps}$ during PV is shifted to positive values for OBT. Significance tests (corrected paired t-tests) on task effects were performed for all the participant groups, $^{*}p < 0.05$ and $^{**}p < 0.01$. PV, passive viewing; OBT, one-back task; FDT, fixation-dot task.

Next, we explored task-dependent LPZ responses in participants with advanced VF defects due to glaucoma. For a qualitative assessment, the fMRI-responses in the visual cortex of a representative participant with glaucoma (GL1) and a healthy control (HC1) with simulated peripheral VF-defect are shown in **Figure 3** for three different stimulation conditions (PV, OBT, FDT). In the healthy control, LPZ responses were largely similar for all stimulation conditions, i.e., negative coherence$_{ps}$ and BOLD modulations. In contrast, LPZ responses in the glaucoma patient resulted in positive coherence$_{ps}$ and BOLD modulations for OBT, while negative coherence$_{ps}$ and negative BOLD modulations, as for the control, were obtained only for PV and FDT. Taken together, the response signatures for the participant with glaucoma resembled those reported for RP (**Supplementary Figure 1**).

In a quantitative assessment, the above task dependence of the LPZ-responses in glaucoma was further confirmed at the group level. Each participant's mean phase-specified coherence (coherence$_{ps}$) was extracted from NPZ and LPZ voxels for each of the three stimulation conditions. The mean coherence$_{ps}$ of the three participant groups is depicted for V1 in **Figure 2**. For all participant groups, in NPZ we observed a strong positive coherence$_{ps}$, which was enhanced for OBT. In contrast, in LPZ the negative coherence$_{ps}$ for PV turned positive for OBT in the glaucoma and RP group, while it remained negative, albeit reduced, for the control group. This differential effect between patient and control groups in LPZ was also directly evident from the inspection of the average single-cycle BOLD time series in LPZ. As depicted in **Figure 4** for the group averages, only for glaucoma and RP did negative responses during stimulation (first 12 s) for PV shift to positive responses for OBT. As a consequence the BOLD-peak for OBT shifts from the second block (12–24 s) in healthy controls to the first block (first 12 s) in RP and glaucoma.

The significance of the task effect on V1 coherence$_{ps}$ and its difference across participant groups were assessed with two-way repeated measures ANOVA [between-subject factor: *group* (glaucoma, RP, control); within-subject factor: *task* (PV, OBT, FDT)] for the LPZ and NPZ separately. The effect of *task* was

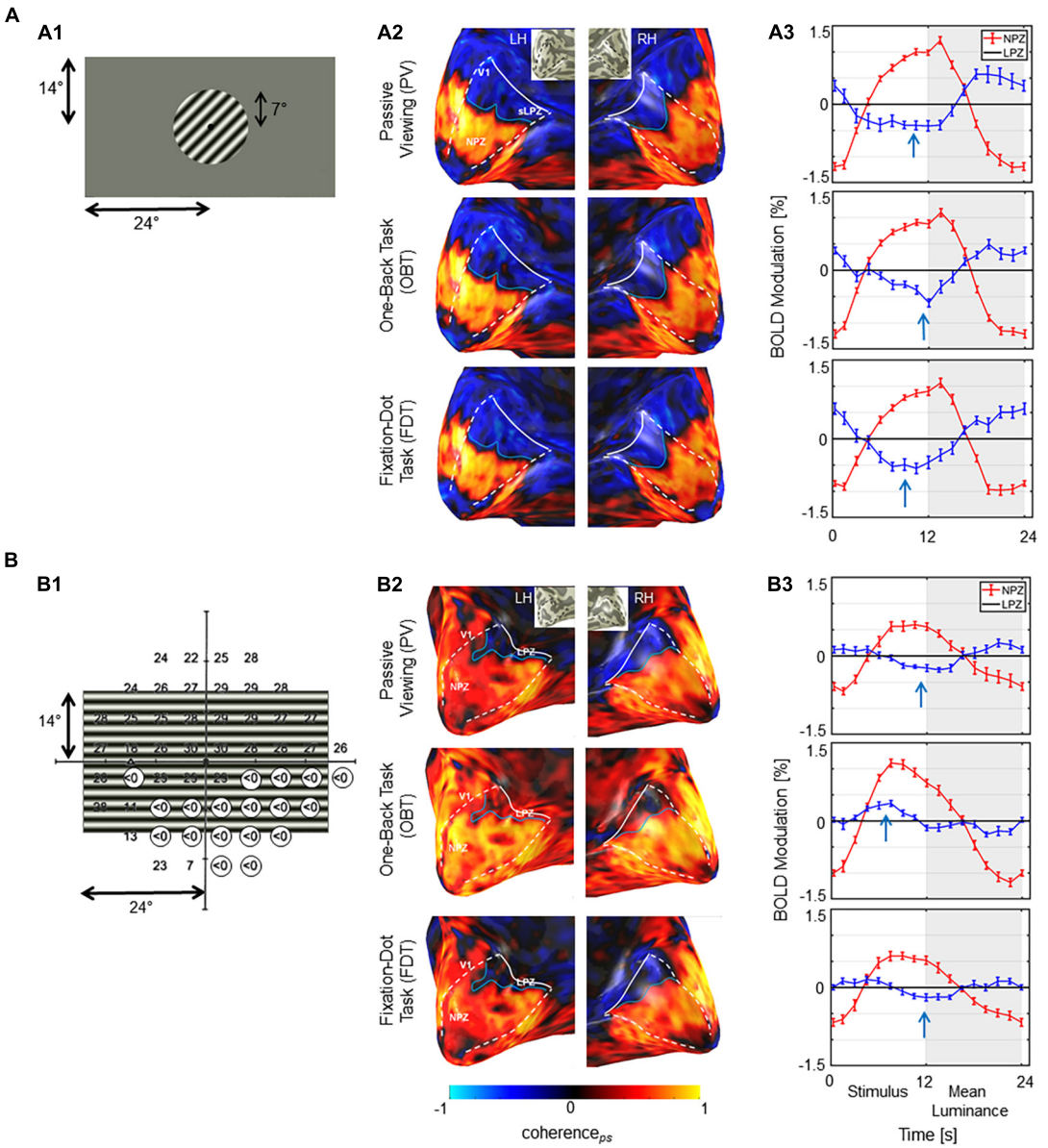

FIGURE 3 | Stimulus schematics and fMRI-based activations. **(A)** Control HC1 **(A1)** Illustration of stimulated visual field for the controls with the simulation of a scotoma by peripheral masking beyond 7°. **(A2)** BOLD-activations (coherence$_{ps}$) for the three task conditions projected onto the inflated occipital lobe as false-color overlays. V1 boundaries (white dashed) and the anterior extent (white solid line) were determined from the participants pRF mapping; NPZ and LPZ are indicated. **(A3)** Average single-cycle BOLD time series for the three conditions in the NPZ (red) and LPZ (blue) ROIs. White and gray zones indicate motion and blank blocks, respectively. The induced BOLD response is shifted due to the hemodynamic delay. Stimulus related BOLD modulations in LPZ are negative, irrespective of the task condition, as indicated by the arrows. **(B)** Glaucoma participant GL1. **(B1)** Visual field sensitivities for the study eye (left eye SAP) as determined perimetrically are superimposed onto stimulus layout (absolute scotomas are highlighted by white discs). **(B2)** BOLD-activations (coherence$_{ps}$) depicted as for A2. V1 was determined from the participants pRF mapping data informed by atlas mapping as detailed in section "Materials and Methods.". **(B3)** Average single-cycle BOLD time series depicted as for A3. Depending on task, LPZ responses were negative (PV/FDT) or positive (OBT), as indicated by the arrows. NPZ, normal projection zone; LPZ, lesion projection zone; RH, right hemisphere; LH, left hemisphere.

significant for both LPZ and NPZ ($p < 0.001$; see **Supplementary Table 1**), but the effect of *group* was significant only for the LPZ ($p < 0.05$). No significant interactions (*task* × *group*) were observed. *Post hoc* tests (corrected) were performed to identify the significant comparisons as indicated in **Figure 2A**. To assess the task-dependence of LPZ responses in glaucoma, the comparisons of the conditions OBT and PV in the control and glaucoma group are of particular relevance: for glaucoma there was a significant difference ($t = 5.4$; $p = 0.024$), but not for the controls. This effect was also significant in glaucoma V3 ($t = 10.2$; $p = 0.006$), while the same trend in V2 ($t = 2.8$; $p = 0.069$) failed to reach significance (**Figures 2B,C**). We further tested in

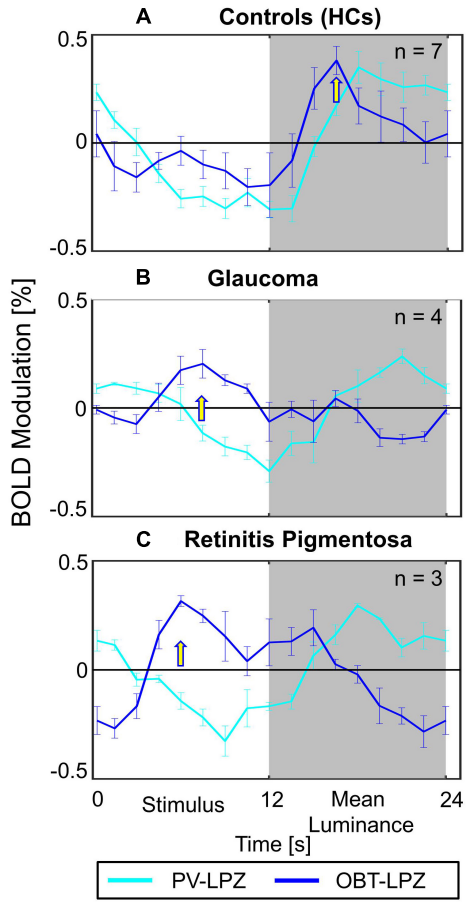

FIGURE 4 | Average single-cycle BOLD time series ± SEM. Group-averaged fMRI response modulation across participants of V1 LPZ during PV (cyan) and OBT (blue) conditions. The panels show the plots for **(A)** HCs **(B)** Glaucoma **(C)** Retinits Pigmentosa. Yellow arrows indicate time-points with peak responses for OBT; the BOLD-peak for OBT shifts from the second block (12–24 s) in HC to the first block (first 12 s) in RP and glaucoma.

glaucoma for any hierarchical effects of task-dependence in V1, V2, and V3 by calculating the effect size (computed as Cohen's d) of the observed task-related coherence$_{ps}$ modulations in LPZ. We observed a stronger effect size in V1 (d = 0.70) and relatively lower effect size for V2 (d = 0.50) and V3 (d = 0.51). However, a repeated measures one-way ANOVA with *visual areas* (V1–V3) as the within-subject factor did not show any significant difference on the task-dependent effects across the visual areas [$F_{(2,\ 6)}$ = 1.1; p = n.s.]. Finally, it was assessed whether the FDT-condition might serve as a better reference condition than PV by resulting in more negative coherence$_{ps}$ values in LPZ. However, this was not the case, modulations for FDT fell short of that for PV, an effect that reached significance in glaucoma for V1 and V2.

LPZ Responses as a Function of Clinical Characteristics

Considering that our patients (both glaucoma and RP) demonstrated significant task-dependent LPZ responses, we employed an exploratory approach to investigate the relationship of the magnitude of difference in coherence$_{ps}$ (i.e., OBT minus PV) with patient specific clinical characteristics. Specifically, the clinical measures included visual acuity (VA), disease duration, percentage of visual field loss (VF$_{loss}$), mean deviation (MD), foveal sensitivity. VF$_{loss}$ was computed from the SAP-based VFs as the ratio of number of non-responsive test points vs. the total number of test points and considered only the regions of the VF representing our fMRI stimulus size. The relationship of the percentage of differential coherence$_{ps}$ in LPZ with these clinical measures was tested with a simple linear regression model [R^2(adjusted), $p < 0.05$]. We did not find a significant association of the task-dependent responses with any of the afore-mentioned clinical correlates, except for MD and task-effect in the visual area V2. Nonetheless, based on the magnitude of R^2, a negative trend in the task-effect with both MD (V1: 0.29; V2: 0.49) and the percentage of VF$_{loss}$ (V1: 0.18; V2: 0.38) in V1 and V2 was indicated, but not for V3.

Cortical Thickness as a Measure of Structural Integrity

In an exploratory analysis, we probed for the presence of structural changes of the visual cortex following visual field deficits in patients compared to the controls. Freesurfer derived cortical thickness estimates, measured as the distance between the gray/white boundary and the pial surface (Fischl and Dale, 2000) was used as the indicator for structural integrity. For each participant and visual area (V1–V3) voxel-wise cortical thickness was extracted. Based on eccentricity estimates from a participant-specific anatomy driven retinotopic atlas (Benson et al., 2014), 12 ROIs of 2° eccentricity bins (0–24°) were created for each visual area and the mean cortical thickness was computed for each ROI. To investigate for differences in cortical thickness across groups a repeated measure ANOVA with *participant group* (patients and controls) as between-subject factor and *eccentricity* (0–24°) and *visual areas* (V1–V3) as within-subject factors was performed. The subject-specific global cortical thickness was included as a covariate to account for participant variability. While there was an overall trend for smaller cortical thickness in the *patient group* [cortical thickness controls vs. patients (mm) mean ± SEM: 1.76 ± 0.03 vs. 1.65 ± 0.02 (V1); 1.99 ± 0.05 vs. 1.93 ± 0.05 (V2); 2.31 ± 0.07 vs. 2.08 ± 0.05 (V3)], this did not reach significance. No other significant main effects or interaction were found. In addition, we tested for any potential association between the duration of visual field deficits and cortical thickness across the patients and did not find any significant relationship [R^2: 0.08 (V1); 0.12 (V2); 0.20 (V3)].

DISCUSSION

We report that activations in the LPZ of the early visual cortex were strongly related to performing a one-back task in glaucoma and retinitis pigmentosa (RP), but not in controls with simulated LPZ. This indicates that the limited remapping, previously reported in RP and MD, is also a feature in glaucoma. These results thus suggest that strong limits of bottom-up plasticity

are a general feature of the early human visual cortex that was de-afferented due to acquired lesions at the level of the retinal photoreceptors or ganglion cells.

The response pattern we observed, i.e., LPZ activation for visual stimulus-locked tasks, had previously not been reported for glaucoma. At the same time, it fits well into the context of other studies on visual plasticity in acquired retinal defects (for e.g., MD, Masuda et al., 2008, 2020; Baseler et al., 2011; RP, Masuda et al., 2010; Ferreira et al., 2019). From the initial apparent heterogeneity of reports on the scope of plasticity in the LPZ of human V1, ranging from the absence of relevant cortical remapping (Sunness et al., 2004; Baseler et al., 2011) to large-scale reorganization (Baker et al., 2008; Dilks et al., 2009), the picture of limited bottom-up plasticity in human V1 has eventually emerged (Wandell and Smirnakis, 2009; Morland, 2015). Accordingly, Masuda et al. (2008) observed LPZ-responses in V1 during the performance of stimulus-related visual tasks and concluded that they were associated with task-dependent feedback instead of bottom-up plasticity in MD (Masuda et al., 2008) and RP (Masuda et al., 2010). In a larger RP cohort, Ferreira et al. (2019) demonstrated similar task-dependent responses using spatial specific stimulation, as opposed to full-field stimulation employed by Masuda and colleagues (2020). This, in addition to recent findings of LPZ responsiveness to be modality independent [i.e., induced also by auditory and tactile stimulation associated tasks (Masuda et al., 2020)], adds further evidence to the hypothesis of LPZ responses to be dependent on the demands of task. In conclusion, we here demonstrate that these mechanisms are not specific to the rare disease RP, but they also apply to the much more prevalent disease entity of glaucoma.

Early Visual Cortex Stability and Plasticity

The potential of remapping in V1 in acquired defects is often inferred from adult animal models (Kaas et al., 1990; Gilbert and Wiesel, 1992; Giannikopoulos and Eysel, 2006). While some degree of developmental V1 plasticity has been reported for congenital vision disorders (Baseler et al., 2002), the nature and magnitude of a large-scale reorganization in adulthood is questionable (Wandell and Smirnakis, 2009) and still warrants quantitative ascertainment. The differential comprehension in the above literature on LPZ activation primarily arises from the variable definitions of cortical reorganization and remapping (Morland, 2015). While the proponents of plasticity speculate that the mere presence of abnormal LPZ responses is sufficient evidence, the critiques point out the need for such responses to be non-explainable by the normal visual cortex organization following visual field loss. In the context of the latter definition of cortical reorganization, from our data, bottom-up large-scale reorganization appears an unlikely cause of the reported LPZ activation in glaucoma, as it would lead to LPZ responses irrespective of the condition, i.e., task. While this supports top-down effects as a cause of the task-related LPZ responses, these do not appear to strictly follow the inverse visual hierarchy, i.e., a decreasing effect size from V3 to V1, as might be expected for top-down modulations. In fact, the differential activation (reflected by Cohen's d) we observed in V1 was not exceeded by those in V2 and V3 and did not reach statistical significance in a respective ANOVA. A stronger effect size in the extra-striate areas (i.e., V3 > V2 > V1) would have added further evidence to a top-down hypothesis. Further research is necessary to decipher the nature of the top-down modulations. One rewarding avenue to pursue for this purpose is paved by the advent of MRI at submillimeter resolution (Ress et al., 2007; Yakupov et al., 2017; Fracasso et al., 2018; Kashyap et al., 2018). It opens the possibility to recover information on the directionality of information flow in the cortex via laminar imaging (Dumoulin et al., 2018; Lawrence et al., 2019) that allows to dissociate activations in cortical input and output layers. Consequently, future studies measuring layer-specific functional activity in the visual cortex might unravel the missing pieces of information, i.e., origin and directionality of task-related LPZ activations, to validate or invalidate existing theories on the aberrant cortical activity observed in patients with de-afferented visual cortex.

Clinical Relevance in the Context of Emerging Therapeutic Interventions

A subset of glaucoma patients continues advancing toward blindness regardless of disease management. While restoration therapies might offer treatment options for this patient entity, it has been suggested that vision loss associated changes at the level of visual cortex might be a reason for treatment failure in such cases (Gupta and Yücel, 2007; Davis et al., 2016; Nuzzi et al., 2018). Remarkably, the existence of cortical responses in the de-afferented visual cortex, as demonstrated in the present study, suggests that the LPZ is still to some degree operational. These finding are of particular importance for current promising initiatives to restore the visual input to the cortex (Roska and Sahel, 2018), which include retinal gene (Ashtari et al., 2015; Aguirre, 2017; Russell et al., 2017) and stem-cell therapy (Schwartz et al., 2015; Jutley et al., 2017; Mead et al., 2018; Wang et al., 2020), and retinal (da Cruz et al., 2016; Edwards et al., 2018) and visual cortex implants (Beauchamp et al., 2020). Our findings demonstrate the relevance of fMRI-investigations of the functionality of the visual cortex for the preparation of such demanding vision restoration procedures, e.g., via the individualized prediction of their clinical effectiveness.

Relationship of Cortical Responses With Clinical Correlates

The presence and magnitude of LPZ task-dependent responses are likely also related to the patient's clinical characteristics and their variability (Ferreira et al., 2019). Testing this, we observed a non-significant trend for the task-elicited LPZ responses to be negatively associated with the VF loss, i.e., the smaller the deficit the larger the response. This might suggest that the task-dependent LPZ-activations do not depend on the presence of extensive scotomas. Given the limited sample size in the present study, this explorative observation disserves following up in future studies. Nevertheless, the findings emphasize the benefits

of patient stratification strategies for the investigation of disease related changes in the visual cortex.

Limitations and Future Directions

As a primary limitation in the study, we acknowledge the small sample size of glaucoma patients, which was still fully sufficient to identify the relevant effects. It should be noted, that our target patients were those with strongly advanced VF defects. Consequently, as glaucoma is an age-progressive disorder, such patients are mostly in their later stages of life and likely to have at least one MRI-related contraindication, which makes them a rare cohort for fMRI investigations. Studies investigating the dynamics of the observed task-dependent LPZ responses in patients with different stages of the pathology are limited (Ferreira et al., 2017, 2019) which should be addressed by future research and more importantly aim to uncover the mechanisms underlying such responses with submillimeter laminar fMRI imaging.

Our definition of the lesion projection zone (LPZ) was based on negative modulations observed with full-field visual stimulation in accordance with previous studies (Masuda et al., 2010; 2008), but not on explicit spatial VF mapping. In consideration to previous studies (Plank et al., 2017) reporting changes in BOLD response modulation with stimulus type (for e.g., faces vs. checkerboard), it is to be noted that there might be a marginally differential characterization of LPZ with a full-field stimulus (in this case, gratings) compared to a spatial mapping stimulus. Importantly, in the context of population receptive field properties, distinctions in the cortical representation of visual field has been even reported for different spatial mapping-based approaches (Alvarez et al., 2015). As we tested for the presence of task-dependent responses in advanced glaucoma with substantial VF loss, full-field stimulation eliciting robust fMRI responses was preferred over a precise spatial delineation of the LPZ with spatially specific stimuli. Given the fact, irrespective of the stimulus type, keeping it consistent across the different conditions sufficed for our objective, the choice of stimulus could be rationalized. Nevertheless, a comparative analysis of LPZ definitions with different stimulation approaches might be of relevant interest to understand the dynamics of LPZ boundaries.

Some of our patients (GL2, RP2, and RP3) had quite low visual acuity and one of these patients (RP3) was predicted to have unreliable fixation with fundus-controlled perimetry, and the quantitative eye tracking data might have been informative. Despite this limitation, the qualitative monitoring and evaluation of the stimulated eye during scanning indicated all our participants to have good fixation of the stimulus in the scanner. In addition, given that the intact VF of our low visual acuity patients was largely constricted to central few degrees, we believe the responsive central visual field to be well within the stimulus window for potential small or moderate eye movements, thereby mitigating any possible eye-movement related influence in the fMRI response.

We also acknowledge a potential confound in our study with one RP patient also diagnosed with secondary glaucoma. Considering that, RP is not the primary disease under investigation in this study and used as a reference cohort to demonstrate the replicability and reproducibility of previous reports of task-dependent LPZ responses, we did not see a reason to exclude this patient in our analysis.

It should also be noted that our characterization of artificial scotoma was based on a generalized pattern of VF deficits as observed in peripheral vision disorders and not aiming at the simulation of our patient cohort's idiosyncratic individual VF deficits. Although we acknowledge benefits of the latter approach, as our primary aim was to look at the task-dependent effects at a group level rather than individual patient-to-control comparison, the employed approach in the present study has the benefit of better within-group comparability. In addition, future research should also explore alternative methods to efficiently simulate artificial scotomas which closely correspond to patient like VF deficits, for e.g., via retinal bleaching (Magnussen et al., 2001; Gaffney et al., 2013) with high luminance levels and temporarily desensitizing the locations intended to represent an artificial scotoma.

CONCLUSION

In summary, we demonstrated in patients with advanced glaucoma, the existence of aberrant cortical responses in the supposedly de-afferented regions of the early visual cortex. The fMRI modulations are more likely to be driven by task-elicited top-down neural mechanisms than bottom-up cortical reorganization. Given similar findings in glaucoma as in RP and MD, the results are indicative of a general mechanism behind such aberrant cortical responses that is not limited to the distinct pathophysiology of a specific disease. We believe that these insights are of importance for the development of treatment and rehabilitation schemes in glaucoma and beyond.

DATA AVAILABILITY STATEMENT

The raw data supporting the conclusions of this article will be made available by the authors, without undue reservation.

ETHICS STATEMENT

The studies involving human participants were reviewed and approved by the Ethics Committee—University of Magdeburg. The patients/participants provided their written informed consent to participate in this study.

AUTHOR CONTRIBUTIONS

GP: conceptualization, methodology, formal analysis, investigation and data curation, and writing—original draft. MH: conceptualization, methodology, supervision, writing—review and editing, and funding acquisition. KA-N: investigation and writing—review and editing. CT: methodology and writing—review and editing. MW: investigation and writing—review and editing. HT: writing—review

and editing. All authors contributed to the article and approved the submitted version.

FUNDING

This project was supported by the European Union's Horizon 2020 Research and Innovation Programme under the Marie Skłodowska-Curie grant agreements No. 675033 (EGRET plus) and by the German research foundation (DFG: HO2002/20-1) to MH. The funding organization did not have any role in the study design, collection, analysis and interpretation of the data, or publication of this research.

ACKNOWLEDGMENTS

We also thank Katharina Jürse for her assistance with the recruitment of participants and Denise Scheermann for her support of the MRI measurements. We also thank the reviewers for their valuable comments and suggestions which have greatly helped us improve the manuscript.

SUPPLEMENTARY MATERIAL

The Supplementary Material for this article can be found online at: https://www.frontiersin.org/articles/10.3389/fnins.2021.653632/full#supplementary-material

REFERENCES

Aguirre, G. D. (2017). Concepts and strategies in retinal gene therapy. *Invest. Ophthalmol. Vis. Sci.* 58, 5399–5411. doi: 10.1167/iovs.17-22978

Ahmadi, K., Fracasso, A., Puzniak, R. J., Gouws, A. D., Yakupov, R., Speck, O., et al. (2020). Triple visual hemifield maps in a case of optic chiasm hypoplasia. *NeuroImage* 215:116822. doi: 10.1016/j.neuroimage.2020.116822

Ahmadi, K., Fracasso, A., van Dijk, J. A., Kruijt, C., van Genderen, M., Dumoulin, S. O., et al. (2019). Altered organization of the visual cortex in FHONDA syndrome. *NeuroImage* 190, 224–231. doi: 10.1016/j.neuroimage.2018.02.053

Alvarez, I., de Haas, B., Clark, C. A., Rees, G., and Schwarzkopf, D. S. (2015). Comparing different stimulus configurations for population receptive field mapping in human FMRI. *Front. Hum. Neurosci.* 9:96. doi: 10.3389/fnhum.2015.00096

Ashtari, M., Zhang, H., Cook, P. A., Cyckowski, L. L., Shindler, K. S., Marshall, K. A., et al. (2015). Plasticity of the human visual system after retinal gene therapy in patients with leber's congenital amaurosis. *Sci. Transl. Med.* 7:296ra110. doi: 10.1126/scitranslmed.aaa8791

Bach, M. (1996). The freiburg visual acuity test–automatic measurement of visual acuity. *Optom. Vis. Sci.* 73, 49–53.

Baker, C. I., Dilks, D. D., Peli, E., and Kanwisher, N. (2008). Reorganization of visual processing in macular degeneration: replication and clues about the role of foveal loss. *Vis. Res.* 48, 1910–1919. doi: 10.1016/j.visres.2008.05.020

Barton, B., and Brewer, A. A. (2015). FMRI of the rod scotoma elucidates cortical rod pathways and implications for lesion measurements. *Proc. Natl. Acad. Sci. U.S.A.* 112, 5201–5206. doi: 10.1073/pnas.1423673112

Baseler, H. A., Brewer, A. A., Sharpe, L. T., Morland, A. B., Jägle, H., and Wandell, B. A. (2002). Reorganization of human cortical maps caused by inherited photoreceptor abnormalities. *Nat. Neurosci.* 5, 364–370. doi: 10.1038/nn817

Baseler, H. A., Gouws, A., Haak, K. V., Racey, C., Crossland, M. D., Tufail, A., et al. (2011). Large-scale remapping of visual cortex is absent in adult humans with macular degeneration. *Nat. Neurosci.* 14, 649–655. doi: 10.1038/nn.2793

Beauchamp, M. S., Oswalt, D., Sun, P., Foster, B. L., Magnotti, J. F., Niketeghad, S., et al. (2020). Dynamic stimulation of visual cortex produces form vision in sighted and blind humans. *Cell* 181, 774–783. doi: 10.1016/j.cell.2020.04.033

Benson, N. C., Butt, O. H., Brainard, D. H., and Aguirre, G. K. (2014). Correction of distortion in flattened representations of the cortical surface allows prediction of v1-v3 functional organization from anatomy. *PLoS Comput. Biol.* 10:e1003538. doi: 10.1371/journal.pcbi.1003538

Borges, V. M., Danesh-Meyer, H. V., Black, J. M., and Thompson, B. (2015). Functional effects of unilateral open-angle glaucoma on the primary and extrastriate visual cortex. *J. Vis.* 15:9. doi: 10.1167/15.15.9

Boucard, C. C., Hanekamp, S., Ćurčić-Blake, B., Ida, M., Yoshida, M., and Cornelissen, F. W. (2016). Neurodegeneration beyond the primary visual pathways in a population with a high incidence of normal-pressure glaucoma. *Ophthalmic Physiol. Opt.* 36, 344–353. doi: 10.1111/opo.12297

Brainard, D. H. (1997). The psychophysics toolbox. *Spat. Vis.* 10, 433–436.

da Cruz, L., Dorn, J. D., Humayun, M. S., Dagnelie, G., Handa, J., Barale, P.-O., et al. (2016). five-year safety and performance results from the argus II retinal prosthesis system clinical trial. *Ophthalmology* 123, 2248–2254. doi: 10.1016/j.ophtha.2016.06.049

Dai, H., Morelli, J. N., Ai, F., Yin, D., Hu, C., Xu, D., et al. (2013). Resting-state functional mri: functional connectivity analysis of the visual cortex in primary open-angle glaucoma patients. *Hum. Brain Mapp.* 34, 2455–2463. doi: 10.1002/hbm.22079

Davis, B. M., Crawley, L., Pahlitzsch, M., Javaid, F., and Cordeiro, M. F. (2016). Glaucoma: the retina and beyond. *Acta Neuropathol.* 132:807. doi: 10.1007/s00401-016-1609-2

Dilks, D. D., Baker, C. I., Peli, E., and Kanwisher, N. (2009). Reorganization of visual processing in macular degeneration is not specific to the preferred retinal locus. *J. Neurosci.* 29, 2768–2773. doi: 10.1523/JNEUROSCI.5258-08.2009

Dumoulin, S. O., Fracasso, A., van der Zwaag, W., Siero, J. C. W., and Petridou, N. (2018). Ultra-high field MRI: advancing systems neuroscience towards mesoscopic human brain function. *NeuroImage* 168, 345–357. doi: 10.1016/j.neuroimage.2017.01.028

Dumoulin, S. O., and Wandell, B. A. (2008). Population receptive field estimates in human visual cortex. *NeuroImage* 39, 647–660. doi: 10.1016/j.neuroimage.2007.09.034

Duncan, R. O., Sample, P. A., Weinreb, R. N., Bowd, C., and Zangwill, L. M. (2007). Retinotopic organization of primary visual cortex in glaucoma: comparing FMRI measurements of cortical function with visual field loss. *Prog. Retin. Eye Res.* 26, 38–56. doi: 10.1016/j.preteyeres.2006.10.001

Edwards, T. L., Cottriall, C. L., Xue, K., Simunovic, M. P., Ramsden, J. D., Zrenner, E., et al. (2018). Assessment of the electronic retinal implant alpha AMS in restoring vision to blind patients with end-stage retinitis pigmentosa. *Ophthalmology* 125, 432–443. doi: 10.1016/j.ophtha.2017.09.019

Ferreira, S., Pereira, A. C., Quendera, B., Reis, A., Silva, E. D., and Castelo-Branco, M. (2017). Primary visual cortical remapping in patients with inherited peripheral retinal degeneration. *NeuroImage* 13, 428–438. doi: 10.1016/j.nicl.2016.12.013

Ferreira, S., Pereira, A. C., Quendera, B., Reis, A., Silva, E. D., and Castelo-Branco, M. (2019). Enhanced visual attentional modulation in patients with inherited peripheral retinal degeneration in the absence of cortical degeneration. *Neural Plast.* 2019:8136354. doi: 10.1155/2019/8136354

Fischl, B., and Dale, A. M. (2000). Measuring the thickness of the human cerebral cortex from magnetic resonance images. *Proc. Natl. Acad. Sci. U.S.A.* 97, 11050–11055. doi: 10.1073/pnas.200033797

Fracasso, A., Luijten, P. R., Dumoulin, S. O., and Petridou, N. (2018). Laminar imaging of positive and negative bold in human visual cortex at 7T. *NeuroImage* 164, 100–111. doi: 10.1016/j.neuroimage.2017.02.038

Frezzotti, P., Giorgio, A., Motolese, I., De Leucio, A., Iester, M., Motolese, E., et al. (2014). Structural and functional brain changes beyond visual system in patients with advanced glaucoma. *PloS One* 9:e105931. doi: 10.1371/journal.pone.0105931

Gaffney, A. J., Binns, A. M., and Margrain, T. H. (2013). The effect of pre-adapting light intensity on dark adaptation in early age-related macular degeneration. *Doc. Ophthalmol.* 127, 191–199. doi: 10.1007/s10633-013-9400-3

Giannikopoulos, D. V., and Eysel, U. T. (2006). Dynamics and specificity of cortical map reorganization after retinal lesions. *Proc. Natl. Acad. Sci. U.S.A.* 103, 10805–10810. doi: 10.1073/pnas.0604539103

Gilbert, C. D., and Wiesel, T. N. (1992). Receptive field dynamics in adult primary visual cortex. *Nature* 356, 150–152. doi: 10.1038/356150a0

Gupta, N., and Yücel, Y. H. (2007). Glaucoma as a neurodegenerative disease. *Curr. Opin. Ophthalmol.* 18, 110–114. doi: 10.1097/ICU.0b013e3280895aea

Haak, K. V., Cissen, F. W., and Morland, A. B. (2012). Population receptive field dynamics in human visual cortex. *PloS One* 7:e37686. doi: 10.1371/journal.pone.0037686

Hoffmann, M. B., and Dumoulin, S. O. (2015). Congenital visual pathway abnormalities: a window onto cortical stability and plasticity. *Trends Neurosci.* 38, 55–65. doi: 10.1016/j.tins.2014.09.005

Hoffmann, M. B., Kaule, F. R., Levin, N., Masuda, Y., Kumar, A., Gottlob, I., et al. (2012). Plasticity and stability of the visual system in human achiasma. *Neuron* 75, 393–401. doi: 10.1016/j.neuron.2012.05.026

Holm, S. (1979). A simple sequentially rejective multiple test procedure. *Scand. J. Stat.* 6, 65–70.

Jonas, J. B., Aung, T., Bourne, R. R., Bron, A. M., Ritch, R., and Panda-Jonas, S. (2017). Glaucoma. *Lancet* 390, 2183–2193. doi: 10.1016/S0140-6736(17)31469-1

Jutley, G., Luk, S. M., Dehabadi, M. H., and Francesca Cordeiro, M. (2017). Management of glaucoma as a neurodegenerative disease. *Neurodegener. Dis. Manag.* 7, 157–172. doi: 10.2217/nmt-2017-0004

Kaas, J. H., Krubitzer, L. A., Chino, Y. M., Langston, A. L., Polley, E. H., and Blair, N. (1990). Reorganization of retinotopic cortical maps in adult mammals after lesions of the retina. *Science* 248, 229–231. doi: 10.1126/science.2326637

Kapetanakis, V. V., Chan, M. P. Y., Foster, P. J., Cook, D. G., Owen, C. G., and Rudnicka, A. R. (2016). Global variations and time trends in the prevalence of primary open angle glaucoma (POAG): a systematic review and meta-analysis. *Br. J. Ophthalmol.* 100, 86–93. doi: 10.1136/bjophthalmol-2015-307223

Kashyap, S., Ivanov, D., Havlicek, M., Sengupta, S., Poser, B. A., and Uludağ, K. (2018). Resolving laminar activation in human V1 using ultra-high spatial resolution FMRI at 7T. *Sci. Rep.* 8:17063. doi: 10.1038/s41598-018-35333-3

Lawrence, S. J. D., Formisano, E., Muckli, L., and de Lange, F. P. (2019). Laminar FMRI: applications for cognitive neuroscience. *NeuroImage* 197, 785–791. doi: 10.1016/j.neuroimage.2017.07.004

Liu, T., Cheung, S.-H., Schuchard, R. A., Glielmi, C. B., Hu, X., He, S., et al. (2010). Incomplete cortical reorganization in macular degeneration. *Investig. Ophthalmol. Vis. Sci.* 51, 6826–6834. doi: 10.1167/iovs.09-4926

Magnussen, S., Spillmann, L., Stürzel, F., and Werner, J. S. (2001). Filling-in of the foveal blue scotoma. *Vis. Res.* 41, 2961–2967.

Masuda, Y., Dumoulin, S. O., Nakadomari, S., and Wandell, B. A. (2008). V1 projection zone signals in human macular degeneration depend on task, not stimulus. *Cereb. Cortex* 18, 2483–2493. doi: 10.1093/cercor/bhm256

Masuda, Y., Horiguchi, H., Dumoulin, S. O., Furuta, A., Miyauchi, S., Nakadomari, S., et al. (2010). Task-dependent V1 responses in human retinitis pigmentosa. *Investig. Ophthalmol. Vis. Sci.* 51, 5356–5364. doi: 10.1167/iovs.09-4775

Masuda, Y., Takemura, H., Terao, M., Miyazaki, A., Ogawa, S., Horiguchi, H., et al. (2020). V1 projection zone signals in human macular degeneration depend on task despite absence of visual stimulus. *Curr. Biol.* 31, 406–412. doi: 10.1016/j.cub.2020.10.034

Mead, B., Ahmed, Z., and Tomarev, S. (2018). Mesenchymal stem cell–derived small extracellular vesicles promote neuroprotection in a genetic DBA/2J mouse model of glaucoma. *Investig. Ophthalmol. Vis. Sci.* 59, 5473–5480. doi: 10.1167/iovs.18-25310

Morland, A. B. (2015). Organization of the central visual pathways following field defects arising from congenital, inherited, and acquired eye disease. *Ann. Rev. Vis. Sci.* 1, 329–350. doi: 10.1146/annurev-vision-082114-035600

Murphy, M. C., Conner, I. P., Teng, C. Y., Lawrence, J. D., Safiullah, Z., Wang, B., et al. (2016). Retinal structures and visual cortex activity are impaired prior to clinical vision loss in glaucoma. *Sci. Rep.* 6:31464. doi: 10.1038/srep31464

Nuzzi, R., Dallorto, L., and Rolle, T. (2018). Changes of visual pathway and brain connectivity in glaucoma: a systematic review. *Front. Neurosci.* 12:363. doi: 10.3389/fnins.2018.00363

Pelli, D. G. (1997). The videotoolbox software for visual psychophysics: transforming numbers into movies. *Spat. Vis.* 10, 437–442.

Plank, T., Frolo, J., Brandl-Rühle, S., Renner, A. B., Jägle, H., and Greenlee, M. W. (2017). FMRI with central vision loss: effects of fixation locus and stimulus type. *Optom. Vis. Sci.* 94, 297–310. doi: 10.1097/OPX.0000000000001047

Plank, T., Frolo, J., Farzana, F., Brandl-Rühle, S., Renner, A. B., and Greenlee, M. W. (2013). Neural correlates of visual search in patients with hereditary retinal dystrophies. *Hum. Brain Mapp.* 34, 2607–2623. doi: 10.1002/hbm.22088

Prabhakaran, G. T., Carvalho, J., Invernizzi, A., Kanowski, M., Renken, R. J., Cornelissen, F. W., et al. (2020). Foveal PRF properties in the visual cortex depend on the extent of stimulated visual field. *NeuroImage* 222:117250. doi: 10.1016/j.neuroimage.2020.117250

Quigley, H. A., and Broman, A. T. (2006). The number of people with glaucoma worldwide in 2010 and 2020. *Br. J. Ophthalmol.* 90, 262–267. doi: 10.1136/bjo.2005.081224

Ress, D., Glover, G. H., Liu, J., and Wandell, B. (2007). Laminar profiles of functional activity in the human brain. *NeuroImage* 34, 74–84. doi: 10.1016/j.neuroimage.2006.08.020

Roska, B., and Sahel, J.-A. (2018). Restoring vision. *Nature* 557, 359–367. doi: 10.1038/s41586-018-0076-4

Russell, S., Bennett, J., Wellman, J. A., Chung, D. C., Yu, Z.-F., Tillman, A., et al. (2017). Efficacy and safety of voretigene neparvovec (AAV2-HRPE65v2) in patients with RPE65-mediated inherited retinal dystrophy: a randomised, controlled, open-label, phase 3 trial. *Lancet* 390, 849–860. doi: 10.1016/S0140-6736(17)31868-8

Schwartz, S. D., Regillo, C. D., Lam, B. L., Eliott, D., Rosenfeld, P. J., Gregori, N. Z., et al. (2015). human embryonic stem cell-derived retinal pigment epithelium in patients with age-related macular degeneration and stargardt's macular dystrophy: follow-up of two open-label phase 1/2 studies. *Lancet* 385, 509–516. doi: 10.1016/S0140-6736(14)61376-3

Sereno, M. I., Dale, A. M., Reppas, J. B., Kwong, K. K., Belliveau, J. W., Brady, T. J., et al. (1995). Borders of multiple visual areas in humans revealed by functional magnetic resonance imaging. *Science* 268, 889–893.

Song, X., Wang, G., Zhang, T., Feng, L., An, P., and Zhu, Y. (2012). Functional magnetic resonance imaging evaluation of visual cortex activation in patients with anterior visual pathway lesions. *Neural Regen. Res.* 7, 692–696. doi: 10.3969/j.issn.1673-5374.2012.09.009

Sunness, J. S., Taosheng, L., and Steven, Y. (2004). Retinotopic mapping of the visual cortex using functional magnetic resonance imaging in a patient with central scotomas from atrophic macular degeneration. *Ophthalmology* 111, 1595–1598. doi: 10.1016/j.ophtha.2003.12.050

Wandell, B. A., and Smirnakis, S. M. (2009). Plasticity and stability of visual field maps in adult primary visual cortex. *Nat. Rev. Neurosci.* 10, 873–884. doi: 10.1038/nrn2741

Wandell, B. A., Suelika, C., and Benjamin, B. T. (2000). Visualization and measurement of the cortical surface. *J. Cogn. Neurosci.* 12, 739–752. doi: 10.1162/089892900562561

Wang, J., Li, T., Sabel, B. A., Chen, Z., Wen, H., Li, J., et al. (2016). Structural brain alterations in primary open angle glaucoma: a 3T MRI study. *Sci. Rep.* 6:18969. doi: 10.1038/srep18969

Wang, Y., Tang, Z., and Gu, P. (2020). Stem/Progenitor cell-based transplantation for retinal degeneration: a review of clinical trials. *Cell Death Dis.* 11:793. doi: 10.1038/s41419-020-02955-3

Yakupov, R., Lei, J., Hoffmann, M. B., and Speck, O. (2017). False FMRI activation after motion correction. *Hum. Brain Mapp.* 38, 4497–4510. doi: 10.1002/hbm.23677

Yu, L., Xie, L., Dai, C., Xie, B., Liang, M., Zhao, L., et al. (2015). Progressive thinning of visual cortex in primary open-angle glaucoma of varying severity. *PLoS One* 10:e0121960. doi: 10.1371/journal.pone.0121960

Yu, L., Yin, X., Dai, C., Liang, M., Wei, L., Li, C., et al. (2014). Morphologic changes in the anterior and posterior subregions of V1 and V2 and the V5/MT+ in patients with primary open-angle glaucoma. *Brain Res.* 1588, 135–143. doi: 10.1016/j.brainres.2014.09.005

Zhou, W., Muir, E. R., Nagi, K. S., Chalfin, S., Rodriguez, P., and Duong, T. Q. (2017). Retinotopic FMRI reveals visual dysfunction and functional

reorganization in the visual cortex of mild to moderate glaucoma patients. *J. Glaucoma* 26, 430–437. doi: 10.1097/IJG.0000000000000641

Conflict of Interest: The authors declare that the research was conducted in the absence of any commercial or financial relationships that could be construed as a potential conflict of interest.

Publisher's Note: All claims expressed in this article are solely those of the authors and do not necessarily represent those of their affiliated organizations, or those of the publisher, the editors and the reviewers. Any product that may be evaluated in this article, or claim that may be made by its manufacturer, is not guaranteed or endorsed by the publisher.

Chapter 7

Approaches to map VF defects with fMRI

This chapter contains the permitted reprint of the **Mapping visual field defects with fMRI – Impact of approach and experimental conditions"** published in Frontiers in Neuroscience:

Prabhakaran, G.T., Al-Nosairy, K.O., Tempelmann, C., Thieme, H., Hoffmann, M.B., 2021. Mapping Visual Field Defects With fMRI – Impact of Approach and Experimental Conditions. Frontiers in Neuroscience 15, 1180.

https://doi.org/10.3389/fnins.2021.745886

frontiers in Neuroscience

ORIGINAL RESEARCH
published: 08 September 2021
doi: 10.3389/fnins.2021.745886

Mapping Visual Field Defects With fMRI – Impact of Approach and Experimental Conditions

*Gokulraj T. Prabhakaran[1], Khaldoon O. Al-Nosairy[1], Claus Tempelmann[2], Hagen Thieme[1] and Michael B. Hoffmann[1,3]**

[1] Department of Ophthalmology, Otto von Guericke University, Magdeburg, Germany, [2] Department of Neurology, Otto von Guericke University, Magdeburg, Germany, [3] Center for Behavioral Brain Sciences, Magdeburg, Germany

Current initiatives to restore vision emphasize the need for objective assessments of visual field (VF) defects as pursued with functional magnetic resonance imaging (fMRI) approaches. Here, we compared population receptive field (pRF) mapping-based VF reconstructions to an fMRI method that uses more robust visual stimulation (on-off block design) in combination with individualized anatomy-driven retinotopic atlas-information (*atlas-based VF*). We investigated participants with sizable peripheral VF-deficits due to advanced glaucoma (n = 4) or retinitis pigmentosa (RP; n = 2) and controls (n = 6) with simulated scotoma. We obtained (1) standard automated perimetry (SAP) data as reference VFs and 3T fMRI data for (2) pRF-mapping [8-direction bar stimulus, fixation color change task] and (3) block-design full-field stimulation [8-direction drifting contrast patterns during (a) passive viewing (PV) and (b) one-back-task (OBT; reporting successions of identical motion directions) to probe the impact of previously reported task-related unspecific visual cortex activations]. Correspondence measures between the SAP and fMRI-based VFs were accuracy, assisted by sensitivity and specificity. We found an accuracy of *pRF-based VF* from V1 in patients [median: 0.62] that was similar to previous reports and increased by adding V2 and V3 to the analysis [0.74]. In comparison to the pRF-based VF, equivalent accuracies were obtained for the atlas-based VF for both PV [0.67] and, unexpectedly, the OBT [0.59], where, however, unspecific cortical activations were reflected by a reduction in sensitivity [0.71 (PV) and 0.35 (OBT)]. In conclusion, in patients with peripheral VF-defects, we demonstrate that previous fMRI procedures to obtain VF-estimates might be enhanced by: (1) pooling V1-V3 to enhance accuracy; (2) reporting sensitivity and specificity measures to increase transparency of the VF-reconstruction metric; (3) applying atlas-based procedures, if *pRF-based VFs* are not available or difficult to obtain; and (4) giving, counter-intuitively, preference to PV. These findings are expected to provide guidance to overcome current limitations of translating fMRI-based methods to a clinical work-up.

Keywords: vision, human visual cortex, scotoma, perimetry, retinotopy, glaucoma, retinitis pigmentosa, atlas

OPEN ACCESS

Edited by:
Lauren Ayton,
The University of Melbourne, Australia

Reviewed by:
Edgar DeYoe,
Medical College of Wisconsin, United States
Janine Dale Mendola,
McGill University, Canada

****Correspondence:***
Michael B. Hoffmann
michael.hoffmann@med.ovgu.de

Specialty section:
This article was submitted to Perception Science, a section of the journal Frontiers in Neuroscience

Received: *22 July 2021*
Accepted: *19 August 2021*
Published: *08 September 2021*

Citation:
Prabhakaran GT, Al-Nosairy KO, Tempelmann C, Thieme H and Hoffmann MB (2021) Mapping Visual Field Defects With fMRI – Impact of Approach and Experimental Conditions. Front. Neurosci. 15:745886. doi: 10.3389/fnins.2021.745886

INTRODUCTION

Visual field (VF) testing is of critical importance for diagnosis and follow-up in ocular diseases. Standard automated perimetry (SAP) is primarily used for VF-assessment in clinical routine and regarded gold standard. Besides their widespread use, these conventional VF tests suffer from notable limitations. For example, they depend on the participant's ability and compliance in performing the attentionally demanding subjective test and on the tester's experience and skill (Gardiner and Demirel, 2008; Junoy Montolio et al., 2012). Such issues have emphasized the need and motivated the development of objective tests which do not require maximal patient compliance.

Interest in this field has been enhanced by current gene- and cell-based initiatives aiming at the restoration of retinal function in ocular diseases (reviews Jutley et al., 2017; Roska and Sahel, 2018), as these benefit from objective readouts of therapy success. Given the recent therapeutic advances at the level of the visual cortex with cortical implants (Beauchamp et al., 2020), one option for an objective VF assessment is the reconstruction of VF-coverage and identification of VF defects from the response patterns in the visual cortex obtained with functional magnetic resonance imaging (fMRI). This approach is based on the retinotopic layout of the visual information in the visual cortex, which can be directly obtained from fMRI data via (i) individualized VF-mapping, e.g., population receptive field (pRF) mapping (Dumoulin and Wandell, 2008), or (ii) indirectly via the application of a group-informed retinotopic atlas to the individual anatomy (Benson et al., 2014). (i) Individualized VF-mapping has been widely applied not only to map and investigate normal visual cortex functioning in healthy individuals (Harvey and Dumoulin, 2011; Wandell and Winawer, 2015; Prabhakaran et al., 2020), but also to provide insights on the interplay of visual cortex stability and plasticity in vision disorders (Baseler et al., 2011; Barton and Brewer, 2015; Hoffmann and Dumoulin, 2015; Ahmadi et al., 2020, 2019). For each voxel in the visual cortex, a model-based analysis of the participant-specific pRF-mapping data is applied to estimate the preferred eccentricity and receptive field size for a population of neurons in that voxel. Subsequently, this can be projected back to the VF for the reconstruction of a VF-map. Previous studies demonstrated a good correspondence of pRF-based VFs with subjective VF-prediction in both patients with VF-defects (Papanikolaou et al., 2014; Silson et al., 2018; Ritter et al., 2019; Carvalho et al., 2021) and healthy individuals with simulated scotomas (Hummer et al., 2018). (ii) For the atlas-based approach, cortical fMRI responses from full-field stimulation (i.e., non-mapping) can be projected into the VF via information from an anatomically driven participant-specific retinotopic atlas. Despite a potential utility of atlas-based VF-predictions, reports addressing this are very limited (Cideciyan et al., 2015) with most studies restricting the use of retinotopic atlases to only delineate visual areas. In fact, the pRF-based approach is intuitively expected to be of highest accuracy. Accordingly, Ritter et al. reported for the pRF-based reconstruction of peripheral VF defects (similar to the present study's patient cohort) in retinitis pigmentosa (RP) from V1 a median accuracy of 0.85 [range: 0.49–0.98 (n = 7)] (Ritter et al., 2019). It should be noted, however, that this approach is subject to the availability of reliable pRF-mapping data and the patient's reliable fixation of the central fixation target. Importantly, the atlas-based approach is much less dependent on patient's compliance as it applies more robust visual stimulation in a simple on-off block design. To assess its potential, a direct comparison of pRF- and atlas-based approaches is needed. The present investigation is aiming to fill this gap.

We address the question of how atlas-based and pRF-based reconstructions of VF defects compare for V1 and how they benefit from the inclusion of activity in V2 and V3. We ascertain a quantitative comparison of the different fMRI-based VF predictions to the subjective SAP-derived VFs. Further, the effect of adding stimulus-related attention on atlas-based reconstructions is determined. Finally, we assessed the potential improvement of the VF-reconstruction for a combined pRF- and atlas-based approach [Bayesian Benson (here termed "Combined"): Benson and Winawer, 2018].

MATERIALS AND METHODS

Participants

Individuals with sizable peripheral VF-deficits due to advanced glaucoma (n = 4) or RP (n = 2). Age of the patients ranged between 46 and 78. One of the RP patients was also diagnosed with secondary glaucoma. One additional participant with RP was excluded on grounds of unreliable mapping data (not included in the above sample size). Healthy controls (HCs) with normal vision [best-corrected decimal visual acuity $\geq$ 1.0 (Bach, 1996); n = 6] were also included for comparisons. Written informed consents and data usage agreements were signed by all participants. The study was conducted in adherence to the tenets of the Declaration of Helsinki and was approved by the ethics committee of the University of Magdeburg.

Visual Field Testing

Standard automated threshold perimetry (SAP) of the central 30° was performed to measure visual sensitivity using 24-2 Swedish Interactive Threshold Algorithm protocol [Goldmann size III white-on-white stimuli; either: Humphrey Field Analyzer 3 (SITA-Fast); Carl Zeiss Meditec AG; Jena, Germany; or (n = 2): OCTOPUS® Perimeter 101, Haag-Streit International, Switzerland; dG2; dynamic strategy]. The SAP-based VFs served as the reference for the correspondence analysis with fMRI-based reconstructions.

Fixation Stability

An MP-1 microperimeter (Nidek, Padua, Italy) was used in the patient cohort (except GL3) to ascertain the fixation stability of a central fixation target. Fixations were tracked with 25 Hz and the proportion of fixations falling within the central 2° radius was determined using built-in MP1 analysis. All the patients had stability greater than 96%.

Functional Magnetic Resonance Imaging Measurements

All magnetic resonance imaging (MRI) and fMRI data were collected with a 3 Tesla Siemens Prisma scanner (Erlangen, Germany). One high-resolution whole brain anatomical T1-weighted scan (MPRAGE, 1 mm isotropic voxels, TR | TI | TE = 2500 | 1100 | 2.82 ms) was collected for each participant. fMRI scans parallel to the AC–PC line were acquired using a T2*-weighted BOLD gradient-EPI sequence (TR | TE = 1,500 | 30 ms and voxel size = 2.5^3 mm^3). An inversion recovery EPI sequence (TR | TI | TE = 4,000 | 1,100 | 23 ms) with spatial coverage (FOV) and resolution identical to the T2* EPI was obtained to aid in the alignment of structural and functional data. The visual stimuli for fMRI were generated with Psychtoolbox-3 (Brainard, 1997; Pelli, 1997) in MATLAB (MathWorks, Natick, MA, United States) and back-projected to a screen [resolution: 1,920 × 1,080 pixels] at the rear end of the magnet bore. The visual stimulus was viewed monocularly with the better eye based on SAP [mean deviation (MD) and extent of VF-defect] in the patients and the dominant eye in the controls at a distance of 35 cm via an angled mirror. Only the lower section of a 64-channel head coil was used effectively resulting in a 34-channel coil to allow for an unrestricted view of the entire projection screen. For each participant, we collected in two separate sessions, fMRI data for (1) pRF mapping and (2) block-design full-field stimulation. The block-design data had been analyzed for a previous publication (Prabhakaran et al., 2021), which provided the extraction criteria for the selection of stimulation-driven voxels in our present analysis.

Population Receptive Field (pRF) Mapping

Visual stimulation

For visual stimulation a moving checkerboard stimulus pattern was presented [directions: 8 (2 horizontal, 2 vertical, and 4 diagonal); mean luminance: 109 cd/m^2; contrast: 99%; check size: 1.57°), exposed through a bar aperture [width: 1/4th (3.45°) of the stimulus radius (13.8°)]. The bar propagated across a circular aperture spanning the stimulus radius in 16 steps [step rate = 1.75°/repetition time (TR); TR = 1.5 s] within 24 s per bar directions. The sequence of the bar direction alternated with a horizontal or vertical sweep followed by a diagonal sweep, for which only the first 12 s of the sweep were presented and the later 12 s of the sweep were replaced by a mean luminance gray. For the controls, mapping data were obtained with an artificial peripheral (>7°) and complete lower right quadrant scotoma. Each pRF-mapping scan lasted 192 s and was repeated six times for the patient cohort and four times for the controls. The participants responded to a fixation-dot color change via button press.

Preprocessing and analysis

Freesurfer[1] was used for the automated segmentation of gray-white matter boundaries and ITK gray software[2] for the manual correction of segmentation errors. For each individual participant, within and between-scan head motion artifacts in the fMRI scans were corrected with AFNI[3] and the motion corrected functional images were aligned spatially to the anatomical scan using Kendrick Kay's alignment toolbox.[4] Using MATLAB based Vistasoft tools,[5] the motion-corrected fMRI time series were averaged together and for each voxel, the aggregate receptive field properties of the underlying neuronal population were estimated using a 2D-Gaussian pRF-model. The model is described by three stimulus-referred parameters; pRF-center or the position preferred in the VF (x and y in Cartesian coordinates) and the spatial spread (σ). The time course of the stimulus is convolved with a canonical hemodynamic response function (HRF; Friston et al., 1998) to predict a voxel's fMRI response. Approximately 100,000 predictions were generated for different plausible combinations of pRF parameters (x, y, σ) and the optimal pRF parameters, best fitting the predicted and actual voxel time-series were estimated by minimizing the sum of squared errors (RSS) between the two. Position parameters were used to compute voxel-wise eccentricity $\sqrt{(x^2 y^2)}$ and polar angle $\tan^{-1}(\frac{y}{x})$ and the fitted 2D-Gaussian spatial spread was used to compute the pRF-size. For each participant, borders of the primary (V1) and extra-striate (V2 and V3) visual cortex were delineated by following the phase reversals in the polar angle data (Sereno et al., 1995) projected onto their inflated cortical surface.

Visual field coverage

We generated the coverage maps by back projecting the voxel-wise pRF estimates to a high resolution matrix (128 × 128) representing the VF. The coverage map shows the locations in the VF that elicit a significant response from the cortical voxels. Only voxels with an explained variance ≥15% were included for the generation of the VF-maps. The threshold was chosen based on existing literature (Baseler et al., 2011; Haak et al., 2012; Barton and Brewer, 2015). The pRF-center of each voxel along with its width (2D-Gaussian) was overlaid on the VF-matrix. In this way, each location in the VF might be represented by more than one pRF and the one with the maximum value was taken as the coverage measure at that specific location. The pRF coverage ranges between 0 and 1, where lower coverage values indicate a possible scotoma.

Block-Design fMRI

Visual stimulation and data analysis

Participants viewed a high-contrast pattern stimulus within a rectangular aperture [width: 48°; height: 28°] drifting in eight different directions, while maintaining fixation on a centrally located fixation dot. fMRI data were obtained during (a) passive viewing (PV) and (b) one-back-task (OBT; reporting the succession of identical motion directions) of the stimulus. In the controls, we simulated an artificial peripheral scotoma exposing only the central 7° of the stimulus through a circular aperture. The temporal sequence of each run followed a block design with 10 cycles of 12 s motion block (stimulus presentation) alternating with 12 s of mean luminance gray (24 s per cycle). Within each motion block, the direction of the contrast pattern

[1]https://surfer.nmr.mgh.harvard.edu/

[2]https://github.com/vistalab/itkgray

[3]https://afni.nimh.nih.gov/

[4]https://github.com/kendrickkay/alignvolumedata

[5]https://github.com/vistalab/vistasoft

was randomly changed every second (i.e., 12 trials per block). In each 1 s trial, the stimulus was presented for 750 ms followed by a 250 ms mean luminance gray. This fMRI data-set was analyzed previously for the assessment of task-dependences of the fMRI responses (Prabhakaran et al., 2021). Since, we use the results from these data exclusively for the selection of voxels for the VF-reconstruction analysis of the present study, we refer to the publication for details on preprocessing and analysis steps. Briefly, fMRI BOLD responses for the two conditions were quantified via voxel-wise phase specified coherence at the stimulation frequency [coherence$_{ps}$ (Masuda et al., 2008)].

Visual field reconstruction

For our non-mapping based VF-reconstruction a two-step strategy was employed, i.e., as first step we extracted pRF estimates from the retinotopic atlas for the voxels activated by the fMRI stimulus, as second step we reconstructed the VF based on these estimates. Specifically, we extracted the voxel coordinates which will be used for generating the VF-coverage maps from the fMRI data [threshold: coherence$_{ps} \geq 0.30$; $p < 0.001$ (uncorrected) (Silver et al., 2005)] and applied pRF-estimates from an atlas-defined retinotopic template to these voxels (Benson et al., 2014). The atlas has previously been demonstrated to predict the retinotopic organization of the visual cortex with high accuracy using only a participant's brain anatomy. The anatomical retinotopic template is based on fMRI-based retinotopic mapping data and T1-weighted anatomy from 25 healthy participants as detailed in Benson et al. (2014). For the application of this template to the data-sets of the present study, a 3D cortical surface was generated from the anatomy of each participant and is inflated and flattened to a 2D surface. The patterns of the gyral and sulcal curvatures are used to register the 2D cortical surface between participants. Based on algebraic functions describing the topographic organization of the visual cortex (Schira et al., 2010), positions in the VF are mapped to points in the cortical surface. This algebraic retinotopic model is registered to the aggregate functional imaging data across the participants to construct the anatomical retinotopic template. With the voxel-wise pRF estimates from the template, we generated the VF-coverage maps applying the same procedure that was employed with the pRF mapping data. Separate coverage maps were computed for PV and OBT, respectively.

In addition, a Bayesian adaptation of the atlas-based approach (Benson and Winawer, 2018), i.e., combining participant-specific pRF-data with the retinotopic atlas, was also evaluated (here termed "Combined"). Coverage maps were generated similarly to the atlas-only approach.

Quantification of Correspondence

On a participant-to-participant basis, the MD samples located in the central 14° of the SAP VFs were upsampled to match the spatial resolution [128 × 128] of the fMRI-derived coverage maps for a quantitative comparison. Subsequently, the coverage maps were binarized into responsive and non-responsive locations for the detection of absolute scotomas (threshold: MD −26 dB, i.e., sensitivity < 0 5dB). Similarly, fMRI-based VF-coverage maps were thresholded at a value of 0.7, in accordance with Ritter et al. (2019) for better comparability. Exploratory analysis with other threshold values below and above 0.7 resulted in suboptimal correspondence. VF-locations corresponding to the blind spot were not included in the analysis.

The primary correspondence between SAP and fMRI-based VFs was determined as in Ritter et al. (2019) and is defined by:

$$Accuracy = \frac{\text{Number of matched VF locations (fMRI and SAP)}}{\text{Total number of VF locations tested}}$$

The range of *Accuracy* is between 0 and 1, with higher values indicating a better agreement between the compared coverage maps.

For further exploratory evaluation, we also computed the sensitivity and specificity of fMRI for the scotoma detection as auxiliary measures.

$$Sensitivity = \frac{\text{Number of matched non responsive locations (fMRIand SAP)}}{\text{Number of non responsive locations (SAP)}}$$

$$Specificty = \frac{\text{Number of matched responsive locations (fMRIand SAP)}}{\text{Number of responsive locations (SAP)}}$$

Statistical Analysis

Data for the statistical analysis were prepared in MATLAB (MathWorks, Natick, MA, United States) and statistics were performed with the software "R," version 3.4.1. Shapiro Wilk's test was used to test the normality assumptions of the data and an appropriate test was chosen based on its outcome. For within group statistics, one-sample *t*-test of the differences between measures, conditions or approaches were used and for between-group statistics two-sample independent *t*-tests were employed. It should be noted that the statistics for the additional auxiliary measures, i.e., sensitivity and specificity, were not corrected for multiple comparisons, due to their exploratory nature.

RESULTS

In patients with advanced peripheral VF defects and controls with artificial scotomas, we investigated the scope of fMRI as an objective tool for VF-predictions. In a comparative approach with SAP-derived VFs, we determined the accuracy of different fMRI-based VF-reconstruction approaches [based on (1) pRF-mapping; (2) participant-specific anatomy driven retinotopic atlas for PV; and (3) OBT] and assessed the association of the fMRI-SAP correspondence with clinical characteristics.

Cortical Representation of the VF-Defects

In all participants, we found a qualitative correspondence of the SAP-VF and the fMRI-based cortical VF maps. As an example of the cortical maps obtained, the eccentricity map derived from pRF mapping in a representative glaucoma participant (GL1) is depicted in **Figure 1A**. The maps clearly demonstrate a restricted representation in the anterior dorsal regions of the primary visual

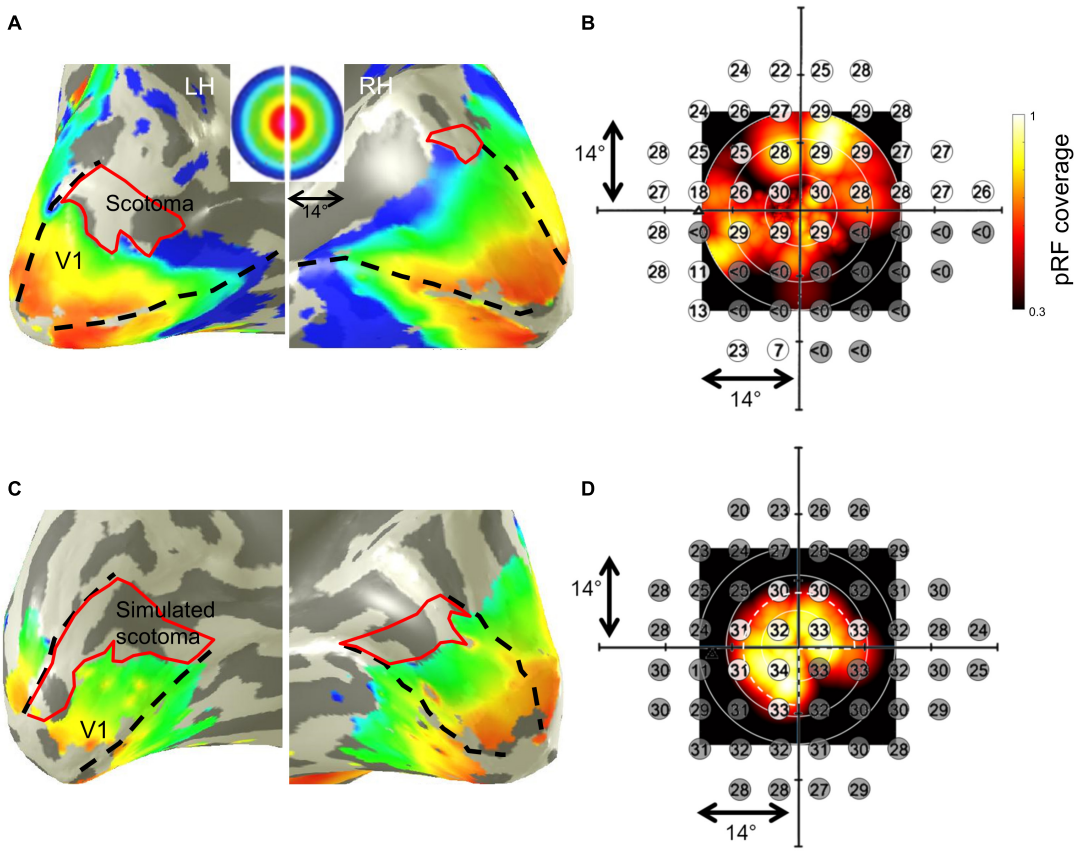

FIGURE 1 | Population receptive field (pRF) mapping derived eccentricities of a representative glaucoma participant (GL1; stimulation of left eye) with lower VF-defect (scotoma) **(A)** and a control (HC5; stimulation of left eye) with simulated peripheral (>7°) and lower right quadrant scotoma **(C)** mapped on their subjective inflated right and left visual cortex, respectively. Dashed black lines in panels **(A,C)** illustrate the primary visual cortex V1 boundaries. False-color representation from dark orange to dark blue illustrates the retinotopic progression of eccentricities from 0° to 14°. Restricted representations are visualized in the regions of the cortex corresponding to the VF-deficits (depicted by the red borders). Panels **(B,D)** show the subjective VFs predicted by SAP overlaid on the pRF-based VF coverage map of the glaucoma patient and control, respectively. In panel **(B)**, sensitivity < 0 dB (indicated by gray discs) indicates absolute scotoma location in the glaucoma participant. In panel **(D)**, the white dashed pie represents the boundary of stimulated VF in the controls; the simulated scotomatous VF locations are indicated by the gray discs in the control. The superimposed plots clearly demonstrate the correspondence between the SAP-based and pRF-based VF-reconstructions for both, patient and control.

cortex (V1), which topographically corresponds to the lower peripheral VF defect of this participant. The superposition of the participant's SAP-based VFs on the pRF-derived coverage maps (**Figure 1B**), demonstrates qualitatively the correspondence between the MRI and SAP-based VF-predictions. In controls with artificial scotoma, we report a similar correspondence between the two modalities, as depicted for a representative control participant in **Figures 1C,D**.

Population Receptive Field-Based VF Reconstruction – Quantification of Agreement

How Does V1 pRF-Based VF Reconstruction Compare to Previous Reports?

We observed a strong correspondence between SAP-based and pRF-based VFs in our patient cohort (n = 6) with advanced peripheral deficits caused by glaucoma or RP [median accuracy (range): 0.62 (0.32–0.88)], which is similar to previous reports [e.g., RP patients in Ritter et al., 2019; accuracy (range): 0.85 (0.49–0.98)]. Remarkably, in our further separate evaluations of sensitivity and specificity in the patient cohort, we observed not only a high sensitivity of pRF-mapping in predicting VF-defects [median (range): 0.91 (0.74–1.0)], but also large false positive predictions of VF-defects [low specificity: 0.24 (0.11–0.99)]. We report a similar pattern in the sensitivity-specificity profile for our control cohort [accuracy: 0.74 (0.63–0.83); sensitivity: 1.0 (1.0–1.0); specificity: 0.41 (0.16–0.63)], which indicates this effect to be not patient-specific. Such an increase in false positives in the detection of VF-defects is likely associated with signal dropouts that are not exclusive to the regions of the visual cortex deprived of visual input, but that also affect the visually intact cortex (e.g., due to cortical folding patterns or venous anatomy), i.e., false-positive scotoma detection. Therefore, we investigated whether the low specificity arising from false-positive scotoma can be

mitigated by pooling information from the early visual cortex (V1 through V3).

Does the Accuracy, Sensitivity, Specificity Benefit From Including V1–V3?

To address the issue of asymmetric sensitivity-specificity profiles observed in the above V1-based VF reconstructions, we tested how accuracy, sensitivity and specificity measures for scotoma detection compare between V1–V3-pooled and V1-only data. In the patients, we observed as expected a trend to higher accuracies [median (range): 0.74 (0.62–0.92)] and an increased balance between the sensitivity [0.86 (0.6–1.0)] and specificity [0.58 (0.33–1.0)] than for the reconstructions based on V1-only [accuracy: 0.62 (0.32–0.88); sensitivity: 0.91 (0.74–1.0); specificity: 0.24 (0.11–0.99)]. In the controls with simulated scotoma an even higher correspondence of SAP and fMRI-based VF predictions was observed [accuracy: 0.83 (0.71–0.87); sensitivity: 1.0 (0.98–1.0); specificity: 0.63 (0.32–0.73)] compared to measures from V1-only [accuracy: 0.74 (0.63–0.83); sensitivity: 1.0 (1.0–1.0); specificity: 0.41 (0.16–0.63)] (see also **Figure 2**). The individual VF reconstructions are depicted in **Figures 3**, **4** for patients and controls, respectively. At the individual level, in comparison to V1-only metrics, a quantitative assessment of the VF-reconstructions for V1–V3-pooled data demonstrated a better correspondence accuracy between SAP and pRF-based VFs for 5/6 patients (exception: GL4; $t(5) = 1.3$, $p = 0.255$) and for all (6/6) controls [$t(5) = 3.5$, $p = 0.017$]. Taken together, there was a trend to increased accuracies for V1–V3 based VF-reconstructions, which reached significance in the controls. Consequently, we performed all subsequent analyses for the V1-V3-pooled data.

Atlas-Based VF Reconstruction

Subsequent to the demonstration of a strong correspondence of pRF-based and SAP-based VFs, we investigated the feasibility of non-mapping based fMRI for VF predictions, as it has the potential to increase the utility and availability of fMRI-based objective VF-testing and its translation to clinical routine.

How Do pRF-Based and Atlas-Based VF Reconstructions of VF-Defects Compare?

In the patients, compared to mapping-based predictions [accuracy: 0.74 (0.62–0.92); sensitivity: 0.86 (0.6–1.0); specificity [0.58 (0.33–1.0)], we report for our anatomy informed retinotopic atlas and full-field stimulation (PV) approach equivalent accuracies [0.67 (0.41–0.89)] and a symmetric sensitivity [0.71 (0.39–0.91)] and specificity profile [0.7 (0.37–0.93] (**Figure 2**). In the controls, we observed very similar correspondence measures of the atlas-based (PV) and pRF-based approach [accuracy: 0.79 (0.7–0.81) vs. 0.83 (0.71–0.87); sensitivity: 0.9 (0.76–1.0) vs. 1.0 (0.98–1.0); specificity: 0.64 (0.58–0.85) vs. 0.63 (0.32–0.73)]. Only for the sensitivity measure, a significant decrease at the individual level for PV was found in both patients [$t(5) = 3.2$, $p = 0.025$] and controls [$t(5) = 3.1$, $p = 0.026$], which might be a consequence of the difference in the stimulation schemes between the two approaches. Taken together, the findings demonstrate the anatomy-based VF reconstructions with non-mapping full-field stimulation fMRI to be highly comparable to pRF-mapping based VF reconstructions [see **Figures 3** (patients) and **4** (controls) for participant-specific atlas-based coverage maps and correspondence measures].

Benefits From Combined pRF- and Atlas-Based VF-Reconstruction?

In our additional analysis with combined pRF- and atlas-based data (Benson and Winawer, 2018) compared to the conventional atlas-based approach, we only observed marginal non-significant differences in the reconstruction accuracy [patients (combined vs. atlas-based): 0.74 (0.34–0.84) vs. 0.67 (0.41–0.89); controls: 0.77 (0.7–0.8) vs. 0.79 (0.7–0.81)]. However, a small but significant increase in the specificity with the combined approach was reported for patients [0.75 (0.42–0.94) vs. 0.7 (0.37–0.93; $t(5) = 3.5$, $p = 0.017$] and controls [0.77 (0.58–0.89) vs. 0.64 (0.58–0.85); $t(5) = 3.4$, $p = 0.018$], which is suggestive of potential benefits from a combined pRF-mapping and atlas-based approach, subject to the availability of mapping data.

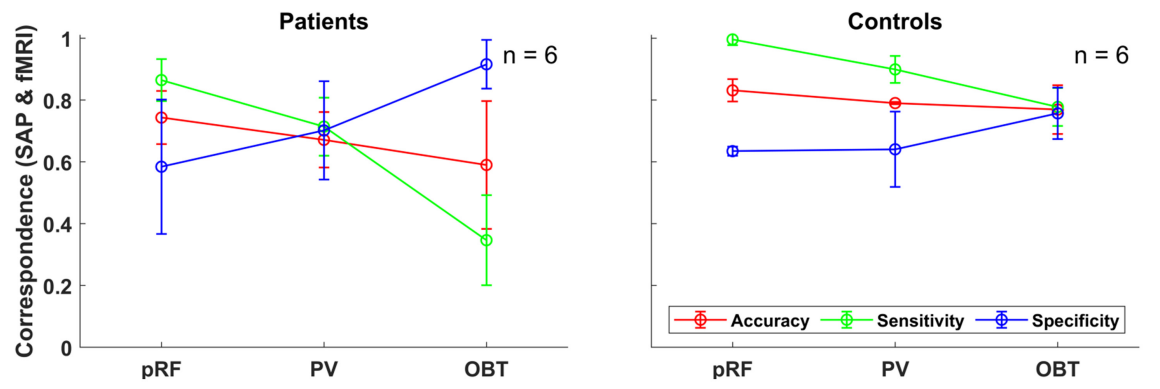

FIGURE 2 | Group-level fMRI-SAP correspondence measures (accuracy; sensitivity; and specificity) of the early visual cortex (V1–V3-pooled) for the different fMRI approaches (pRF, PV, and OBT) visualized as line plots for the patients ($n = 6$) and controls ($n = 6$). Each data point and error bars represent the median of the corresponding measure and its median absolute deviation (MAD) around the median.

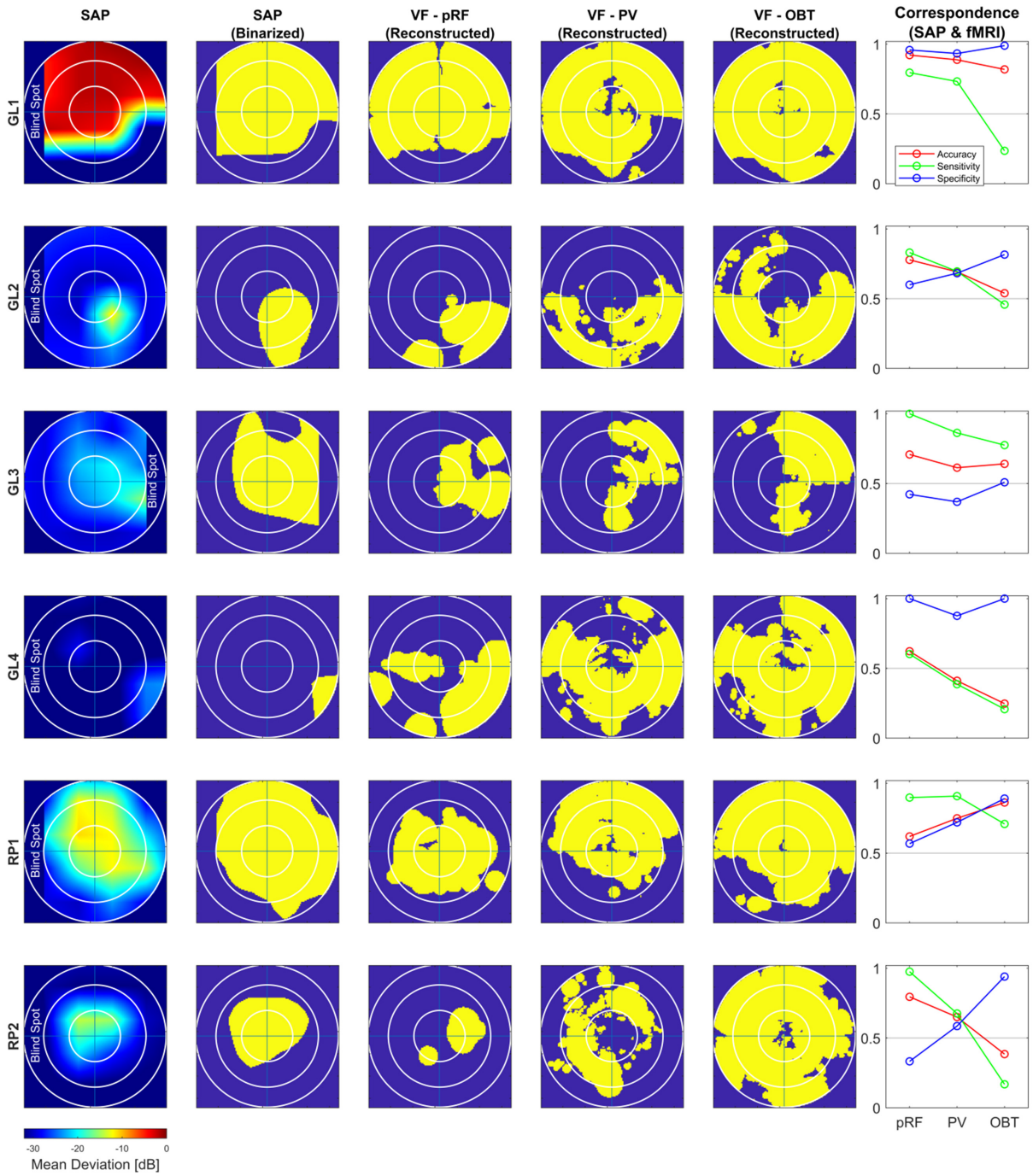

FIGURE 3 | Comparison of subjective (SAP) and objective (fMRI) VF-reconstruction (V1–V3-pooled) in patients. Each row represents one participant, the description for the columnar subplots are as follows: SAP: Upsampled and interpolated SAP VFs for the central 14° (radius); SAP (Binarized): Binarization was performed by thresholding the SAP VFs into responsive (yellow) (MD $\leq$ –26) and non-responsive (scotoma) (MD $>$ –26) locations; Columns VF – pRF, PV and OBT: Binarized pRF-based and atlas-based (PV and OBT) coverage maps, thresholded at a pRF coverage of 0.7; Correspondence (SAP and fMRI): accuracy; sensitivity; specificity for the different fMRI approaches (pRF, PV, and OBT) visualized as line plots.

Influence of Stimulus-Related Task (OBT) on Atlas-Based VF-Reconstruction?

We tested the informative value of the atlas-based VF-reconstruction approach and the three different performance measures (accuracy, sensitivity, and specificity) further. For this purpose, we applied the approach, in addition to the PV condition of the full-field stimulus, to the experimental condition OBT, which renders the cortical signature of the VF-defects in

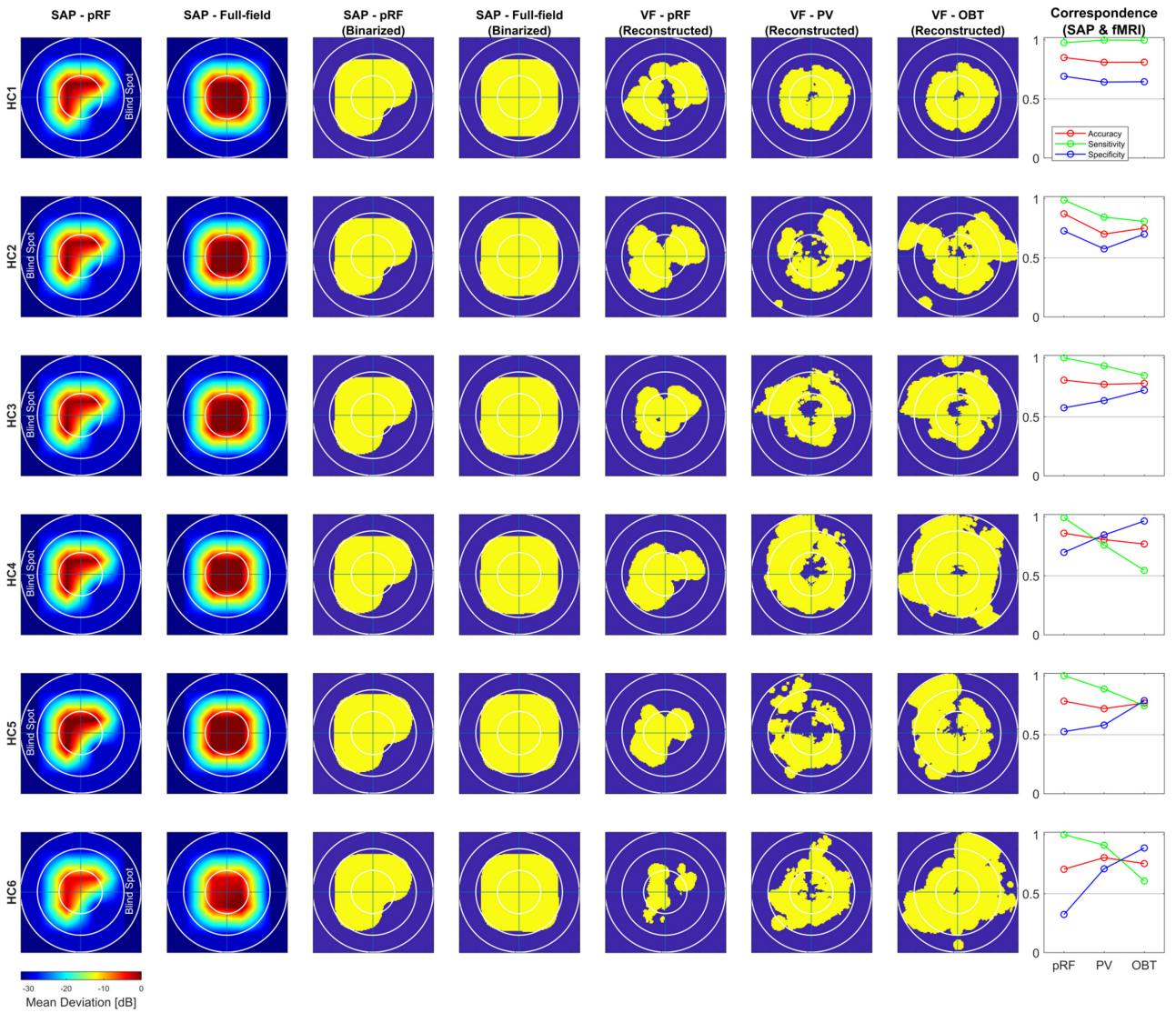

FIGURE 4 | Comparison of subjective (SAP) and objective (fMRI) VF-reconstruction (V1–V3-pooled) in controls. Each row represents one participant, the description for the columnar subplots are as follows: Columns SAP-pRF and SAP-Full-field: Upsampled and interpolated SAP VFs for the central 14° (radius) for comparison with pRF-based and atlas-based coverage maps, respectively. The reason for two different SAP-VFs is, in addition to a peripheral artificial scotoma (>7°), the pRF-mapping stimulus had a quadrantopic scotoma stimulation as well. SAP-pRF and Full-field (Binarized): Binarization procedure for the two SAP-based VFs followed same convention as in **Figure 3**. Columns VF – pRF, PV, and OBT: Binarized pRF-based and atlas-based (PV and OBT) coverage maps, thresholded at a pRF coverage of 0.7; Correspondence (SAP and fMRI): conventions same as **Figure 3**.

patients, but not controls, less specific (Masuda et al., 2010, 2008; Prabhakaran et al., 2021). For a meaningful measure, it is expected that the correspondence measures between SAP and atlas-based VF-reconstruction change for OBT compared to PV in patients, but not in controls.

Remarkably, for the patients' OBT, we found accuracies [0.59 (0.25–0.86)] closely similar to PV [0.67 (0.41–0.89); $t(5) = 1.5$, $p = 0.192$]. In contrast, the expected reduced performance for OBT was evident for sensitivities [median sensitivity for PV and OBT (range): 0.71 (0.39–0.91) and 0.35 (0.17–0.78), respectively; $t(5) = 4.0$, $p = 0.011$] and specificities [PV: 0.70 (0.37–0.93); OBT: 0.92 (0.51–1.0), respectively; $t(5) = -3.9$, $p = 0.011$]. **Figure 5** demonstrates that, at the individual level, all patients showed a considerable decrease in sensitivity and an increase in specificity of the OBT driven atlas-based approach. As anticipated, in controls with a simulated peripheral scotoma, a difference in the accuracy [PV: 0.79 (0.7–0.81); OBT: 0.77 (0.75–0.81); $t(5) = -0.2$, $p = 0.851$] was not observed. Unexpectedly, we did find a significant difference in the sensitivity [PV: 0.9 (0.76–1.0); OBT: 0.78 (0.55–1.0); $t(5) = 2.7$, $p = 0.041$] and specificity [PV: 0.64 (0.58–0.85); OBT: 0.76 (0.65–0.96); $t(5) = -4.1$, $p = 0.010$], similar to the patients. However, a further exploratory two-sample independent t-test (patients > controls) demonstrated the patients to have a greater magnitude of PV-OBT difference

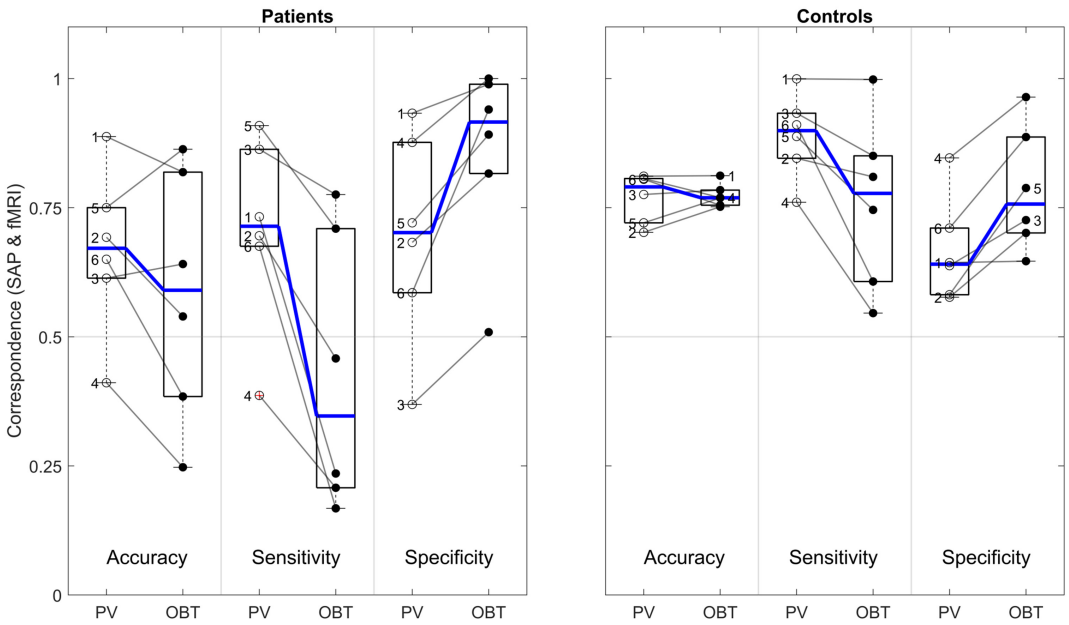

FIGURE 5 | Difference in atlas-based correspondence measures (V1–V3-pooled) for PV and OBT in patients (left panel) and controls (right panel). Subpanels delineated by transparent gray lines encompass the boxplots for PV (left) and OBT (right) for accuracy, sensitivity and specificity, respectively. Thick horizontal blue lines within the box plot represent the median of the measure and the blue lines connecting the PV and OBT box plots indicates the slope of median difference between them. Participant-specific correspondence measures, superimposed on the box plots (PV – open dots and OBT – closed black dots) are connected by a line to indicate the slope of the difference. Numbers 1–4 in the patients' panel represents the glaucoma participants GL1–GL4 and 5 and 6 represent RP1 and RP2. In the controls panel, 1–6 represents HC1–HC6, respectively.

than controls [sensitivity ($t(10) = 1.8$, $p = 0.05$); specificity ($t(10) = 2.1$, $p = 0.031$)]. Nevertheless, from our observations for PV and OBT, task-dependent dynamics in the correspondence measures is noticeable in both patient and controls. This suggests a simple full-field stimulus without an explicit task to be the optimal choice for atlas-based VF-reconstruction approaches.

Correlation With Clinical Characteristics

Insights into the association of fMRI-based VF predictions with patient-specific clinical characteristics are critical for its translation to clinical routine. Therefore, we investigated this relationship in the patients of the present study. Specifically, we explored the dependence of the correspondence measures on the MD as predicted by SAP (**Figure 6**) using a simple linear regression model [R^2 (coefficient of determination)]. All analyses were confined to the central 14° VF. For the atlas-based approach (PV), we observed a strong significant linear relationship between fMRI reconstruction accuracy and MD [$R^2 = 0.80$, $p = 0.014$]. This did not apply to the pRF-based approach [$R^2 = 0.29$, $p = 0.796$]. There was no significant association for sensitivity and specificity, irrespective of the reconstruction approach.

DISCUSSION

In the present study, we investigated for a group of patients with advanced peripheral VF-deficits (glaucoma and RP) and for HCs with simulated peripheral scotoma, the potential of various fMRI-based approaches for the reconstruction of VFs. We report a strong correspondence between the SAP-based and pRF-mapping-based VF reconstructions especially for pooled data from V1-V3. Equivalent correspondences were observed for VF-reconstructions that were based on simple block-design full-field stimulation fMRI data combined with an individualized anatomy-driven retinotopic atlas. In addition to our primary metric of correspondence, i.e., correspondence accuracy, we found the use of supplementary metrics to assess VF-defect prediction, i.e., sensitivity and specificity, to be critical to pinpoint and understand factors that might be of influence on the quality of fMRI-based reconstructions.

Qualitatively, the cortical response signatures observed in our patients corresponded to the location of their VF-defects, which is in accordance with the well-established application of retinotopic fMRI in mapping retinal lesions in the visual cortex (Duncan et al., 2007; Baseler et al., 2011; Barton and Brewer, 2015; Ferreira et al., 2017). Our finding of a moderate quantitative correspondence accuracy between SAP- and pRF-based VFs from V1-only data are in line with previous reports (Papanikolaou et al., 2014; Silson et al., 2018; Ritter et al., 2019; Carvalho et al., 2021). This prompts the question, why the correspondence of SAP and pRF-based VFs is not higher. We would like to indicate three potential reasons for this observation. (i) Cross-modality comparison. The comparison is done between two modalities, SAP vs. fMRI, that are fundamentally different, in terms of the entire approach, i.e., threshold detection of a spot-light vs. cortical responses to a temporally modulated high

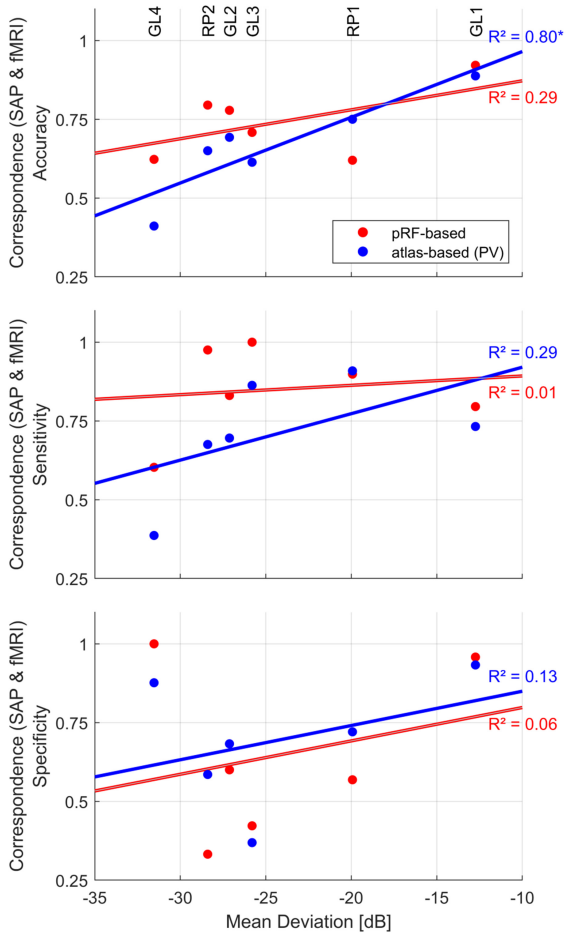

FIGURE 6 | Dependence of fMRI-SAP correspondence measures [pRF-based (red) and atlas-based PV (blue)] on mean deviation (MD) of the central 14° VF. Patient-specific measures are plotted as scatter-dot plots. Solid lines depict the best fitting regression. The strength of the association was evaluated as coefficient of determination (linear regression model); "*" indicates a significant *p*-value.

contrast checker-board exposed through a bar sweeping across the screen. (ii) Different sampling of the VF. For fMRI-based VF reconstruction, the VF is sampled much more densely than for SAP (one data point covered 6° × 6°). As a consequence, the SAP-results were upsampled for the comparison with fMRI-VFs, which likely contributed to a mismatch in the inter-modal comparison. (iii) Correspondence metric. The add-on metric of specificity indicated fMRI susceptibility to false-positive detection of VF-defects, i.e., overestimation of the scotoma, to be a critical factor in determining the correspondence. The proportion of false-positives was observed to follow an inverse relationship with the extent of the VF-defects. In fact, this is plausible, as an individual with a very large scotoma would have fewer responsive locations to be mislabeled as non-responsive.

As we report these false-positive detections even in the controls, we reason the cause to be of methodological origin rather than physiological, for e.g., signal dropouts as a result of reduced modulation of cortical responses or morphological limitations as in venous anatomy or cortical folding patterns generating local magnetic field inhomogeneities. This is complemented by our observations of reduced false-positive scotoma detection and consequent increase in accuracy with pooling of V1–V3 mapping-data for the reconstruction. Pooling V1–V3 appears to help in covering the VF-locations with signal dropouts for V1-only data. Considering V2 and V3 receive their primary input from V1 neurons, a potential logic for the observed effect of pooling might be that the neurons in a voxel associated with signal dropout may still drive voxels in V2 and V3. Thus pooling data from the three visual areas increases the likelihood of an fMRI response from at least one of the areas thereby contributing to the VF. However, the smaller surface area of V2 and V3 retinotopic maps in comparison to V1's and consequent coarse sampling might result in less precise and crude VF maps with the pooled data. Moreover, the increase in pRF sizes along the visual hierarchy might also add-up to this imprecision. Taken together, it should be noted that while pooling V1-V3 might ameliorate the incidence of false positives, it may also limit the ability to detect small scotomas due to a filling-in type of effect. Nevertheless, identifying the exact mechanisms behind the reported increase in accuracy of correspondence with pooled data is beyond the scope of this study and warrants future research, as information on VF-predictions based on individual visual areas are critical for establishing fMRIs likely role in therapeutic decisions.

Recent promising advancements in cell-, gene-, and microelectronics based vision restoration procedures (Ashtari et al., 2015; Aguirre, 2017; Roska and Sahel, 2018; Beauchamp et al., 2020) led to an increased fundamental interest in fMRI as a tool for objective visual function assessment. These upcoming therapeutic interventions require precise information of the VF representation in the visual cortex following VF-loss, which is provided by mapping-based fMRI. A bottleneck, however, is acquiring this information in patients where fMRI-based mapping is not feasible, for instance due to unstable fixation, very advanced VF loss or inability to comply with demanding task requirements. The VF-reconstruction approach employed here, using simple fMRI stimulus driven cortical responses in combination with an individualized retinotopic atlas demonstrated a performance that is equivalent to the pRF-based approach. The utility of this atlas-based approach also finds support from a previous report on two patients with Leber congenital amaurosis to investigate changes in fixation location (pseudo fovea) pre and post retinal gene therapy (Cideciyan et al., 2015). The stimulus used by Cideciyan and colleagues was a flickering uniform luminance screen whereas we employed a high contrast moving grating stimulus. Technically, the approach is expected to be robust to the use of any simple and salient stimulus, nevertheless it would be of interest for future work to test for any stimulus-type dependent effects on the approaches VF-reconstruction capability.

The use of spatially specific stimuli for pRF-mapping makes the approach susceptible to eye movements (Hummer et al., 2016). The full-field stimulus used in the atlas-based approach has the advantage to be less sensitive to fixation instabilities.

Although in our experiment the participants were presented with a fixation dot and instructed to focus their attention, it should, in fact be possible to discard the fixation and apply a free-viewing approach to the stimulus. This was not achievable with the current setup of our fMRI visual stimulation system which had a limited stimulus window size [width × height: 48° × 28°] and this limitation could be overcome by the use of wide-field stimulus displays (Wu et al., 2013; Greco et al., 2016).

We found a significantly reduced sensitivity for the detection of VF-defects with the atlas-based approach, when a stimulus-related task (OBT) was introduced. This indicates that the quality of VF-reconstructions is task-dependent and reduced if attention is directed to the visual stimulus. While this is at first sight counter-intuitive finding, it corresponds well with earlier reports on patients with central and peripheral VF deficits, where a stimulus-related tasks drove responses in the deafferented regions of the visual cortex (Baker et al., 2008; Masuda et al., 2010, 2008; Ferreira et al., 2019). The origin of these task-dependent responses is still under debate and beyond the scope of this study, for the purpose of atlas-based VF assessments. Still we can draw an important conclusion from our current findings, i.e., that including a stimulus-related attention task is, counter-intuitively, not recommended as it induces unspecific activations in deafferented cortex. It should be noted, however, that we here tested for effects of global attention as opposed to spatially varying attention. Consequently, it is unknown, whether there would be any differential effects of spatially-specific attention to the stimulus-aperture, e.g., in the pRF-stimulation sequence. It is to be noted that even in the absence of a task (PV) we did observe a marginal, but significant decrease in the sensitivity compared to pRF-based reconstruction. There might be two reasons for this, (1) the distinction between the pRF-mapping and PV stimulus by itself might drive the cortex differentially, and (2) participants performing OBT subconsciously even during PV, as the instructions for both PV and OBT were given pre-scanning. Nevertheless, our data show that the stimulus used in the atlas-based (PV) reconstruction performs equivalently well as the mapping-based approach in reconstructing VFs. This suggests that a simple block design stimulus without an explicit task is the optimal choice.

We acknowledge the small sample size, which was still sufficient for a statistical inference of the results. As we included patients with very advanced VF-defects, most of the recruited patients were aged and consequently resulted in a high rate of exclusions due to at least one MRI-related contraindication. The small sample size also limits our ability to correlate the performance of fMRI-based VFs with patient-specific clinical characteristics, when in fact a linear trend was observed with MD from SAP. Information on the relationship with clinical correlates is critical for translation of fMRI to clinical routine, which must be addressed by future research with patients with different stages of pathology using wide-field stimulation approaches.

In studies with patients who are prone to suffer from unreliable fixation, for instance, as a result of low visual acuity or large VF defects, the availability of quantitative eye-tracking data adds validation to the inference of results. While some of our patients fall in the aforementioned category, all of them were able to fixate quite well (fixation stability for the central 2° radius > 96%), as determined with fundus-controlled perimetry and a qualitative monitoring of stimulated eye in the scanner using an eye-tracker. This was also evident from their ability to perform a fixation dot task for the pRF-mapping experiment, subsequently confirmed by an overall good quality of retinotopic maps. Nevertheless, the lack of quantitative eye-tracking data should still be considered a constraint and we underscore the importance of eye-tracking in studies involving patients with vision disorders.

Although other mapping-based fMRI approaches, as in temporal phase-encoding (conventional rings and wedges) have also been employed in mapping VF defects in patients (Morland et al., 2001; Furuta et al., 2009; DeYoe et al., 2015), due to the prevalent adoption of pRF-mapping in recent years, we chose the latter approach for VF-mapping here. A few important similarities and differences with these approaches should be noted. (1) The stimulus used for both the pRF-mapping and phase-encoding methods are spatially-selective and suffer from the same limitations of requirement for stable fixation and attention from the patients. (2) In contrast to the phase-encoding method, the model-based analysis of pRF-mapping data provides a direct estimation of neuronal receptive field size (pRF-size) and this information is expected to enhance the accuracy of the reconstructed VFs. (3) pRF-mapping data provides precise VF-maps to the center of the foveal representation (Dumoulin and Wandell, 2008). (4) Although the acquisition time for these approaches are quite similar, analysis of conventional mapping data is less time-consuming. In consideration to the above-mentioned pros and cons, we believe a critical discussion on the situation-dependent suitability of the methods might help in making an informed decision on the choice of the mapping technique. For example, for the purpose of a time-constraint surgical planning which might not require a highly precise VF-map, fMRI-reconstruction based on phase-encoding approach might suffice.

The anatomy driven retinotopic atlas used in the atlas-based approach is based on pRF-mapping data from HCs and could be argued as a bias when used in patients with VF-defects. This could be asserted in consideration to studies that report altered pRF properties (specifically shifting of pRF position and enlargement of pRFs) in such patients (Ferreira et al., 2017; Zhou et al., 2017) and suggestive of cortical reorganization. It is to be noted, however, there is no clear consensus on this as there is a growing body of evidence demonstrating similar changes in receptive field properties even in controls with simulated scotomas (Baseler et al., 2011; Haak et al., 2012; Prabhakaran et al., 2020). Ideally, resolving this would require the creation of separate atlases specific for the patient population, but given the heterogeneity manifested in vision disorders it seems to be far-fetched at this point of time. Taking into account, the limited scope of long-term reorganization of the adult visual cortex in acquired vision disorders (Wandell and Smirnakis, 2009), we do not see the use of a control-based atlas as a potential limitation in the study.

Finally, it should be acknowledged that in the present study the atlas-based reconstruction of VFs is based on the assumptions

of undistorted central representation and absence of retinotopic re-organization. This might limit the method's utility to acquired peripheral vision disorders. Considering this, based on our current data and results, we exercise caution and warrant future research to investigate the applicability of the approach to: (1) central vision disorders (e.g., macular degeneration) even though with pRF-mapping being previously demonstrated to be a feasible tool to map central VF-defects (Hummer et al., 2018; Ritter et al., 2019), (2) congenital vision disorders with possible reorganization (Baseler et al., 2002), and (3) pediatric and very young individuals who would still be in the developmental phase of their brain anatomy.

CONCLUSION

In summary, we demonstrated in patients with advanced peripheral VF-defects (glaucoma and RP) and in controls with simulated scotomas the feasibility of fMRI as a tool for objective assessment of VFs. We report a good agreement between the VFs predicted by pRF-mapping and SAP, which is consistent with existing reports, thereby affirming the reliability of the technique. Importantly, we observed the atlas-based approach with a full-field simple block design stimulus perform equally well in reconstructing VFs based on cortical responses. Consequently, the results serve as a proof of concept for the atlas-based procedure to be a surrogate fMRI method in the absence of mapping data and to be of substantial benefit in studies involving patients with peripheral VF-defects. These findings are expected to provide guidance to overcome current limitations of translating fMRI-based methods to a clinical work-up.

DATA AVAILABILITY STATEMENT

The raw data supporting the conclusions of this article will be made available by the authors, without undue reservation.

ETHICS STATEMENT

The studies involving human participants were reviewed and approved by ethics committee – the University of Magdeburg. The patients/participants provided their written informed consent to participate in this study.

AUTHOR CONTRIBUTIONS

GP: conceptualization, methodology, formal analysis, investigation, data curation, and writing – original draft. MH: conceptualization, methodology, supervision, writing – review and editing, and funding acquisition. KA-N: investigation, writing – review, and editing. CT: methodology, writing – review, and editing. HT: writing – review and editing. All authors contributed to the article and approved the submitted version.

FUNDING

This project was supported by European Union's Horizon 2020 Research and Innovation Program under the Marie Skłodowska -Curie grant agreements No. 675033 and the German research foundation (DFG: HO2002/20-1). The funding organization did not have any role in the study design, collection, analysis and interpretation of the data, or publication of this research.

ACKNOWLEDGMENTS

We thank Katharina Jürse for her assistance with the recruitment of participants and Denise Scheermann for her support of the MRI measurements. We also thank the reviewers for their valuable comments and suggestions which have greatly helped us improve the manuscript.

REFERENCES

Aguirre, G. D. (2017). Concepts and strategies in retinal gene therapy. *Invest. Ophthalmol. Vis. Sci.* 58, 5399–5411. doi: 10.1167/iovs.17-22978

Ahmadi, K., Fracasso, A., Puzniak, R. J., Gouws, A. D., Yakupov, R., Speck, O., et al. (2020). Triple visual hemifield maps in a case of optic chiasm hypoplasia. *NeuroImage* 215:116822. doi: 10.1016/j.neuroimage.2020.116822

Ahmadi, K., Fracasso, A., van Dijk, J. A., Kruijt, C., van Genderen, M., Dumoulin, S. O., et al. (2019). Altered organization of the visual cortex in FHONDA syndrome. *Neuroimage* 190, 224–231. doi: 10.1016/j.neuroimage.2018.02.053

Ashtari, M., Zhang, H., Cook, P. A., Cyckowski, L. L., Shindler, K. S., Marshall, K. A., et al. (2015). Plasticity of the human visual system after retinal gene therapy in patients with Leber's congenital amaurosis. *Sci. Transl. Med.* 7:296ra110. doi: 10.1126/scitranslmed.aaa8791

Bach, M. (1996). The Freiburg Visual Acuity test–automatic measurement of visual acuity. *Optom. Vis. Sci.* 73, 49–53.

Baker, C. I., Dilks, D. D., Peli, E., and Kanwisher, N. (2008). Reorganization of visual processing in macular degeneration: replication and clues about the role of foveal loss. *Vision Res.* 48, 1910–1919. doi: 10.1016/j.visres.2008.05.020

Barton, B., and Brewer, A. A. (2015). fMRI of the rod scotoma elucidates cortical rod pathways and implications for lesion measurements. *PNAS* 112, 5201–5206. doi: 10.1073/pnas.1423673112

Baseler, H. A., Brewer, A. A., Sharpe, L. T., Morland, A. B., Jägle, H., and Wandell, B. A. (2002). Reorganization of human cortical maps caused by inherited photoreceptor abnormalities. *Nat. Neurosci.* 5, 364–370. doi: 10.1038/nn817

Baseler, H. A., Gouws, A., Haak, K. V., Racey, C., Crossland, M. D., Tufail, A., et al. (2011). Large-scale remapping of visual cortex is absent in adult humans with macular degeneration. *Nat. Neurosci.* 14, 649–655. doi: 10.1038/nn.2793

Beauchamp, M. S., Oswalt, D., Sun, P., Foster, B. L., Magnotti, J. F., Niketeghad, S., et al. (2020). Dynamic stimulation of visual cortex produces form vision in sighted and blind humans. *Cell* 181, 774–783.e5. doi: 10.1016/j.cell.2020.04.033

Benson, N. C., and Winawer, J. (2018). Bayesian analysis of retinotopic maps. *eLife* 7:e40224. doi: 10.7554/eLife.40224

Benson, N. C., Butt, O. H., Brainard, D. H., and Aguirre, G. K. (2014). Correction of distortion in flattened representations of the cortical surface allows prediction of V1-V3 functional organization from anatomy. *PLoS Comput. Biol.* 10:e1003538. doi: 10.1371/journal.pcbi.1003538

Brainard, D. H. (1997). The psychophysics toolbox. *Spat. Vis.* 10, 433–436.

Carvalho, J., Invernizzi, A., Martins, J., Jansonius, N. M., Renken, R. J., and Cornelissen, F. W. (2021). Visual field reconstruction using fMRI-based techniques. *Trans. Vis. Sci. Tech.* 10:25. doi: 10.1167/tvst.10.1.25

Cideciyan, A. V., Aguirre, G. K., Jacobson, S. G., Butt, O. H., Schwartz, S. B., Swider, M., et al. (2015). Pseudo-Fovea formation after gene therapy for RPE65-LCA. *Invest. Ophthalmol. Vis. Sci.* 56, 526–537. doi: 10.1167/iovs.14-15895

DeYoe, E. A., Ulmer, J. L., Mueller, W. M., Sabsevitz, D. S., Reitsma, D. C., and Pillai, J. J. (2015). Imaging of the functional and dysfunctional visual system. *Semin. Ultrasound CT MR* 36, 234–248. doi: 10.1053/j.sult.2015.05.015

Dumoulin, S. O., and Wandell, B. A. (2008). Population receptive field estimates in human visual cortex. *Neuroimage* 39, 647–660. doi: 10.1016/j.neuroimage.2007.09.034

Duncan, R. O., Sample, P. A., Weinreb, R. N., Bowd, C., and Zangwill, L. M. (2007). Retinotopic organization of primary visual cortex in glaucoma: comparing fMRI measurements of cortical function with visual field loss. *Prog. Retin. Eye Res.* 26, 38–56. doi: 10.1016/j.preteyeres.2006.10.001

Ferreira, S., Pereira, A. C., Quendera, B., Reis, A., Silva, E. D., and Castelo-Branco, M. (2019). Enhanced visual attentional modulation in patients with inherited peripheral retinal degeneration in the absence of cortical degeneration. *Neural Plast* 2019:8136354. doi: 10.1155/2019/8136354

Ferreira, S., Pereira, A. C., Quendera, B., Reis, A., Silva, E. D., and Castelo-Branco, M. (2017). Primary visual cortical remapping in patients with inherited peripheral retinal degeneration. *Neuroimage Clin.* 13, 428–438. doi: 10.1016/j.nicl.2016.12.013

Friston, K. J., Fletcher, P., Josephs, O., Holmes, A., Rugg, M. D., and Turner, R. (1998). Event-related fMRI: characterizing differential responses. *Neuroimage* 7, 30–40. doi: 10.1006/nimg.1997.0306

Furuta, A., Nakadomari, S., Misaki, M., Miyauchi, S., and Iida, T. (2009). Objective perimetry using functional magnetic resonance imaging in patients with visual field loss. *Exp. Neurol.* 217, 401–406. doi: 10.1016/j.expneurol.2009.03.030

Gardiner, S. K., and Demirel, S. (2008). Assessment of patient opinions of different clinical tests used in the management of glaucoma. *Ophthalmology* 115, 2127–2131. doi: 10.1016/j.ophtha.2008.08.013

Greco, V., Frijia, F., Mikellidou, K., Montanaro, D., Farini, A., D'Uva, M., et al. (2016). A low-cost and versatile system for projecting wide-field visual stimuli within fMRI scanners. *Behav. Res.* 48, 614–620. doi: 10.3758/s13428-015-0605-0

Haak, K. V., Cornelissen, F. W., and Morland, A. B. (2012). Population receptive field dynamics in human visual cortex. *PLoS One* 7:e37686. doi: 10.1371/journal.pone.0037686

Harvey, B. M., and Dumoulin, S. O. (2011). The relationship between cortical magnification factor and population receptive field size in human visual cortex: constancies in cortical architecture. *J. Neurosci.* 31, 13604–13612. doi: 10.1523/JNEUROSCI.2572-11.2011

Hoffmann, M. B., and Dumoulin, S. O. (2015). Congenital visual pathway abnormalities: a window onto cortical stability and plasticity. *Trends Neurosci.* 38, 55–65. doi: 10.1016/j.tins.2014.09.005

Hummer, A., Ritter, M., Tik, M., Ledolter, A. A., Woletz, M., Holder, G. E., et al. (2016). Eyetracker-based gaze correction for robust mapping of population receptive fields. *NeuroImage* 142, 211–224. doi: 10.1016/j.neuroimage.2016.07.003

Hummer, A., Ritter, M., Woletz, M., Ledolter, A. A., Tik, M., Dumoulin, S. O., et al. (2018). Artificial scotoma estimation based on population receptive field mapping. *Neuroimage* 169, 342–351. doi: 10.1016/j.neuroimage.2017.12.010

Junoy Montolio, F. G., Wesselink, C., Gordijn, M., and Jansonius, N. M. (2012). Factors that influence standard automated perimetry test results in glaucoma: test reliability, technician experience, time of day, and season. *Invest. Ophthalmol. Vis. Sci.* 53, 7010–7017. doi: 10.1167/iovs.12-10268

Jutley, G., Luk, S. M., Dehabadi, M. H., and Cordeiro, M. F. (2017). Management of glaucoma as a neurodegenerative disease. *Neurodegener. Dis. Manag.* 7, 157–172. doi: 10.2217/nmt-2017-0004

Masuda, Y., Dumoulin, S. O., Nakadomari, S., and Wandell, B. A. (2008). V1 projection zone signals in human macular degeneration depend on task, not stimulus. *Cereb. Cortex* 18, 2483–2493. doi: 10.1093/cercor/bhm256

Masuda, Y., Horiguchi, H., Dumoulin, S. O., Furuta, A., Miyauchi, S., Nakadomari, S., et al. (2010). Task-Dependent V1 responses in human retinitis pigmentosa. *Invest. Ophthalmol. Vis. Sci.* 51, 5356–5364. doi: 10.1167/iovs.09-4775

Morland, A. B., Baseler, H. A., Hoffmann, M. B., Sharpe, L. T., and Wandell, B. A. (2001). Abnormal retinotopic representations in human visual cortex revealed by fMRI. *Acta Psychol. (Amst)* 107, 229–247. doi: 10.1016/s0001-6918(01)00025-7

Papanikolaou, A., Keliris, G. A., Papageorgiou, T. D., Shao, Y., Krapp, E., Papageorgiou, E., et al. (2014). Population receptive field analysis of the primary visual cortex complements perimetry in patients with homonymous visual field defects. *Proc. Natl. Acad. Sci. U.S.A.* 111, E1656–E1665. doi: 10.1073/pnas.1317074111

Pelli, D. G. (1997). The VideoToolbox software for visual psychophysics: transforming numbers into movies. *Spat. Vis.* 10, 437–442.

Prabhakaran, G. T., Al-Nosairy, K. O., Tempelmann, C., Wagner, M., Thieme, H., and Hoffmann, M. B. (2021). Functional dynamics of de-afferented early visual cortex in glaucoma. *Front. Neurosci.* 15:653632. doi: 10.3389/fnins.2021.653632

Prabhakaran, G. T., Carvalho, J., Invernizzi, A., Kanowski, M., Renken, R. J., Cornelissen, F. W., et al. (2020). Foveal pRF properties in the visual cortex depend on the extent of stimulated visual field. *NeuroImage* 222:117250. doi: 10.1016/j.neuroimage.2020.117250

Ritter, M., Hummer, A., Ledolter, A. A., Holder, G. E., Windischberger, C., and Schmidt-Erfurth, U. M. (2019). Correspondence between retinotopic cortical mapping and conventional functional and morphological assessment of retinal disease. *Br. J. Ophthalmol.* 103, 208–215. doi: 10.1136/bjophthalmol-2017-311443

Roska, B., and Sahel, J.-A. (2018). Restoring vision. *Nature* 557, 359–367. doi: 10.1038/s41586-018-0076-4

Schira, M. M., Tyler, C. W., Spehar, B., and Breakspear, M. (2010). Modeling magnification and anisotropy in the primate foveal confluence. *PLoS Comput. Biol.* 6:e1000651. doi: 10.1371/journal.pcbi.1000651

Sereno, M. I., Dale, A. M., Reppas, J. B., Kwong, K. K., Belliveau, J. W., Brady, T. J., et al. (1995). Borders of multiple visual areas in humans revealed by functional magnetic resonance imaging. *Science* 268, 889–893.

Silson, E. H., Aleman, T. S., Willett, A., Serrano, L. W., Pearson, D. J., Rauschecker, A. M., et al. (2018). Comparing clinical perimetry and population receptive field measures in patients with *Choroideremia*. *Invest. Ophthalmol. Vis. Sci.* 59, 3249–3258. doi: 10.1167/iovs.18-23929

Silver, M. A., Ress, D., and Heeger, D. J. (2005). Topographic maps of visual spatial attention in human parietal cortex. *J. Neurophysiol.* 94, 1358–1371. doi: 10.1152/jn.01316.2004

Wandell, B. A., and Smirnakis, S. M. (2009). Plasticity and stability of visual field maps in adult primary visual cortex. *Nat. Rev. Neurosci.* 10, 873–884. doi: 10.1038/nrn2741

Wandell, B. A., and Winawer, J. (2015). Computational neuroimaging and population receptive fields. *Trends Cogn. Sci.* 19, 349–357. doi: 10.1016/j.tics.2015.03.009

Wu, J., Wang, B., Yang, J., Hikino, Y., Takahashi, S., Yan, T., et al. (2013). Development of a method to present wide-view visual stimuli in MRI for peripheral visual studies. *J. Neurosci. Methods* 214, 126–136. doi: 10.1016/j.jneumeth.2013.01.021

Zhou, W., Muir, E. R., Nagi, K. S., Chalfin, S., Rodriguez, P., and Duong, T. Q. (2017). Retinotopic fMRI reveals visual dysfunction and functional reorganization in the visual cortex of mild to moderate glaucoma patients. *J. Glaucoma* 26, 430–437. doi: 10.1097/IJG.0000000000000641

Conflict of Interest: The authors declare that the research was conducted in the absence of any commercial or financial relationships that could be construed as a potential conflict of interest.

Publisher's Note: All claims expressed in this article are solely those of the authors and do not necessarily represent those of their affiliated organizations, or those of the publisher, the editors and the reviewers. Any product that may be evaluated in this article, or claim that may be made by its manufacturer, is not guaranteed or endorsed by the publisher.

Chapter 8

General discussion

Using fMRI and neuro-computational models in patients with peripheral VF deficits (glaucoma and RP) and healthy individuals with simulated peripheral scotomas, the main objective of the studies presented in this thesis work revolves around the assessment of the scope and limits of neuroplasticity of the human visual cortex. More specifically, by evaluation of the receptive field properties of the visual neurons (chapter 5) and cortical response patterns in the visual cortex (chapter 6), I have established the limited ability of the adult visual cortex to modify its functional organization following VF loss. Given these findings, I also evaluated the feasibility of fMRI-based approaches for the assessment of visual dysfunction (chapter 7) and demonstrated its utility as a viable clinical tool. The following paragraphs briefly discuss the main findings of the studies presented in the thesis and their significance.

8.1 Summary of main findings and discussion

8.1.1 Altered receptive fields are not an exclusive indication of cortical reorganization

Changes in the receptive field characteristics of neuronal population (pRFs) are commonly reported in patients with VF dysfunction (Barton and Brewer, 2015; Ferreira et al., 2017; Zhou et al., 2017). It is established now, at the least in central vision disorders (for e.g. MD) that similar alterations are also observed in healthy individuals when patient-like conditions are simulated (Baseler et al., 2011; Haak et al., 2012). Such findings have challenged the claims on the remapping ability of adult visual cortex. Chapter 5 addresses this issue in the context of VF restrictions due to peripheral retinal pathologies, which was currently lacking from the literature.

In a comparative approach, we evaluated in a cohort of healthy participants, the dynamics of RF characteristics in the foveal neuronal population when simulated with artificial retinal lesions in the peripheral VF. The retinal lesions and associated VF-restrictions were simulated indirectly by reducing the extent of the stimulated VF. The findings from the study revealed the controls to exhibit modified receptive fields (specifically shifts in the preferred position and enlargement of pRFs) as a function of simulated retinal lesion size. Previously similar findings were reported in

patients with natural peripheral scotomas and taken as evidence of large scale cortical reorganization (Ferreira et al., 2017; Zhou et al., 2017). In consideration to our results, it is now plausible to assume such dynamics of receptive fields in patients to reflect normal cortical response behavior in a context of reduced peripheral stimulation and not necessarily straightforward evidence of neuroplasticity. These findings have significant implications with regards to the definition of cortical reorganization and also in exerting caution for selecting appropriate and comparable control conditions in studies addressing plasticity. For this purpose, forthcoming research should investigate RF properties from patients and controls with and without comparable experimental conditions.

A key question that warrants attention from our findings concerns the mechanisms underlying the dynamics of receptive field changes. Although the main objective of the study was not to deduce this, a review of various plausible causes in the context of both methodological biases and physiological origins was discussed in the article. We provide a concise overview of the same below. Firstly, in contrast to central vision disorders, where neurons with ectopic RFs are shown change the characteristics of foveal neuronal population (Haak et al., 2012), this seems not plausible in our case. This conclusion is in consideration to the magnitude and direction of the shifts and the proportion of voxels contributing to the reported changes. Secondly, methodological biases associated with pRF mapping technique can be addressed in terms of modeling approaches and conditions and stimulus configurations (Alvarez et al., 2015; Binda et al., 2013). We did direct our study to address some of these biases. For instance, we (1) compared two modeling approaches (Bayesian Markov Chain Monte Carlo (MCMC) (Zeidman et al., 2018) and conventional pRF mapping) and (2) evaluated models taking into account of the scotoma information. These variations however did not yield a significantly different result in our case. Nevertheless, there is plausibility for methodological biases to alter pRF properties and result in changes similar to those we report here. However, it is to be noted that over manipulation of modeling and stimulus properties might make replication of studies difficult. Given this, an effective way to tackle any potential methodological biases is to maintain closely matched experimental and analysis conditions between the patients and controls. This in a way emphasizes the main conclusion from our study indicating the need to use comparable control conditions. Thirdly, from the perspective of physiological mechanisms, (1) iso-oriented stimulus in the surround decreases fMRI responses (Kastner et al., 2001; Williams et al., 2003). Lack of peripheral stimulation (surround suppression) in the case of scotomas might have an impact on the collective neural response modulation changing the RF characteristics of the neuronal population. (2) Voluntary attention modulates fMRI responses and influences RF estimates (Desimone and Duncan, 1995; Kastner and Ungerleider, 2000). Although the attention of our participants was kept in focus with a fixation task, the masking of stimulus might invoke an exogenous (involuntary) attention towards the stimulus border and might consequently resulting in RF variations, we report in the study. Future research, for

e.g. using different models incorporating surround suppression (Zuiderbaan et al., 2012), attention (Klein et al., 2014) or without apriori pRF shape (Carvalho et al., 2019), should be employed to provide further insights the origin and nature of these RF variations associated with the introduction of scotoma.

8.1.2 Abnormal LPZ responses are driven by task-elicited demands

Brain activity in the regions of the visual cortex deprived of visual input due to retinal lesions (LPZ) might be interpreted as indication for cortical remapping (Baker et al., 2005; Dilks et al., 2009). This view has been challenged by reports demonstrating the nature of these functional responses to be more of a task-dependent effect, as shown previously in MD and RP (Masuda et al., 2010, 2008).

In chapter 6, we extended these reports to advanced glaucoma, which despite its global prevalence is still understudied in this regard. Patients with RP and healthy individual with simulated peripheral scotomas were also included in the study as reference cohorts. We showed the presence of aberrant LPZ responses in the early visual cortex which were strongly related to the performance of a stimulus related task in both glaucoma and RP, similar to existing literature. The findings have critical implications in suggesting strong limitations of bottom-up plasticity in the adult visual cortex and addressing the behavior of cortical organization and functioning in glaucoma. In addition, observing these effects across a spectrum of disorders (glaucoma and RP from our study and MD from previous independent work) also implies the mechanism driving them to be not pathology or disease specific, but to be a general feature of the early visual cortex (Masuda et al., 2020, 2010, 2008).

In line with existing reports (Masuda et al., 2010), a plausible mechanism behind the LPZ responses might be feedback from higher visual areas, which becomes the prominent signal in the absence of the primary feed-forward visual input. Ascertaining this origin of these responses however requires insights on the direction of information flow in the deafferented cortex and this is not possible to obtain at the spatial resolution of conventional 3T fMRI. To overcome this and provide further knowledge, future research employing ultra-high-field fMRI (7T) with submillimeter resolution (Ahmadi et al., 2020; Fracasso et al., 2018; Ress et al., 2007) should attempt to dissociate functional activity in the cortical input and output layers and thereby revealing the origin and directionality of task-related LPZ activations.

The findings reported in the study also garners high clinical relevance in the context of emerging initiatives to restore visual input to the cortex as information on the functionality of visual cortex is quite important in the preparation of these vision restoration and rehabilitation procedures. For e.g. regardless of proper disease management, a proportion of glaucoma patients continue progressing which raises the suspicion of the involvement of vision loss associated changes in the visual

cortex (Gupta and Yücel, 2007; Nuzzi et al., 2018). Our investigation on the cortical signatures of retinal lesions provides relevant insights into understanding the afore-mentioned relationship. For instance, the presence of cortical responses in the LPZ related to a visual input is suggestive of a stable functional architecture even after vision loss. In addition, we also reported no significant change in the cortical thickness of the visual cortex between the age-matched controls and patients. Taken together, our findings suggest well preserved functional and structural integrity, which should be further assessed in future research with a larger samples.

Finally, we also reported a non-significant negative association between the magnitude of the task-elicited LPZ responses and size of the VF-defect. Given the smaller sample size, future studies in a larger and heterogeneous cohort of patients might aid in getting a clearer picture on the relationship. Nevertheless, the findings underscore the benefits of patient-stratification strategies in studying disease associated changes in the visual cortex.

8.1.3 Translating fMRI to clinical routine – It is possible!

Translation of fMRI-based approaches to clinical routine regardless of its necessity and usefulness is limited by its availability and complexity, and more importantly the question on the limits of plasticity of the human visual cortex. For instance, in the wake of promising advances from gene therapy to cortical implants (Beauchamp et al., 2020; Jutley et al., 2017; Roska and Sahel, 2018), objective assessments of visual function based on cortical responses can provide complementary information that might not be available form standard ophthalmological test and help make better informed decisions on disease management and treatment strategies. Given that evidences from our work (chapters 5 & 6) and earlier studies point to an absence of long term reorganization in acquired vision disorders, in Chapter 7, we have established the utility of fMRI as a tool for VF assessments (Cideciyan et al., 2015; Ritter et al., 2019) in patients with advanced peripheral VF loss.

Specifically, we demonstrated a good correspondence of the pRF-based VFs with the VFs predicted by the gold standard approach, the SAP. In addition to the primary correspondence metric i.e. accuracy as used in earlier reports, we also measured the sensitivity and specificity of fMRI to detect VF-defects. These add-on measures were found to greatly benefit in providing further insights into the factors that might influence the quality of fMRI-based reconstructions. For instance, considering the measure of specificity, we were able to note an increased false-positive detection of VF-defects by fMRI that had an association with the size of the scotoma. Based on this inference, we also found that VF reconstructions based on pooled data from the early visual cortex (V1 – V3) results in a reduction of the afore-mentioned false positives and consequently a better congruence with SAP than using data from V1 alone. This appears to be achieved by the mitigation of some methodological biases, e.g. pooling of data reduces signal dropouts associated with morphological

characteristics as in venous anatomy or cortical folding patterns. Because of this reason, the conclusions derived from the study were based on the results from the pooled data. Nevertheless, forthcoming research should investigate the mechanisms that might influence the use of responses from individual visual areas in VF-reconstructions, as this will be critical for substantiating fMRI as a robust tool for clinical purpose.

A key bottleneck with pRF mapping or in general any mapping-based approaches, however, is the need for patient compliance and attention, for it to provide unbiased estimates. To overcome this, we employed an alternative approach based on cortical responses driven by a simpler full-field fMRI stimulus and individualized retinotopic atlas (atlas-based approach) (Cideciyan et al., 2015). We demonstrated the performance of the approach to be equivalent to that of the pRF-based method in predicting VFs. This finding establishes the potential of the atlas-based approach in patient population where mapping-based approaches are not feasible, for e.g. patients with fixation instability, severe VF-defects and/or those unable to perform tasks. Although, in theory, it is possible to employ a free-viewing approach to the stimulus, we asked the participants to fixate on a dot in the middle due to the limited stimulus window size in our fMRI visual stimulation system (a common problem with most fMRI setups). Nevertheless, the findings are expected to motivate research groups with wide-field stimulus displays to validate the atlas-based method without fixation requirements on the basis of empirical data. Based on our findings of task-dependent changes in the cortical signature of the visual cortex (chapter 6), we investigated the effect of this dynamics in the VF-reconstruction metrics and found a significant reduction in sensitivity with the introduction of a stimulus-related task. Given this finding, a simpler stimulus with no explicit task appears to be the optimal choice for the atlas-based approach. Future research is required to validate the atlas-based approach in a larger sample size in different stages of pathology and also to establish the generalizability of the approach across the spectrum of vision disorders (e.g. central vision disorders, congenital conditions).

8.2 Concluding remarks

A key question in the field of visual neuroscience is the assessment of the ability of adult human visual cortex to change or adapt with loss of visual function – and if it is plastic, then to what extent can it change? Using fMRI, the studies presented in this thesis work investigated the afore-mentioned questions from the perspective of peripheral visual field restrictions. In chapter 5, I demonstrated that the receptive field characteristics of a neuronal population can be altered even in healthy individuals when subjected to patient-like visual field restrictions. In chapter 6, I demonstrated the presence of aberrant cortical responses in the deafferented regions of visual cortex does not necessarily indicate remapping, but can be explained by task-elicited demands. The findings from both the studies indicate no definitive evidence for bottom-up large-scale neuroplasticity and also exert caution in

interpreting evidence for remapping by adhering to comparable and appropriate control conditions. The complementary information fMRI might provide in addition to ophthalmic tests are of benefit only when fMRI-based results can be translated appropriately to clinical routine. For this purpose, in chapter 7, I demonstrated the plausibility of conventional and alternative fMRI-based approaches, which can be employed even in challenging conditions (e.g. patients with fixation instability or less compliance) as an efficient tool for objective assessment of visual function. In conclusion, the results presented in this thesis are expected to fill important knowledge gaps insights into understanding the scope of neuroplasticity in the visual cortex, paving way for better disease management and treatment strategies in vision disorders.

List of abbreviations

BOLD	blood oxygen level dependent
EPI	echo planar imaging
fMRI	functional magnetic resonance imaging
IOP	intra-ocular pressure
LGN	lateral geniculate nucleus
LPZ	lesion projection zone
MCMC	markov chain monte carlo
MD	macular degeneration
MT	medial temporal visual area
NPZ	normal projection zone
pRF	population receptive field
RF	receptive field
RNFL	retinal nerve fiber layer
RGC	retinal ganglion cell
RP	retinitis pigmentosa
SAP	standard automated perimetry
TR	repetition time
V1	primary visual cortex
V2-V3	extrastriate visual areas
VF	visual field

Bibliography

Aguirre, G.D., 2017. Concepts and Strategies in Retinal Gene Therapy. Invest. Ophthalmol. Vis. Sci. 58, 5399–5411. https://doi.org/10.1167/iovs.17-22978

Ahmadi, K., Fracasso, A., Puzniak, R.J., Gouws, A.D., Yakupov, R., Speck, O., Kaufmann, J., Pestilli, F., Dumoulin, S.O., Morland, A.B., Hoffmann, M.B., 2020. Triple visual hemifield maps in a case of optic chiasm hypoplasia. NeuroImage 215, 116822. https://doi.org/10.1016/j.neuroimage.2020.116822

Alvarez, I., de Haas, B., Clark, C.A., Rees, G., Schwarzkopf, D.S., 2015. Comparing different stimulus configurations for population receptive field mapping in human fMRI. Front Hum Neurosci 9, 96. https://doi.org/10.3389/fnhum.2015.00096

Ashtari, M., Nikonova, E.S., Marshall, K.A., Young, G.J., Aravand, P., Pan, W., Ying, G.-S., Willett, A.E., Mahmoudian, M., Maguire, A.M., Bennett, J., 2017. The Role of the Human Visual Cortex in Assessment of the Long-Term Durability of Retinal Gene Therapy in Follow-on RPE65 Clinical Trial Patients. Ophthalmology 124, 873–883. https://doi.org/10.1016/j.ophtha.2017.01.029

Ashtari, M., Zhang, H., Cook, P.A., Cyckowski, L.L., Shindler, K.S., Marshall, K.A., Aravand, P., Vossough, A., Gee, J.C., Maguire, A.M., Baker, C.I., Bennett, J., 2015. Plasticity of the human visual system after retinal gene therapy in patients with Leber's congenital amaurosis. Sci Transl Med 7, 296ra110. https://doi.org/10.1126/scitranslmed.aaa8791

Authié, C.N., Berthoz, A., Sahel, J.-A., Safran, A.B., 2017. Adaptive Gaze Strategies for Locomotion with Constricted Visual Field. Frontiers in Human Neuroscience 11, 387. https://doi.org/10.3389/fnhum.2017.00387

Baker, C.I., Dilks, D.D., Peli, E., Kanwisher, N., 2008. Reorganization of visual processing in macular degeneration: replication and clues about the role of foveal loss. Vision Res 48, 1910–1919. https://doi.org/10.1016/j.visres.2008.05.020

Baker, C.I., Peli, E., Knouf, N., Kanwisher, N.G., 2005. Reorganization of Visual Processing in Macular Degeneration. J. Neurosci. 25, 614–618. https://doi.org/10.1523/JNEUROSCI.3476-04.2005

Barton, B., Brewer, A.A., 2015. fMRI of the rod scotoma elucidates cortical rod pathways and implications for lesion measurements. PNAS 112, 5201–5206. https://doi.org/10.1073/pnas.1423673112

Baseler, H.A., Brewer, A.A., Sharpe, L.T., Morland, A.B., Jägle, H., Wandell, B.A., 2002. Reorganization of human cortical maps caused by inherited photoreceptor abnormalities. Nat. Neurosci. 5, 364–370. https://doi.org/10.1038/nn817

Baseler, H.A., Gouws, A., Haak, K.V., Racey, C., Crossland, M.D., Tufail, A., Rubin, G.S., Cornelissen, F.W., Morland, A.B., 2011. Large-scale remapping of visual cortex is absent in adult humans with macular degeneration. Nat. Neurosci. 14, 649–655. https://doi.org/10.1038/nn.2793

Beauchamp, M.S., Oswalt, D., Sun, P., Foster, B.L., Magnotti, J.F., Niketeghad, S., Pouratian, N., Bosking, W.H., Yoshor, D., 2020. Dynamic Stimulation of Visual Cortex Produces Form Vision in Sighted and Blind Humans. Cell 181, 774-783.e5. https://doi.org/10.1016/j.cell.2020.04.033

Binda, P., Thomas, J.M., Boynton, G.M., Fine, I., 2013. Minimizing biases in estimating the reorganization of human visual areas with BOLD retinotopic mapping. J Vis 13, 13. https://doi.org/10.1167/13.7.13

Boucard, C.C., Hernowo, A.T., Maguire, R.P., Jansonius, N.M., Roerdink, J.B.T.M., Hooymans, J.M.M., Cornelissen, F.W., 2009. Changes in cortical grey matter density associated with long-standing retinal visual field defects. Brain 132, 1898–1906. https://doi.org/10.1093/brain/awp119

Callaway, E.M., 2004. Feedforward, feedback and inhibitory connections in primate visual cortex. Neural Netw 17, 625–632. https://doi.org/10.1016/j.neunet.2004.04.004

Carvalho, J., Invernizzi, A., Ahmadi, K., Hoffmann, M.B., Renken, R.J., Cornelissen, F.W., 2019. Micro-probing enables fine-grained mapping of neuronal populations using fMRI. Neuroimage 116423. https://doi.org/10.1016/j.neuroimage.2019.116423

Cattaneo, Z., Vecchi, T., 2011. Blind Vision: The Neuroscience of Visual Impairment. MIT Press, Cambridge, MA, USA.

Cideciyan, A.V., Aguirre, G.K., Jacobson, S.G., Butt, O.H., Schwartz, S.B., Swider, M., Roman, A.J., Sadigh, S., Hauswirth, W.W., 2015. Pseudo-Fovea Formation After Gene Therapy for RPE65-LCA. Invest Ophthalmol Vis Sci 56, 526–537. https://doi.org/10.1167/iovs.14-15895

Cunningham, S.I., Shi, Y., Weiland, J.D., Falabella, P., Olmos de Koo, L.C., Zacks, D.N., Tjan, B.S., 2015. Feasibility of Structural and Functional MRI Acquisition with Unpowered Implants in Argus II Retinal Prosthesis Patients: A Case Study. Transl Vis Sci Technol 4, 6. https://doi.org/10.1167/tvst.4.6.6

Curcio, C.A., Sloan, K.R., Kalina, R.E., Hendrickson, A.E., 1990. Human photoreceptor topography. Journal of Comparative Neurology 292, 497–523. https://doi.org/10.1002/cne.902920402

Desimone, R., Duncan, J., 1995. Neural mechanisms of selective visual attention. Annu. Rev. Neurosci. 18, 193–222. https://doi.org/10.1146/annurev.ne.18.030195.001205

Dilks, D.D., Baker, C.I., Peli, E., Kanwisher, N., 2009. Reorganization of visual processing in macular degeneration is not specific to the “preferred retinal locus.” J Neurosci 29, 2768–2773. https://doi.org/10.1523/JNEUROSCI.5258-08.2009

Dougherty, R.F., Koch, V.M., Brewer, A.A., Fischer, B., Modersitzki, J., Wandell, B.A., 2003. Visual field representations and locations of visual areas V1/2/3 in human visual cortex. J Vis 3, 586–598. https://doi.org/10.1167/3.10.1

Dowling, J.E., Joseph L. Dowling, Jr., 2016. Vision: How It Works and What Can Go Wrong. The MIT Press. https://doi.org/10.7551/mitpress/9780262034616.001.0001

Dumoulin, S.O., Wandell, B.A., 2008. Population receptive field estimates in human visual cortex. Neuroimage 39, 647–660. https://doi.org/10.1016/j.neuroimage.2007.09.034

Duncan, R.O., Boynton, G.M., 2003. Cortical Magnification within Human Primary Visual Cortex Correlates with Acuity Thresholds. Neuron 38, 659–671. https://doi.org/10.1016/S0896-6273(03)00265-4

Duncan, R.O., Sample, P.A., Weinreb, R.N., Bowd, C., Zangwill, L.M., 2007a. Retinotopic Organization of Primary Visual Cortex in Glaucoma: Comparing fMRI Measurements of

Cortical Function with Visual Field Loss. Prog Retin Eye Res 26, 38–56. https://doi.org/10.1016/j.preteyeres.2006.10.001

Duncan, R.O., Sample, P.A., Weinreb, R.N., Bowd, C., Zangwill, L.M., 2007b. Retinotopic organization of primary visual cortex in glaucoma: a method for comparing cortical function with damage to the optic disk. Invest. Ophthalmol. Vis. Sci. 48, 733–744. https://doi.org/10.1167/iovs.06-0773

Engel, S.A., Glover, G.H., Wandell, B.A., 1997. Retinotopic organization in human visual cortex and the spatial precision of functional MRI. Cerebral Cortex 7, 181–192. https://doi.org/10.1093/cercor/7.2.181

Ferreira, S., Pereira, A.C., Quendera, B., Reis, A., Silva, E.D., Castelo-Branco, M., 2017. Primary visual cortical remapping in patients with inherited peripheral retinal degeneration. Neuroimage Clin 13, 428–438. https://doi.org/10.1016/j.nicl.2016.12.013

Fracasso, A., Luijten, P.R., Dumoulin, S.O., Petridou, N., 2018. Laminar imaging of positive and negative BOLD in human visual cortex at 7T. NeuroImage, Pushing the spatio-temporal limits of MRI and fMRI 164, 100–111. https://doi.org/10.1016/j.neuroimage.2017.02.038

Glover, G.H., 2011. Overview of Functional Magnetic Resonance Imaging. Neurosurg Clin N Am 22, 133–139. https://doi.org/10.1016/j.nec.2010.11.001

Grill-Spector, K., Kourtzi, Z., Kanwisher, N., 2001. The lateral occipital complex and its role in object recognition. Vision Research 41, 1409–1422. https://doi.org/10.1016/S0042-6989(01)00073-6

Gupta, N., Yücel, Y.H., 2007. Glaucoma as a neurodegenerative disease. Curr Opin Ophthalmol 18, 110–114. https://doi.org/10.1097/ICU.0b013e3280895aea

Haak, K.V., Cornelissen, F.W., Morland, A.B., 2012. Population receptive field dynamics in human visual cortex. PLoS ONE 7, e37686. https://doi.org/10.1371/journal.pone.0037686

Hamel, C., 2006. Retinitis pigmentosa. Orphanet J Rare Dis 1, 40. https://doi.org/10.1186/1750-1172-1-40

Jonas, J.B., Aung, T., Bourne, R.R., Bron, A.M., Ritch, R., Panda-Jonas, S., 2017. Glaucoma. Lancet 390, 2183–2193. https://doi.org/10.1016/S0140-6736(17)31469-1

Jutley, G., Luk, S.M., Dehabadi, M.H., Cordeiro, M.F., 2017. Management of glaucoma as a neurodegenerative disease. Neurodegener Dis Manag 7, 157–172. https://doi.org/10.2217/nmt-2017-0004

Kastner, S., De Weerd, P., Pinsk, M.A., Elizondo, M.I., Desimone, R., Ungerleider, L.G., 2001. Modulation of sensory suppression: implications for receptive field sizes in the human visual cortex. J. Neurophysiol. 86, 1398–1411. https://doi.org/10.1152/jn.2001.86.3.1398

Kastner, S., Ungerleider, L.G., 2000. Mechanisms of visual attention in the human cortex. Annu. Rev. Neurosci. 23, 315–341. https://doi.org/10.1146/annurev.neuro.23.1.315

Klein, B.P., Harvey, B.M., Dumoulin, S.O., 2014. Attraction of position preference by spatial attention throughout human visual cortex. Neuron 84, 227–237. https://doi.org/10.1016/j.neuron.2014.08.047

Kourtzi, Z., Kanwisher, N., 2000. Activation in Human MT/MST by Static Images with Implied Motion. Journal of Cognitive Neuroscience 12, 48–55. https://doi.org/10.1162/08989290051137594

Kupfer, C., Chumbley, L., Downer, J.C., 1967. Quantitative histology of optic nerve, optic tract and lateral geniculate nucleus of man. J Anat 101, 393–401.

Lamme, V.A., Supèr, H., Spekreijse, H., 1998. Feedforward, horizontal, and feedback processing in the visual cortex. Curr Opin Neurobiol 8, 529–535. https://doi.org/10.1016/s0959-4388(98)80042-1

Logothetis, N.K., Wandell, B.A., 2004. Interpreting the BOLD signal. Annu Rev Physiol 66, 735–769. https://doi.org/10.1146/annurev.physiol.66.082602.092845

Malach, R., Reppas, J.B., Benson, R.R., Kwong, K.K., Jiang, H., Kennedy, W.A., Ledden, P.J., Brady, T.J., Rosen, B.R., Tootell, R.B., 1995. Object-related activity revealed by functional magnetic resonance imaging in human occipital cortex. Proc Natl Acad Sci U S A 92, 8135–8139.

Mansfield, P., 1977. Multi-planar image formation using NMR spin echoes. J. Phys. C: Solid State Phys. 10, L55–L58. https://doi.org/10.1088/0022-3719/10/3/004

Masuda, Y., Dumoulin, S.O., Nakadomari, S., Wandell, B.A., 2008. V1 projection zone signals in human macular degeneration depend on task, not stimulus. Cereb. Cortex 18, 2483–2493. https://doi.org/10.1093/cercor/bhm256

Masuda, Y., Horiguchi, H., Dumoulin, S.O., Furuta, A., Miyauchi, S., Nakadomari, S., Wandell, B.A., 2010. Task-Dependent V1 Responses in Human Retinitis Pigmentosa. Invest Ophthalmol Vis Sci 51, 5356–5364. https://doi.org/10.1167/iovs.09-4775

Masuda, Y., Takemura, H., Terao, M., Miyazaki, A., Ogawa, S., Horiguchi, H., Nakadomari, S., Matsumoto, K., Nakano, T., Wandell, B.A., Amano, K., 2020. V1 Projection Zone Signals in Human Macular Degeneration Depend on Task Despite Absence of Visual Stimulus. Current Biology. https://doi.org/10.1016/j.cub.2020.10.034

Morland, A.B., 2015. Organization of the Central Visual Pathways Following Field Defects Arising from Congenital, Inherited, and Acquired Eye Disease. Annu Rev Vis Sci 1, 329–350. https://doi.org/10.1146/annurev-vision-082114-035600

Muckli, L., De Martino, F., Vizioli, L., Petro, L.S., Smith, F.W., Ugurbil, K., Goebel, R., Yacoub, E., 2015. Contextual Feedback to Superficial Layers of V1. Curr Biol 25, 2690–2695. https://doi.org/10.1016/j.cub.2015.08.057

Murphy, M.C., Conner, I.P., Teng, C.Y., Lawrence, J.D., Safiullah, Z., Wang, B., Bilonick, R.A., Kim, S.-G., Wollstein, G., Schuman, J.S., Chan, K.C., 2016. Retinal Structures and Visual Cortex Activity are Impaired Prior to Clinical Vision Loss in Glaucoma. Sci Rep 6, 31464. https://doi.org/10.1038/srep31464

Nuzzi, R., Dallorto, L., Rolle, T., 2018. Changes of Visual Pathway and Brain Connectivity in Glaucoma: A Systematic Review. Front Neurosci 12. https://doi.org/10.3389/fnins.2018.00363

Ogawa, S., Lee, T.M., Kay, A.R., Tank, D.W., 1990a. Brain magnetic resonance imaging with contrast dependent on blood oxygenation. PNAS 87, 9868–9872. https://doi.org/10.1073/pnas.87.24.9868

Ogawa, S., Lee, T.M., Nayak, A.S., Glynn, P., 1990b. Oxygenation-sensitive contrast in magnetic resonance image of rodent brain at high magnetic fields. Magn Reson Med 14, 68–78. https://doi.org/10.1002/mrm.1910140108

Provis, J.M., Diaz, C.M., Dreher, B., 1998. Ontogeny of the primate fovea: a central issue in retinal development. Prog Neurobiol 54, 549–580. https://doi.org/10.1016/s0301-0082(97)00079-8

Ress, D., Glover, G.H., Liu, J., Wandell, B., 2007. Laminar profiles of functional activity in the human brain. NeuroImage 34, 74–84. https://doi.org/10.1016/j.neuroimage.2006.08.020

Ritter, M., Hummer, A., Ledolter, A.A., Holder, G.E., Windischberger, C., Schmidt-Erfurth, U.M., 2019. Correspondence between retinotopic cortical mapping and conventional functional and morphological assessment of retinal disease. British Journal of Ophthalmology 103, 208–215. https://doi.org/10.1136/bjophthalmol-2017-311443

Roska, B., Sahel, J.-A., 2018. Restoring vision. Nature 557, 359–367. https://doi.org/10.1038/s41586-018-0076-4

Rovamo, J., Virsu, V., 1979. An estimation and application of the human cortical magnification factor. Exp Brain Res 37, 495–510. https://doi.org/10.1007/BF00236819

Schoth, F., Burgel, U., Dorsch, R., Reinges, M.H.T., Krings, T., 2006. Diffusion tensor imaging in acquired blind humans. Neurosci Lett 398, 178–182. https://doi.org/10.1016/j.neulet.2005.12.088

Sereno, M.I., Dale, A.M., Reppas, J.B., Kwong, K.K., Belliveau, J.W., Brady, T.J., Rosen, B.R., Tootell, R.B., 1995. Borders of multiple visual areas in humans revealed by functional magnetic resonance imaging. Science 268, 889–893.

Smirnakis, S.M., 2016. Probing Human Visual Deficits with Functional Magnetic Resonance Imaging 28.

Wandell, B.A., Dumoulin, S.O., Brewer, A.A., 2007. Visual field maps in human cortex. Neuron 56, 366–383. https://doi.org/10.1016/j.neuron.2007.10.012

Wandell, B.A., Winawer, J., 2015. Computational neuroimaging and population receptive fields. Trends Cogn Sci 19, 349–357. https://doi.org/10.1016/j.tics.2015.03.009

Wang, J., Li, T., Sabel, B.A., Chen, Z., Wen, H., Li, J., Xie, X., Yang, D., Chen, W., Wang, N., Xian, J., He, H., 2016. Structural brain alterations in primary open angle glaucoma: a 3T MRI study. Scientific Reports 6, 1–9. https://doi.org/10.1038/srep18969

Williams, A.L., Singh, K.D., Smith, A.T., 2003. Surround modulation measured with functional MRI in the human visual cortex. J. Neurophysiol. 89, 525–533. https://doi.org/10.1152/jn.00048.2002

Zeidman, P., Silson, E.H., Schwarzkopf, D.S., Baker, C.I., Penny, W., 2018. Bayesian population receptive field modelling. Neuroimage 180, 173–187. https://doi.org/10.1016/j.neuroimage.2017.09.008

Zhou, W., Muir, E.R., Nagi, K.S., Chalfin, S., Rodriguez, P., Duong, T.Q., 2017. Retinotopic fMRI Reveals Visual Dysfunction and Functional Reorganization in the Visual Cortex of Mild to Moderate Glaucoma Patients. J. Glaucoma 26, 430–437. https://doi.org/10.1097/IJG.0000000000000641

Zuiderbaan, W., Harvey, B.M., Dumoulin, S.O., 2012. Modeling center-surround configurations in population receptive fields using fMRI. J Vis 12, 10. https://doi.org/10.1167/12.3.10

Publications

*Prabhakaran, G.T., Carvalho, J., Invernizzi, A., Kanowski, M., Renken, R.J., Cornelissen, F.W., Hoffmann, M.B., 2020. Foveal pRF properties in the visual cortex depend on the extent of stimulated visual field. NeuroImage 222, 117250. https://doi.org/10.1016/j.neuroimage.2020.117250

*Prabhakaran, G.T., Al-Nosairy, K.O., Tempelmann, C., Wagner, M., Thieme, H., Hoffmann, M.B., 2021. Functional dynamics of de-afferented early visual cortex in glaucoma. Front. Neurosci. 15. https://doi.org/10.3389/fnins.2021.653632

*Prabhakaran, G.T., Al-Nosairy, K.O., Tempelmann, C., Thieme, H., Hoffmann, M.B., 2021. Mapping visual field defects with fMRI – impact of approach and experimental conditions. Frontiers in Neuroscience 15, 1180. https://doi.org/10.3389/fnins.2021.745886

Puzniak, R.J., Prabhakaran, G.T., Hoffmann, M.B., 2021b. Deep learning-based detection of malformed optic chiasms from MRI images. Frontiers in Neuroscience 15, 1332. https://doi.org/10.3389/fnins.2021.755785

Al-Nosairy, K. O., Prabhakaran, G. T., Pappelis, K., Thieme, H., & Hoffmann, M. B. 2020. Combined multi-modal assessment of glaucomatous damage with electroretinography and optical coherence tomography/angiography. Translational Vision Science & Technology, 9(12), 7–7. https://doi.org/10.1167/tvst.9.12.7

Hoffmann, M.B., Choritz, L., Thieme, H., Prabhakaran, G.T., Puzniak, R.J., 2021. [Neuro-computational approaches for objective assessment of visual function]. Ophthalmologe 118, 900–906. https://doi.org/10.1007/s00347-021-01404-6

Puzniak, R.J., Prabhakaran, G.T., Buentjen, L., Schmitt, F.C., Hoffmann, M.B., 2021a. Tracking the visual system—from the optic chiasm to primary visual cortex. Z. Epileptol. 34, 57–66. https://doi.org/10.1007/s10309-020-00384-y

* Publications presented in this thesis.